




Universitetet
i Stavanger

FACULTY OF SCIENCE AND TECHNOLOGY

MASTER'S THESIS

Study programme/specialisation: MSc in Offshore Technology/ Marine and Subsea Technology	Spring / Autumn semester, 2018 Open/ Confidential
Author: Eirinaios Chatzillari	 (signature of author)
Faculty supervisor: External supervisor:	Dr. Daniel Karunakaran, Ph.D., Adjunct Professor, University of Stavanger and Chief Engineer - Technical Authority, Subsea 7 Håkon Thingstad, Discipline Manager, Structural Design for Operations, Subsea 7
Title of master's thesis: Design of a handling mechanism for deployment of multiple concrete mattresses in a single lift	
Credits: 30	
Keywords: - Installation frame - Concrete mattress - Multi-deployment mechanism - Structural analysis - Spur gears - ROV - Torque tool	Number of pages: ...129..... + Appendix: ...77..... Stavanger, ... 15/06/2018 date/year



In collaboration with



**Design of a handling mechanism for
deployment of multiple concrete mattresses in
a single lift**

by

Eirinaios Chatzillari

University of Stavanger

Department of Mechanical and Structural Engineering and Materials Science

A thesis submitted in partial fulfillment of the requirements for the degree of

Master of Science in Offshore Technology

Specialization in Marine and Subsea Technology

Stavanger, spring 2018

This page is intentionally left blank

Abstract

If one could imagine a single pipeline spanning approximately 11,000 km from Oslo, Norway to Bangkok, Thailand, this would be similar to the total length of the Norwegian oil and gas pipeline network combined [1]. The hydrocarbon resources located in the cold waters of subsea fields offshore Norway, are transported via pipelines to either an onshore processing facility or directly exported to consumers in the UK and European Union area. Long sections of this transportation pipeline network require protection from potential hazards, such as trawling-shipping activities and dropped objects. One common method of pipeline protection is the installation of concrete mattresses on top of the pipeline. Concrete mattresses are also utilized where soil stabilization and foundation support is needed.

Despite a large number of concrete mattress installation projects is performed annually, the current deployment method is relatively inefficient, as each mattress is individually lifted and installed. The present thesis proposes a handling mechanism for the deployment of multiple concrete mattresses in a single lift.

Initially, Subsea 7 proposed a concept for a multi-installation tool. The concept comprised a steel frame that would facilitate six concrete mattresses and embody a handling mechanism with rotating pipes and gears. The mattresses will be lowered to the seabed through the mechanism with the assistance of a ROV torque tool. The key feature of the project is the study of the handling mechanism, and more specifically, to resolve the concept under certain requirements, elaborate on its operational and installation aspects, and assess the structural integrity of the finalized solution.

The initial concept is thoroughly presented and examined. The operational procedure and the functionality of each component is also discussed. The design phase starts with the dimensioning of the rotating parts of the mechanism, which yield the required design values of the gearset.

In the sequel, an arrangement of spur gears is designed according to the limitations that have been set. The strength of the gearset is evaluated with the use of analytical solutions. Additionally, a finite element analysis of the response of the gearset is performed for verification and comparison purposes.

Finally, the current thesis work concludes to a new configuration of the handling mechanism with the use of alternative ROV tooling aids. The design of the new setup is presented and the structural integrity of the new components is assessed. Lastly, some recommendations for future work are given.

Acknowledgements

Firstly, I would like to thank my academic supervisor Daniel Karunakaran, Professor at University of Stavanger, for his valuable help, guidance and follow-up during the elaboration of the present thesis report. Great thanks go also to my co-supervisor Håkon Thingstad, Discipline Manager at Subsea 7, who first gave me the opportunity to develop a thesis work in the industry and presented me the current subject. His valuable knowledge and advice are truly appreciated.

In the sequel, I would like to thank the person who introduced me to this topic and the originator of the idea to develop it, Kristian Lindtveit, principal engineer at Subsea 7. His valuable time for communicating me his knowledge and ideas has been a great assistance to surpass all the challenges that arose, and his overall contribution gave me a great boost to produce this piece of work. Moreover, I would like to thank Knut Sigmund Lende and Stig Hjorth, engineers at subsea 7, for sharing their expertise in the field of offshore installation and ROV tooling.

I am also grateful to all the people who were part of this indisputable chapter of my life and have contributed to my evolution as an engineer and person. I warmly thank all my good friends, Konstantinos, Thodoris, Luis, Khusal, for all the wonderful moments of my student life in Stavanger, and especially Konstantina Dimoula for being with me alongside this journey, for her patience, understanding and love. I am also thankful to my friend Dimitris Ntroumpis for reading and providing his suggestions to improve my work.

Most of all, I am grateful to my parents and little sister, who wholeheartedly have been always close to me with their full support and love. They have helped me to realize my dreams and aspirations. Thank you!

Eirinaios Chatzillari,

Stavanger, June 15th, 2018

Table of Contents

Abstract	iii
Acknowledgements	iv
Table of Contents	v
List of Figures	ix
List of Tables.....	xii
List of Abbreviations.....	xiii
Chapter 1 Introduction.....	1
1.1 Motivation	1
1.2 Aim of the thesis.....	2
1.3 Structure of the report.....	3
Chapter 2 Background	4
2.1 Pipeline hazards.....	4
2.1.1 Introduction to subsea pipelines and cables.....	4
2.1.2 Fishing activities	6
2.1.3 Dropped objects	8
2.1.4 Shipping activity	9
2.1.5 Other cases for pipeline protection	10
2.2 Methods of pipeline protection and stabilization	11
2.2.1 Increase in the wall thickness	11
2.2.2 Concrete mattresses	11
2.2.3 Trenching and Backfilling	12
2.2.4 Glass Reinforced Plastic (GRP) covers	13
2.2.5 Rock dumping.....	13
2.2.6 Concrete coating	14
2.2.7 Protective structures or tunnels.....	15
2.3 Concrete mattresses	15
2.3.1 History of concrete mattresses.....	15
2.3.2 Manufacture of concrete mattresses	16

2.3.3	Type of concrete mattresses.....	16
2.3.4	Equipment used for deployment.....	17
2.3.5	Lifting and handling devices	18
2.3.6	Multi-deployment tools available on the market.....	19
2.3.7	Rigging of the mattresses on the frame	22
2.3.8	Load-out, mobilization, over-boarding and deployment operations	23
2.3.9	Examples of large scale projects.....	25
2.4	ROV tooling	26
2.4.1	Introduction to ROVs	26
2.4.2	ROV torque tools.....	28
2.4.3	Torque tool failures.....	29
2.4.4	Torque tool controllers	29
2.4.5	International standards for ROV interfaces	30
2.4.6	Torque tool interface.....	31
Chapter 3	Gear theory.....	32
3.1	Introduction to gears.....	32
3.1.1	Type of gears	34
3.2	Gear standards, terminology and nomenclature	38
3.3	Forces on spur gears	42
3.4	Gear failures	44
3.5	Gear tooth strength	46
3.5.1	Bending stresses.....	46
3.5.2	Contact stresses.....	50
3.6	Rotational work and power	53
Chapter 4	Concept presentation	55
4.1	Challenges and requirements.....	55
4.2	Multiple concrete mattress installation frame concept.....	56
4.3	Deployment procedure	60
4.4	Selection of parameters and assumptions.....	62
4.5	Potential savings by the multi-deployment frame.....	65

Chapter 5 Basis of design	67
5.1 Units and material/sectional properties	67
5.2 LRFD method and limit state	68
5.3 Load and material factors	69
5.4 Load factors in marine lifting operations	71
5.5 Presentation of results	74
5.6 Structural checks	74
5.7 Software engineering and design tools.....	76
Chapter 6 Design phase	77
6.1 Input data.....	77
6.2 Load case 1: Lift in air	78
6.2.1 Lower pipe.....	78
6.2.2 Upper pipe	80
6.3 Load case 2: Subsea lift.....	81
Chapter 7 Design of gears.....	83
7.1 Input data for the gear design	83
7.2 Speed of deployment	84
7.3 Generation of gears with Inventor.....	85
7.4 Spur gear design	86
7.4.1 Material of spur gears	86
7.4.2 Geometry of spur gears.....	86
7.4.3 Strength of spur gears	87
Chapter 8 Verification of spur gears strength via FEA	90
8.1 Introduction	90
8.2 Reasons requiring a verification via FEA	90
8.3 Parameters of FEA	91
8.3.1 Model geometry.....	91
8.3.2 Mesh	92
8.3.3 Contact.....	93
8.3.4 Boundary conditions.....	93

8.3.5 Analysis settings	93
8.3.6 Solution.....	94
8.4 Results and discussion of FEA	94
8.5 Comparison of AGMA and FEM results	96
Chapter 9 New solution approach with the use of different ROV tooling.....	98
9.1 ROV torque tool multiplier	98
9.1.1 Lowering speed.....	98
9.2 New configuration of the handling mechanism	99
9.3 Locking mechanism	100
9.4 Design of the new setup	103
9.4.1 ROV Buckets.....	103
9.4.2 Plate incorporating the ROV buckets	104
9.4.3 Panel plate.....	105
9.4.4 Stem.....	106
9.5 Results of the new design.....	106
Chapter 10 Conclusions.....	107
10.1 Concluding remarks	107
10.2 Recommendations for future work.....	109
REFERENCES.....	111
APPENDIX A: Drawings and information sheets	A.1
A1. Drawing and geometry of ROV receptacle [28].....	A.1
A2. Drawing of concrete mattress	A.3
A3. ROV tooling	A.4
APPENDIX B: Staad.Pro analysis.....	B.1
B.1 Spreader beam (lower pipe).....	B.1
B.2 Cylindrical pipe (upper pipe).....	B.18
APPENDIX C: Inventor spur gear design.....	C.1
APPENDIX D: Ansys report.....	D.1
APPENDIX E: Structural checks.....	E.1

List of Figures

Figure 2.1: Different trawling gears, Left: otter trawl gear – Right: beam trawl gear – Bottom: twin trawling gear with clump [7]	7
Figure 2.2: North Sea awareness chart of January 2018 (kis-orca.eu/)	8
Figure 2.3: FEA of pipeline-anchor impact (DNV GL.com).....	10
Figure 2.4: Pipeline crossing (stoprust.com)	10
Figure 2.5: Flexible concrete mattress over a subsea pipeline (oedigital.com)	12
Figure 2.6: Illustration of mechanical trencher (seawayheavylifting.com.cy)	12
Figure 2.7: Deployment of a stack of GRP covers (neil-brown.com)	13
Figure 2.8: Rock dumping through a fall pipe system (seatools.com/)	14
Figure 2.9: Example of typical concrete coating (nord-stream2.com)	14
Figure 2.10: Standard concrete cover shape and its lifting operation (slp-projects.com).....	15
Figure 2.11: Illustration of a frond mattress (pipeshield.com)	17
Figure 2.12: Left-installation by a long spreader beam, Right-short spreader beam drawing	18
Figure 2.13: Mechanical lifting frame	19
Figure 2.14: Multi-deployment frame provided by SPS (youtube.com/sps)	20
Figure 2.15: Multi-deployment frame provided by Submar (Submar.com)	20
Figure 2.16: The mechanical releasing mechanism of the Submar frame (Submar.com).....	21
Figure 2.17: IMF during installation of a concrete mattress (deeoceangroup.com).....	21
Figure 2.18: Left- MDS ³ on quayside, Right- MDS3 during deployment of 3 concrete mattresses (offshorem.com)	22
Figure 2.19: Concrete mattress lifted by 16 x 6m webbing slings of different colors [17]	23
Figure 2.20: Typical seafastening of a concrete mattress stack with cargo straps attached to padeyes	24
Figure 2.21: The process of ROV deployment (seaeye.com/tms.html).....	27
Figure 2.22: Key elements of a standard ROV (courtesy of Subsea 7)	28
Figure 2.23: GUI main window overview (e-sea.bluelogic.no)	30

Figure 2.24: ROV bucket with (left) and without (right) stem (google.images.com)	31
Figure 3.1: Left-The Antikythera mechanism as kept at the National Archaeological Museum in Athens, Right-An artistic illustration of how it may look like (wikipedia.com)	32
Figure 3.2: Classification of gears according to the orientation of the operating shafts [31].....	34
Figure 3.3: Spur gears (science.howstuffworks.com).....	35
Figure 3.4: Illustration of helical gear (https://apps.autodesk.com/FUSION).....	36
Figure 3.5: Single-enveloping worm gears (machinerylubrication.com).....	37
Figure 3.6: Left- Bevel gears with straight teeth, Right-Bevel gears with spiral teeth (wikipedia.com).....	37
Figure 3.7: Basic gear terminology [35]	41
Figure 3.8: Gear tooth characteristics [35].....	42
Figure 3.9: Forces on the gear tooth	43
Figure 3.10: Different modes of gear failure	45
Figure 3.11: Contour lines of maximum spur gear stresses under an applied force on the tip of the tooth [35]	45
Figure 3.12: Values of Lewis form factor Y for standard spur gears [31].....	46
Figure 3.13: Bending strength geometry factor Y_J for 20° pressure angle [34].....	48
Figure 3.14: Bending strength life factor Y_N [34].....	49
Figure 3.15: Pitting resistance life factor Z_N [34].....	53
Figure 3.16: tangential force applied on a shaft (physics.ohio-state.edu).....	54
Figure 4.1: Illustration of the concept proposed by Subsea 7	56
Figure 4.2: Illustration of the handling mechanism	57
Figure 4.3: The attachment points of the mattress with the lower pipe	57
Figure 4.4: The support of the upper pipe to the padeye	58
Figure 4.5: View of the frame with the incorporated gear set	59
Figure 4.6: Procedure of lowering the mattress (only for illustration purposes)	61
Figure 4.7: The process of laying the concrete mattresses on a pipeline (only for illustration purposes).....	62
Figure 6.1: Geometry of the lower pipe and its model at Staad.Pro	79

Figure 6.2: Illustration of different pipe lengths	80
Figure 7.1: Dimensions for the spur gear design	83
Figure 8.1: Interference observed in the output from Inventor spur gear generator	91
Figure 8.2: The final geometry of the spur gears and a zoom on the teeth shape.....	92
Figure 8.3: Refined mesh of the teeth in contact	93
Figure 8.4: Equivalent stresses for torque value of 2.711 kNm on the pinion bore	94
Figure 8.5: Above-The equivalent stresses on the root of the pinion, Below- A zoom in the maximum stresses at the root tooth.....	95
Figure 8.6: Contact stresses of the pinion according to FEA.....	96
Figure 9.1: Final configuration of the multi-handling mechanism	99
Figure 9.2: Side-view of the multi-handling mechanism.....	100
Figure 9.3: Side view of the handling mechanism depicting the locking pin	101
Figure 9.4: Green pin ROV shackle with tapered pin and fishtail-handle	101
Figure 9.5: Front view of the panel plate depicting the protruding-locking flaps	102
Figure 9.6: Direction of the unlocking rotation for the flap-locking mechanism	102
Figure 9.7: ROV bucket bolted on a plate panel (left) and the related intervention loads imposed on the ROV interface [28]	103
Figure 9.8: ROV bucket front view	104
Figure 9.9: Plate incorporating the ROV buckets	104
Figure 9.10: Left- The ROV plate model with the applied forces, Right- The equivalent stresses.....	105
Figure 9.11: Panel plate geometry	105

List of Tables

Table 2.1: Potential external hazards [6]	5
Table 2.2: Impact energies of subsea equipment in a typical North Sea field [11]	9
Table 2.3: Torque interface receptacle classification [28]	31
Table 3.1: Comparison of the different type of gears and their characteristics [32].....	35
Table 3.2: Variables used in the present chapter	38
Table 3.3: Gear formulas and conversions.....	39
Table 3.4: Repeatedly applied allowable bending stress and allowable contact stress for a selection of iron and bronze gear materials at 10^7 cycles and 99% reliability [34] ..	50
Table 3.5: Values of the elastic coefficient Z_E [34]	51
Table 5.1: Design limit states [42]	69
Table 5.2: Load factors γ_f for ULS [41].....	70
Table 5.3: Material factors according to EC3 [40] and NORSOK N-004 [43]	70
Table 5.4: DAF values in air [44]	72
Table 5.5: Values of γ_{cont} according to [45]	73
Table 6.1: Parameters used in STAAD.Pro	77
Table 7.1: Input data for gear design	84
Table 7.2: AGMA factors for root bending stresses	87
Table 7.3: AGMA factors for contact stresses	88
Table 8.1: Results of AGMA [33] calculations and FEA	97
Table 9.1: Summarized results of the components of the new configuration resulting to highest UR.....	106

List of Abbreviations

AGMA	American Gear Manufacturers Association
ALS	Accidental Limit State
CAD	Computer Aid Design
CHS	Circular Hollow Section
CoG	Center of Gravity
DAF	Dynamic Amplification factor
DoL	Depth of Lowering
FE	Finite Element
FEA	Finite Elements Analysis
FEM	Finite Element Method
FLS	Fatigue Limit State
GRP	Glass Reinforced Plastic
GUI	Graphical User Interface
IMCA	International Marine Contractors Association
IMF	Intelligent Mattress Frame
ISO	International Organization for Standardization
LARS	Launch and Recovery System
LRFD	Load and Resistance Factor Design
NCS	Norwegian Continental Shelf
POM	Polyoxymethylene
ROV	Remotely Operated Vehicle
rpm	revolutions per minute
rps	revolutions per second
SHL	Static Hook Load
SLS	Serviceability Limit State
SPS	Subsea Protection Systems
TMS	Tether Management System
ULS	Ultimate Limit State
UR	Utilization Ratio

This page is intentionally left blank

Chapter 1

Introduction

1.1 Motivation

According to the Norwegian Petroleum Directorate [1] the gas sales hit a new record in 2017 as the production rose 6.5% in comparison with 2016. Overall, the total production of oil and gas in the Norwegian Continental Shelf (NCS) rose for the fourth year in a row, and with the current trend in the oil price, the forecasts indicate that it will remain in high levels for at least five more years. The oil and gas industry is still a prosperous and profitable market and new mega projects already being started (e.g. the Mero field in Brazil in 2017) or coming on stream soon (e.g. the Johan Sverdrup in Norway in 2019). The current trend lies in the exploration and development of reserves in ultra-deepwater and in the icy waters of the arctic region. Therefore, a greater need for pipeline construction and subsea structures to transfer safely the produced hydrocarbons is expected. The seabed infrastructure is going to be even more labyrinthian if one considers the existing subsea equipment and the one to be added. Hence, the need for pipeline protection measures is anticipated to increase rapidly following the same pace.

Nowadays, concrete mattresses are recognized as a well-proven technology to surpass challenges faced in the subsea pipeline construction, umbilical deployment and seabed protection/stabilization. Manufacturing costs have been significantly reduced, as well as installation time has, with the use of standard lifting frames and beams [2]. The mattresses have a vast field of application with the following being the most common ones:

- Protection from dropped objects.
- Added weight and stabilization.
- Protection from trawl boards.
- Scour prevention.
- Crossover support/separation for pipelines and umbilicals.
- Supports/Foundations for other subsea activities.

UK Oil & Gas [3] estimates that more than 40,000 concrete mattresses have been installed on the seabed across the North Sea for pipeline protection purposes and foundation support. Additionally, approximately 80,000 mattresses have been deployed in the Gulf of Mexico in a 20 year time interval (1990-2010) by Submar company only [4]. These facts reveal the extensive use of concrete mattresses, especially when developing subsea oil and gas fields.

Hence, a great number of concrete mattresses is expected to be deployed on the seafloor, and as result, the lifting operation should be optimized, efficient and time-effective. Surprisingly, despite that the majority of the available on the market installation tools is capable of lifting more than one mattress per lift, they cannot release them one-by-one on the seafloor. As result, a lot of vessel time is required even for a small scale project. Consequently, there is a need for designing a tool capable of deploying multiple concrete mattresses in a single lift, yielding to substantial economic savings for the installation company.

1.2 Aim of the thesis

Subsea 7, as being a leader in the seabed to surface engineering works, has many concrete mattress installation projects in its portfolio and naturally has a great interest in developing such a tool. After the completion of a summer internship within the company the present topic was proposed to the author. The need for such a product was introduced by one of Subsea 7 principal engineers, who had also conceptualized a design approach for an installation frame capable of handling multiple concrete mattresses. The concept consisted of a steel frame which would facilitate six concrete mattresses and embody a handling mechanism with rotating pipes and gears. The mattresses will be lowered to the seabed through the mechanism with the assistance of a ROV torque tool.

The scope of the current work is to examine the suggested concept, analyze the various design considerations and propose answers to the issues that will arise. The main frame body does not emerge particular engineering challenges, so the focal point will be the complex handling mechanism. The handling tool will be “disassembled” in smaller components, of which their challenges, functionality and structural integrity will be assessed. Ultimately, a conclusion will be presented in regards the function of the mechanism and the operational interface.

1.3 Structure of the report

The thesis report is divided in 10 chapters; the calculation sheets and miscellaneous data are located in the Appendix sections, whereas the present chapter compiles Chapter 1.

Chapter 2 discusses the background and the theoretical aspects of the thesis. Pipeline hazards and relevant protection methods are presented, with a more emphasis on the installation procedures of concrete mattresses.

The gear theory is introduced in Chapter 3. The various types of gears are presented alongside with the most common gear failures. Afterwards, the analytical equations for the assessment of the gear strength are developed.

Chapter 4 thoroughly describes the concept proposed by Subsea 7. The various components and their functionalities are given, while the concept is further elaborated in order to be comprehensible by an engineering student.

Chapter 5 facilitates the design basis that will be followed in the current work. More specifically, the relevant standards, tools, calculation procedures and methodologies are defined.

In Chapter 6 the design and dimensioning of the first components of the handling mechanism is performed. Two load cases are identified for the pipes, with the extreme one governing the dimensioning. The second load case, the operational phase, provides the input for the gear system.

Chapter 7 sets the input requirements of the gear system. The geometry and the material of the spur gears are presented in conjunction with the strength calculations and evaluation of the gear system.

Some concerns and uncertainties arise with the analytical solutions of the gearset. Thus, in Chapter 8, a finite element analysis with Ansys Workbench is carried out, and a comparison between the numerical and the analytical solutions is conducted. The conclusion regarding the structural integrity of the gearset is finally given.

Chapter 9 proposes a solution and reveals a new concept of the design of the handling mechanism, with respect to the limitations and challenges that were identified in the previous chapters. The new components are analyzed and reviewed.

Chapter 10 summarizes the concluding remarks produced by this thesis work and recommends the aspects that need further elaboration and study.

Chapter 2

Background

2.1 Pipeline hazards

2.1.1 Introduction to subsea pipelines and cables

The hydrocarbons produced from the offshore fields need further chemical treatment before they are sold to consumers across the globe. With most of these fields being several kilometers far away from the nearest shore, marine pipelines are used to safely transfer the valuable containment to the processing plants. Considering only the Norwegian oil & gas pipeline network, which is made of 8,800 km of pipeline [1], it is clear how complicated and labyrinthian such a network can be.

In addition to the oil and gas transportation pipelines, even more pipes are laid on the seabed, such as the umbilicals. Umbilicals contain several hydraulic, chemical and power cables incorporated in a single pipe, and act as a mean for controlling and operating the subsea structures (such Christmas trees) from the platform. One single platform can pump oil and gas from several nearby fields of up to 50 km away, and naturally the pipeline network is very dense in close proximity to it.

However, pipelines are not to be related only with oil and gas activities, as subsea power and telecommunication cables span hundreds of kilometers connecting and powering islands with the mainland, cities, countries and even continents. The network cables also transfer enormous volume of data per second, providing internet service to the whole countries. The latter highlights the great value of these cables, as for instance, the Australian government characterizes its subsea cable system to be “vital to the national economy” [5].

Adding the great spanning lengths of the pipelines and cables with the sensitivity of the containment they transfer, it is an absolute requirement to protect them and eliminate accidents, leaks or more severe failures that could result in disastrous consequences. Therefore, based on the activities carried out in the area where these pipelines and cables span, potential hazards should be identified and taken under

consideration during their design, installation and operating lifetime. The focus will mainly be on oil and gas activities.

The most common perils that oil & gas pipelines are subjected to, are due to:

- Crane handling on a platform or rig.
- Fishing activities (bottom trawling).
- Supply vessels and general ship traffic in the area or close to the considered area.
- Subsea operations (e.g. simultaneous operations as drilling, completion and intervention).
- Others (planned construction, maintenance work, etc.).

With reference to DNV-GL standards [6] some possible external hazards for pipelines and their consequences can be viewed in Table 2.1. Apparently, the location of the pipeline is a major factor when determining the dominant ones. More specifically, pipelines near platforms are more prone to damage from dropped objects rather than from trawling, whereas pipelines away from fixed or floating offshore structures are put into jeopardy due to vessel activity and trawling. The major hazards will be discussed in the following clauses.

Table 2.1: Potential external hazards [6]

Operation/Activity	Hazard	Potential consequence to pipeline
Installation of pipeline	Dropped and dragged anchor/anchor chain from pipe lay vessel.	Impact damage
	Vessel collision during laying leading to dropped object, etc.	
	Loss of tension, drop of pipe end, etc.	Damage to pipe/umbilical being laid or other pipes/umbilicals already installed
	Damage during trenching, gravel dumping, installation of protective cover, etc.	Impact damage
	Damage during crossing construction	Impact damage

Heavy lifts	Dropped objects	Impact damage
	Dragged anchor chain	Impact damage
Anchor handling (rig and a vessel operations)	Dropped anchor, breakage of anchor chain, etc.	Impact damage
	Dragged anchor	Hooking (and impact) damage
	Dragged anchor chain	Pull-over and abrasion damage
Lifting activities on platform or rig	Drop of objects into the sea	Impact damage
Subsea simultaneous operations	ROV impact	Impact damage
	Manoeuvring failure during equipment installation/removal	Impact damage
		Pull-over and abrasion damage
Fishing activities	Trawl board impact, pull-over or hooking	Impact and pull-over damage
Tanker, supply vessel and commercial ship traffic	Collision (either powered or drifting)	Impact damage
	Emergency anchoring	Impact and/or hooking damage
	Sunken ships (e.g. after collision with platform)	Impact damage

2.1.2 Fishing activities

When examining hazards due to fishing activities, bottom trawling is of particular interest, as a dragging net is used by the fishing vessel. The arising risks are not only due to the weight of the net and the ancillary gear, but also because of possible snagging (hooking), as the trawl gear may lodge under the pipeline. Figure 2.1 illustrates three common types of trawl gears commonly used, namely otter trawl gear, beam trawl gear and the twin trawling gear with clump.

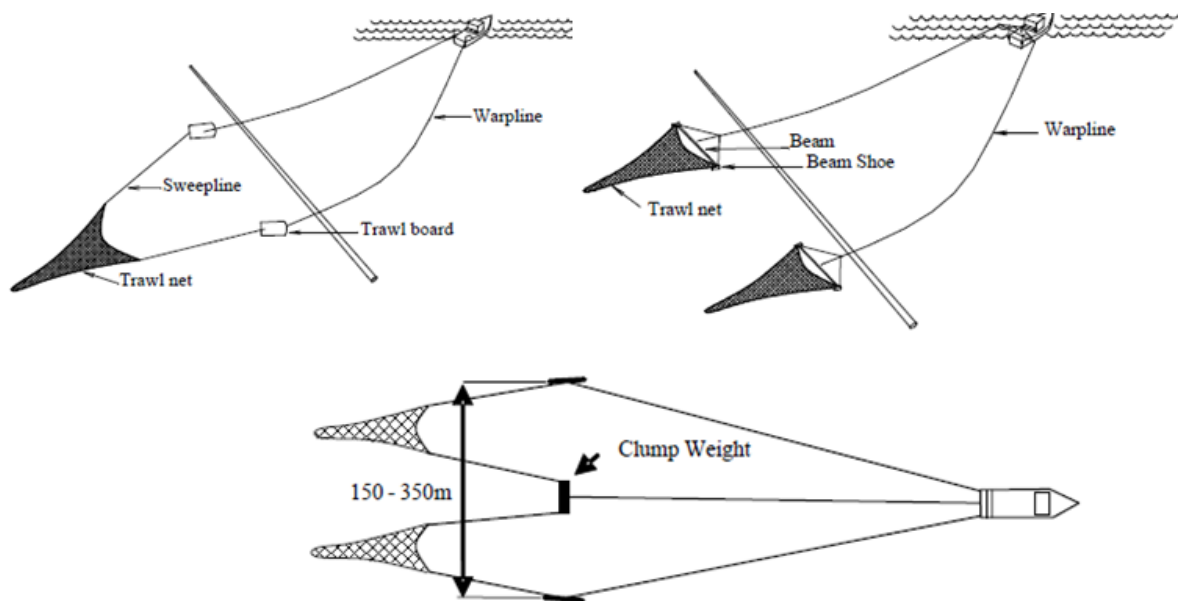


Figure 2.1: Different trawling gears, Left: otter trawl gear – Right: beam trawl gear – Bottom: twin trawling gear with clump [7]

There are three distinct phases of impact between a trawl gear and a pipeline, as explained below:

- Impact phase: the trawling gear, such as the trawl board or beam shoe, instantly hits the pipeline.
- Pull over phase: the trawl gear is pulled over the pipeline causing a global effect-damage.
- Hooking stage: the rarest occurring stage; trawl gear being stuck under the pipeline with disastrous consequences for both the pipeline and the vessel.

As set by DNV [8], in the NCS the non-interference between the subsea equipment and fishing activities is a requirement, unless rationally unavoidable. In other countries the risk is reduced by introducing safety zones, restricted areas, or by using guard vessels. A notable initiative has also been taken by the European Subsea Cables Association in collaboration with RenewableUK, leading to the Kingfisher Information Service – Offshore Renewable and Cable Awareness (KIS-ORCA) project, managed by Kingfisher [9]. The aim of the project is to raise awareness and provide fishermen with correct practical information of subsea cables routes, location of renewable energy structures like wind turbines and buoys (see Figure 2.2). The information is available online, regularly updated, publicly open and are considered as the most accurate and detailed data in Europe.

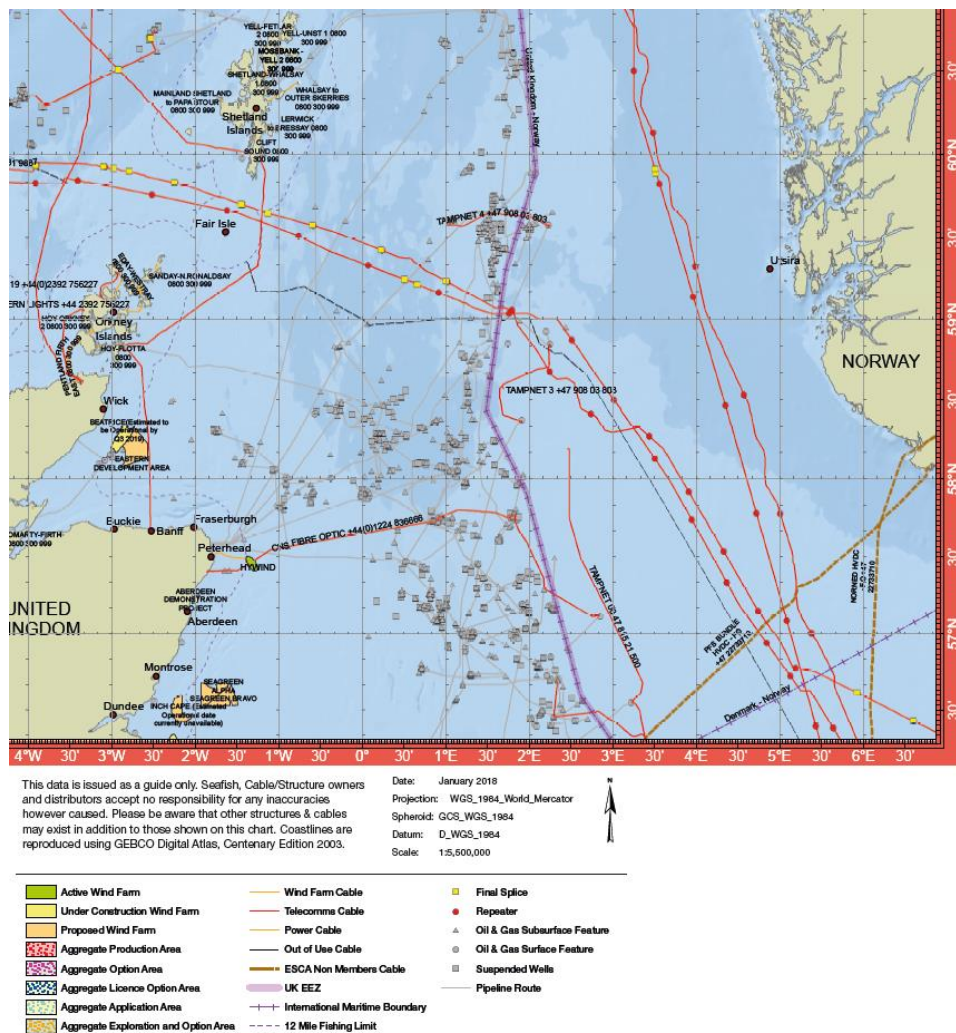


Figure 2.2: North Sea awareness chart of January 2018 (kis-orca.eu/)

2.1.3 Dropped objects

During installation of subsea modules and routine lifting operations on a rig or platform a major hazard is dropped objects. Such objects could be pipes, containers, subsea equipment (e.g. spools, templates) and any other objects that can be dropped into the sea from a platform or vessel. The magnitude of the collision, and thus its consequences, is related to the shape, mass and speed of the hitting object with the pipeline. The resulted damage is also dependent on the angle of collision, the sharpness of the object and the pipeline protection. The most common damage is a dent and the probability of fluid leakage is proportional to the depth of the dent. To demonstrate the aforementioned, an example of a 3 meters container is used, which is considered to be unintentionally dropped into the sea and sink with a velocity of 2m/s. This typical object will transfer approximately 100-200 kJ of energy to the pipeline which can cause severe damage and ultimately a complete failure [10].

Table 2.2 presents some typical impact energies of subsea equipment with a flowline and their frequency of occurrence for a typical North Sea field.

Table 2.2: Impact energies of subsea equipment in a typical North Sea field [11]

Object	Weight (t)	Lift frequency (per well operation)	Impact energy (kJ)	Flowline hit frequency (per well operation)
BOP stack	220	4	20 732	2.0×10^{-15}
Coiled tubing reel	45.0	1	2507	1.9×10^{-10}
Running tool	13.0	1	1816	2.0×10^{-9}
Skid	16.2	3	971	2.9×10^{-10}
X-mas tree	24.4	1	393	2.5×10^{-10}
9 1/2" drill collar	3.0	1	228	6.8×10^{-9}
30" casing	5.5	15	176	1.0×10^{-7}
Container/basket	8.2	~780	133	3.5×10^{-6}
20" casing	2.33	26	48	2.7×10^{-7}
Casing/tubing/pipe	1.25	~160	<15	3.3×10^{-6}
Other			~<40	$\sim 4.0 \times 10^{-7}$
Total hit frequency				7.3×10^{-6}

2.1.4 Shipping activity

There are several hazards to the pipelines related with vessel activities and the main risk is generated by the anchors of the vessels. In a similar way as trawling, a vessel anchor may potentially hook onto the pipeline and/or collide with it, leading to unwanted consequences, especially if the pipeline integrity fails [11]. The cases in which an anchor-pipeline interaction should be considered are [12]:

- Improper anchor deployment.
- Emergency anchoring due to engine or other mechanical failure.
- Anchoring due to severe weather conditions.
- Anchoring activities related with offshore activities (lay-barges, installations vessels etc.)

In a case of anchor-pipeline interaction a consequence analysis should be performed. The major results that will most likely emerge are damage to coating, local denting or punctures, and hooking displacement or rupture [12]. In addition to anchoring, the anchor chains could cause damage to the pipeline as in cases of interaction the abrasion of pipeline walls with the chains is inevitable. Furthermore, the hazards of impact of a sinking vessel or a ROV performing operations with a pipeline should not be omitted and included in a pipeline hazard identification analysis. These environmental and safety risks due to anchor-pipeline interaction are usually identified via a quantitative risk assessment, whereas the structural integrity and response of the pipeline should be addressed with a Finite Elements Analysis (FEA) (see Figure 2.3) [11].

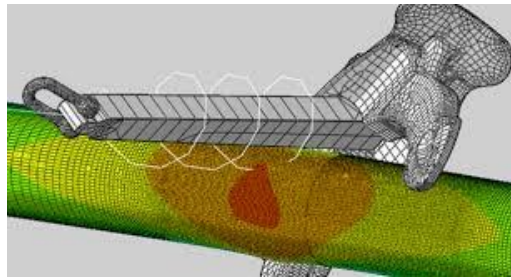


Figure 2.3: FEA of pipeline-anchor impact (DNV GL.com)

A first barrier in the pipeline protection policy from the regulatory bodies across the offshore industry is to set safety zones in the vicinity of pipelines and evaluate the associated risks in the basis of frequency and size of shipping traffic in the area [7].

2.1.5 Other cases for pipeline protection

Sections of pipelines located near shore are vulnerable to breaking waves. As waves approach the shore they become steeper disproportionately with the water depth. A large amount of energy is accumulated which is afterwards dissipated with the breaking of the wave. Experimental results have shown that there substantial hydrodynamic forces induced by plunging breaking waves on unprotected pipelines near the beach [13].

Moreover, pipelines should be protected in a pipeline-crossing (see Figure 2.4). When there is a need that the route of a new pipeline will cross an existing one, the latter should be properly protected and strengthened.

Additional needs that impel pipeline protection are the addition of weight for pipeline stability, protection against scour, separation of pipelines from the umbilicals, riverbank erosion control and protection against seabed gouging by ice [14].

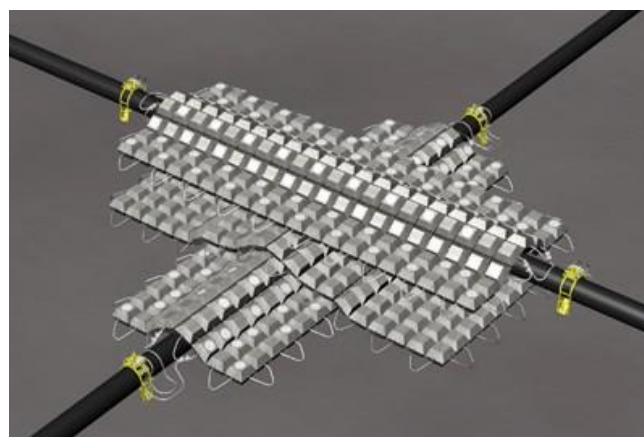


Figure 2.4: Pipeline crossing (stoprust.com)

2.2 Methods of pipeline protection and stabilization

The external hazards encountered by pipelines and cables laid on the seabed were discussed in the previous sections. It was identified that several risks are present with severe economic, safety and social consequences to the nearby population and environment. Consequently, several risk reducing measures have been developed and companies which install and operate pipelines, in most cases utilize protection measures against these hazards. However, the optimal protection method that is to be applied should be considered in the segments that are most vulnerable, for instance pipeline areas near shipping channels and harbors, and not for the whole length of it. Different measures can be used in combination and synthesize a custom-made optimum solution. The major pipeline protection methods are discussed in the below clauses.

2.2.1 Increase in the wall thickness

In cases where small dropped objects or anchors from small vessels seem to be the dominant hazards against pipeline integrity, a simple overdesign of the pipeline could lead to the required resistance. Designing thicker pipeline walls with greater steel quality will result in greater bottom stability, easier reeling operation, and ultimately might be the simplest and most cost-efficient solution in some projects. Yet, there are disadvantages to be considered as thicker walls require more weld consumable and a complex welding procedure.

2.2.2 Concrete mattresses

One widely-used method across the oil and gas industry for the protection of pipelines is the installation of flexible concrete mattresses (also commonly referred to as concrete mats) on top of it. Concrete mattresses can also be used in umbilical deployment and power cable protection. The mattresses are made of high quality concrete blocks moulded with polypropylene ropes in a brick pattern matrix, and usually have dimensions are 6m x 3m x 0.15m (or 0.30m). As result, they have adequate flexibility to follow the shape and contour of a pipeline, umbilical or even the seabed. According to one of the leading suppliers of stabilization equipment more than 20,000 flexible concrete mattresses have been placed on subsea pipeline during the first half of this decade [15].

Despite being one of the most effective ways of protecting a pipeline, some disadvantages are accompanied. With one large and heavy object laying over a pipeline the visual inspection becomes a difficult procedure. Moreover, the mattress itself entails a potential dropped object when being manoeuvred into place during installation. In addition, in the previous years, most of the concrete mats were not

designed and installed without a plan of a later decommissioning, thus making their removal operation rather complex, time consuming and costly. As the deployment of multiple concrete mattresses is the main scope of the present piece of work, a broader elaboration on this topic will follow in the next chapters.



Figure 2.5: Flexible concrete mattress over a subsea pipeline (oedigital.com)

2.2.3 Trenching and Backfilling

Another well-known method for pipeline protection is to bury the pipeline beneath the seabed in a procedure called trenching and backfilling. This approach offers mainly protection against anchor pull-over and trawling gear. The Depth of Lowering (DoL) is a critical parameter and the major cost driver in this activity. It is affected by the mechanical properties of the pipeline, the soil type and parameters, thermal insulation needs, coating type and thickness and the regulatory bodies involved in the specific sea area. Special consideration should be given when calculating the DoL as possible variations in the seabed level due to sediment mobility may occur. Several methods to perform trenching exist; jetting, ploughing, mechanical cutters, dredging tools, dredging vessels and mass flow excavators are the most used in the industry.



Figure 2.6: Illustration of mechanical trencher (seawayheavylifting.com.cy)

After trenching the backfilling takes place, where the excavated soil is used to bury the pipe and thus protect it over trawling and strengthen it against upheaval buckling. The cohesion, adhesion, the internal and the external angle of friction of the soil are some of the key parameters in the sedimentation that takes place. Jetting and ploughing are two widely used methods for trenching and backfilling. In the former, backfilling is done by jetting out the soil and sinking pipe into it, whilst the latter utilizes an additional backfill plough for completion of the process. Ploughing uses powerful machinery to trench up to 2m deep in a V-shape contour and is deemed suitable for all type of soils. Nevertheless, since flexible pipes and umbilicals may ride up the trench walls, the ploughing equipment is possible to endanger their integrity. Another drawback to take into account is that in shallow waters the seabed currents may wash away the side-trench spoil heaps [7].

2.2.4 Glass Reinforced Plastic (GRP) covers

GRP covers are used as a drastic measure of protection against trawler nets, and additionally have a good resistance behaviour in case of objects falling from vessels into the sea. The manufacture material is particularly light, yet strong, and along with the standardization of the shape of the covers, they can be easily transported in stacks, thus saving deck space on the installation vessel (see Figure 2.7).

For inspection and maintenance purposes the covers are designed and manufactured with hatches [7]. In most cases the GRP covers require rock damping for stabilization due to their light weight, which also provides protection of the covers against erosion [6].

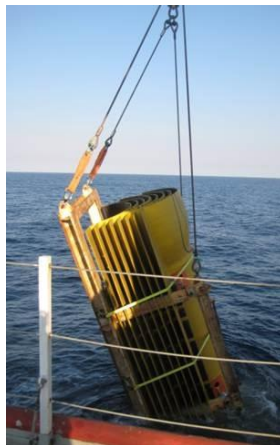


Figure 2.7: Deployment of a stack of GRP covers (neil-brown.com)

2.2.5 Rock dumping

Rock dumping is the process where rocks or gravels are placed on and around the pipeline to offer protection against external loading [7] and sometimes can be a more

cost efficient method than trenching. The possibility of penetrating the pipeline walls should be neglected, yet risks associated with impact and abrasion damage are reduced considerably. A fall pipe system can be used to disperse the rocks in a more controlled manner, so the impact damage due to falling stones can be reduced. The desired accuracy (nowadays is up to 10 cm) is achieved via fall pipe ROVs, which monitor the whole operation (see Figure 2.8).

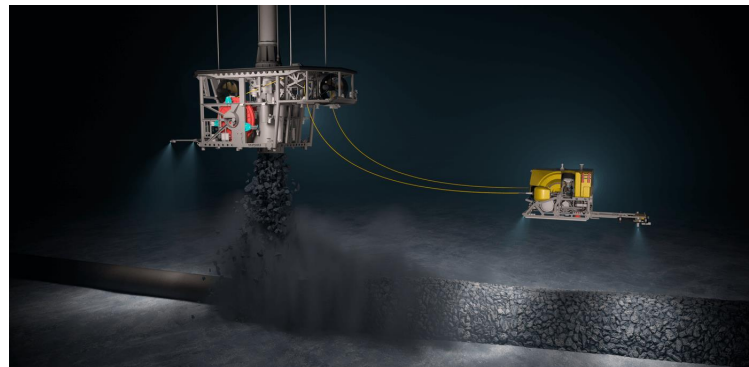


Figure 2.8: Rock dumping through a fall pipe system (seatools.com/)

Rock placement may be a “standalone” protection measure or used in combination with other methods such as GRP covers.

2.2.6 Concrete coating

An extra layer of concrete (see Figure 2.9) is applied on the pipeline circumference, resulting in negative buoyancy and mechanical protection against falling objects or other environmental loading. This additional degree of protection acts as an energy absorber during collision, mainly locally with the formation of micro cracks. The added absorption capacity of the concrete coating can be calculated from the thickness of the coating and the parameters of the impact object (e.g. velocity, shape etc.). Concrete coating is the option that is preferred by companies for large diameter pipelines (greater than 16”) in the NCS. However, specific project requirements (such as cooling of the pipeline) may suggest that this solution is inapplicable.

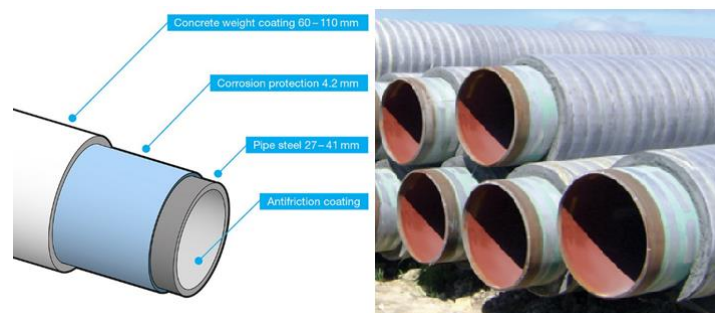


Figure 2.9: Example of typical concrete coating (nord-stream2.com)

2.2.7 Protective structures or tunnels

In the same way as GRP covers, steel or concrete covers can be used and provide the necessary protection over trawling and dropped objects. The resistance of the covers can absorb up to 800 kJ of impact energy due to falling objects and 45 kJ due to trawling equipment [16]. As depicted in Figure 2.10, some standard shapes exist but different covers can be manufactured to meet specific project requirements. This characteristic enables them to be utilized for accommodation of other subsea equipment such as templates and manifolds. As these covers are large objects the installation activity may represent a dropped object hazard as the crane lifting capacity is approached. Therefore, the deployment of steel and concrete covers requires a detailed engineering analysis and it is considered as a complex and time demanding marine operation.



Figure 2.10: Standard concrete cover shape and its lifting operation (slp-projects.com)

2.3 Concrete mattresses

The installation frame studied in the present work is related to deployment of concrete mattresses. Consequently, the main interest in the methods of pipeline protection and stabilization lies in the area of concrete mattresses, and as result a deeper discussion follows.

2.3.1 History of concrete mattresses

It was back in the 70s when the first mattresses came to the spotlight in the offshore industry as a measure for subsea pipeline protection and seabed stabilization, as referred in a report of the International Marine Contractors Association [17]. Concrete was not the primary material to fill the canvas bags of that time, and bituminous material and aggregates was preferred for filling, giving relatively notable stiffness. Consequently, the first ones to be deployed failed to take the pipeline shape or even tore apart when falling into water. Concrete as a mattress material was first

introduced in the early 1980s and gave the required flexibility and versatility, and further expanded while environmental bills by governments and regulatory bodies banned the use of bituminous material [18].

2.3.2 Manufacture of concrete mattresses

Nowadays, with the advances that have been made in manufacturing, concrete mattresses are a standardized product, yet changes can be done according to specific project requirements. The concrete blocks usually have a density of 2400 kg/m^3 , but this figure fluctuates in the range of $1800\text{-}4800 \text{ kg/m}^3$ sometimes. The denser material manages to increase the weight of the blocks laid on the pipeline or achieve better seabed stability [17]. A multi-block form is used for the formation of the concrete mattress, as concrete is poured into a steel mold, and polypropylene rope is laid into it to establish the connection between the blocks. In this way the desired flexibility is achieved without acting against the stiffness of the whole block, which roughly accounts 25 MPa of compressive strength. In some cases, the concrete is coated with a non-abrasive substance or pad (which is left on the supplier's preference) in order to protect the pipeline from the mattress itself. Moreover, the mattresses have rope loops on each side for rigging during installation. The standard industry dimensions are $6\text{m} \times 3\text{m} \times 0.15$ or 0.30m , and standard mattress weight is approximately 4.9 Te in air and 2.8 Te submerged or around 7.5 Te in air and 4.5 Te in water, respectively [17].

2.3.3 Type of concrete mattresses

There is a range of mattress styles which have been commonly used in the North Sea to date. Amongst them, the most used ones are flexible concrete mattresses and fronded mattresses.

- Flexible concrete mattress: this type is the majority of the installed mattresses in the North Sea and it is a well proven technology with a lot of suppliers offering standardized products. The key elements are the articulated concrete blocks which are connected with polypropylene rope and build up a flexible, yet strong arrangement. Due to the high degree of flexibility this type can closely follow the contours of a pipeline/umbilical cable or of an uneven seabed in all 3 dimensions. Once installed, the flexible mats may scour into the seabed to increase the stability and overtrawlability [2]. The dominant supplier is Subsea Protection Systems Ltd (SPS) which owns roughly 80% share on the market. A drawing of a flexible concrete mattress is shown in Appendix A.2.
- Frond Mattress: *“When a solid object, typically a pipeline, offshore platform structure or bridge pier is put in place on a loose sedimentary sea or river bed, the flow of water around this under certain conditions can cause erosion of the*

seabed; this is called scour” [2]. The erosion damage is accumulated and can cause severe problems in the integrity of the whole structure. Scour is reduced naturally by the seaweed which forms an obstacle against the flow leading to a lower velocity of the water. The frond mattresses act as artificial seaweed and replicate the above natural phenomenon; the concept is that the fronds gather silt and sediment to build up a natural bank and help in scour prevention. The mattresses are designed in such way that under their self-weight they sink and gather silt and sediment to build up a natural bank and help prevent scouring. There are two types of frond mattresses available; standard concrete mattresses with fronds (Figure 2.11) and rolled-up spool mounted mattresses completed with artificial seaweed frond clumps.

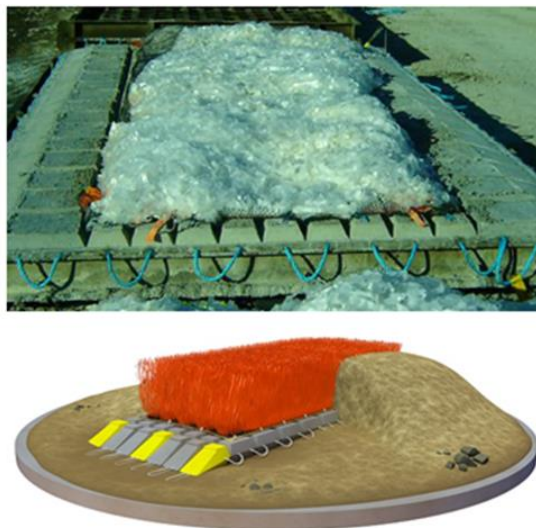


Figure 2.11: Illustration of a frond mattress (pipeshield.com)

Other types of concrete mattresses do exist, such as link-lok mattresses, armoflex mattresses, grout bags and bitumen mattresses. However, most of these types were mainly used in the past, as nowadays they are considered expensive and inefficient.

2.3.4 Equipment used for deployment

The deployment of concrete mattresses is a fairly moderate marine operation, but a comprehensive lifting and rigging study must be carried out. The installation beam or frame must be capable of a safe, accurate and time effective handling of the mattress under dynamic sea conditions. More checks are included, such as on the allowable water depth (especially when using tubular members) and if it is necessary to remove drains/vents, to name a few. Concrete mattresses are mainly installed one-by-one by transferring a single mattress to the seabed at a time. The newly, technologically advanced deployment tools should be ROV friendly, easily controlled by the crane operator and have an as much as possible automated releasement system. The

equipment utilized during installation is lifting frames and beams, ROVs and rigging equipment (shackles, slings etc.) and will be described in the following sections.

2.3.5 Lifting and handling devices

Spreader beams

There are 2 types of spreader beams, the long and the short one. The former is roughly equal to the length of the mattress while the latter is approximately 3 m long or equal to the width of the mattress. The long spreader beam is ideal for longitudinal mattress installation, whereas the short one for transverse installation. Both of them have the same number of hooks as their respective side of the mattress has loops, and lift the mattress according to that side. When in air the mattress hangs in a sharp “U” shape. The example long spreader beam used for illustration in Figure 2.12 is operated by ROV, as the webbing slings are released when the ROV pulls out the lever on top of the beam. Using a spreader bar is a time consuming operation as all individual hooks have to be disconnected one-by-one by the ROV. The latter poses a greater risk of ROV entanglement during rigging.

Mechanical lifting frame

The dimensions of the frame range typically within the length of the mattress as the deployment is usually done in the longitudinal direction. The frame is incorporated with a mechanical release mechanism which releases all straps in one operation. As result, the installation is considered ROV friendly, as only a lever is pulled by the ROV for detachment. As pictured in Figure 2.12, the shape of the lifted mattress is a wide “U” as the frame has an appreciable width dimension.

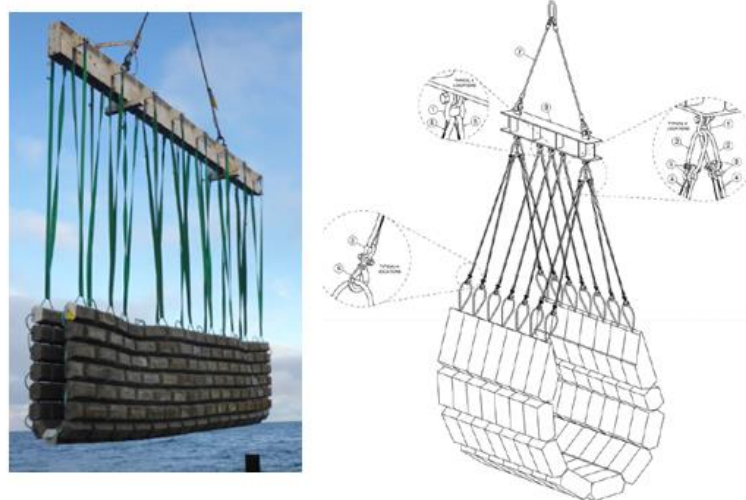


Figure 2.12: Left-installation by a long spreader beam, Right-short spreader beam drawing

Multi-deployment frames

Some service companies (e.g. SPS, OffshoreMM, and Submar) that are specialized in the development and production of subsea equipment and tools have produced frames for deployment of more than one concrete mattress at a time.



Figure 2.13: Mechanical lifting frame

Usually, these tools are used for large scale deep water installations and most of the times are custom made with a lift capacity of 2 or 3 concrete mattresses. They are ROV friendly, equipped with advanced cameras, thrusters and release the mattresses by enabling a hydraulic release system.

2.3.6 Multi-deployment tools available on the market

As discussed above, there exist some advanced multi-deployment frames on market, provided by companies who do specialized work on subsea structures. The most interesting findings that are relevant to the scope of this thesis are described below.

Subsea Production System's frame [2]

Is one of the world's leading manufacturers of concrete mattresses and provides single or double deployment and handling tools for installation. In connection with its products the company supplies relevant frames for their installation. A typical example of frame capable of handling 3 concrete mattresses is shown in Figure 2.14.

Dual Mechanical Release Handling Frame [4]

Submar offers a large selection of versatile erosion control products and specializes in methods or pipeline protection. It provides several handling frames for its concrete mats, with both single and double mechanical release system. The CMDF-40-DR Deployment frame (see Figure 2.15) is capable of installing two sets of concrete

mattresses in different locations in one single deployment trip, by using an upper and lower release steel bar mechanism on each side.



Figure 2.14: Multi-deployment frame provided by SPS ([youtube.com/sps](https://www.youtube.com/sps))

Each bar has attached rods where the sling loops of the mattress are secured for lifting. Shackles are used to fix the straps in one end, whereas the other end is free to pass through the mat rope loops and then hook to each rod. In order to use two sets of mattresses, shorter slings are used for attachment in the upper release bar and longer ones in the lower bar. One ROV/diver operated lever mechanism can be pulled for each release-bar and deploy each set (lower first and upper after) of mattress (see Figure 2.16). The two operations are independent of each other offering a unique feature in this particular frame. The number of the total mattresses that can be lifted depends on their size and weight, but it is relatively limited as stacking mattresses on top of each other, as in Figure 2.15, is not permitted during installation.



Figure 2.15: Multi-deployment frame provided by Submar (Submar.com)



Figure 2.16: The mechanical releasing mechanism of the Submar frame (Submar.com)

Intelligent Mattress Frame (IMF) [19]

IMF (Figure 2.17) is designed and manufactured by DeepOcean, a specialized supplier of a wide range of subsea services and technologies. It might not be a frame that can lift multiple mattresses, but the key of its excellence is that can be remotely operated by a computer on the surface, without the need for ROV or diver intervention. It has a Safe Working Load (SWL) of 15 Te and it is equipped with advanced tools and sensors for monitoring and navigation. A Hydraulic Power Unit (HPU) is attached for powering and enabling the hydraulic release mechanism during deployment.



Figure 2.17: IMF during installation of a concrete mattress (deepoceangroup.com)

MULTI-MATTRESS DEPLOYMENT SYSTEM MDS³ [20]

OffshoreMM offers project-based engineering solutions for the offshore energy industry and supplies highly technologically advanced subsea related products. Its flagship in pipeline protection and soil stabilization using concrete mattresses is MDS³ (see Figure 2.18), a state-of-the-art subsea tool.



Figure 2.18: Left- MDS³ on quayside, Right- MDS³ during deployment of 3 concrete mattresses (offshoremm.com)

This particular tool allows 3 mattresses to be deployed in one lift, speeding substantially the operation and saving costs. Its SWL in air is around 30 Te. Moreover, it is equipped with advanced tools, such as 3 cameras, 2 sonars, 1 fiber optic gyro and sensors for monitoring its movements. Its hydraulic system is composed by 3 pairs of hydraulic actuators that are remotely controlled and operated from a user on the surface, eliminating the need for divers and ROV support.

2.3.7 Rigging of the mattresses on the frame

The concrete mattresses must be attached to the handling frame with sufficient rigging that will provide a safe and simple operational state. The rigging should be inspected, tested and certified according to industry standards (e.g. DNV GL) and designed with good and reliable work practices. The rigging tasks need to be executed by trained, skillful and experienced riggers according to the rigging design study. According to IMCA [17] the equipment that is most likely to be used is:

- Safety bow shackles between frame and slings.
- Webbing slings.
- Safety bow shackles at lower end of the webbing slings.
- Safety ROV release systems, attached to the concrete mattress polypropylene rope loops.
- Split pins for all shackles.

An adequate vertical clearance should be maintained between the handling tool and the mattress, usually roughly 4m or greater. Webbing slings of 8m should be therefore used, especially for mechanical handling devices where ROVs may work beneath it. The heave motion of the vessel and the type of the crane used (either with heave compensation or not) should be considered and also determine the appropriate length of the webbing slings. Different rigging colors should be also used for each side of the frame to assist the ROV/diver work, in combination with plastic sleeves for protection and alignment (see Figure 2.19).

During the rigging design procedure adequate safety factors should be incorporated, such as dynamic factors for weight in air and water, added mass coefficients and effects, dynamic factors including the splash zone effect and unequal loading of the slings linking the mattress to the lifting device due to flexibility in the mattress [21].

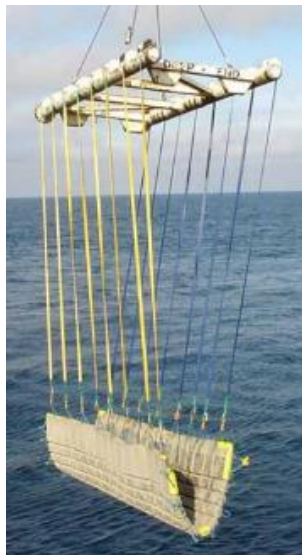


Figure 2.19: Concrete mattress lifted by 16 x 6m webbing slings of different colors [17]

2.3.8 Load-out, mobilization, over-boarding and deployment operations

A quayside or vessel crane is used for the load-operation and the allowable crane load radius curves determine the vessel proximity to the trailer (or truck) access. The operation is carried out according to accurate, detailed and approved lift plans where the exact route of the crane and all possible obstacles are noted [17]. The mattress is lifted and positioned to the predefined, marked location where the crane rigging is detached and vessel seafastening is required.

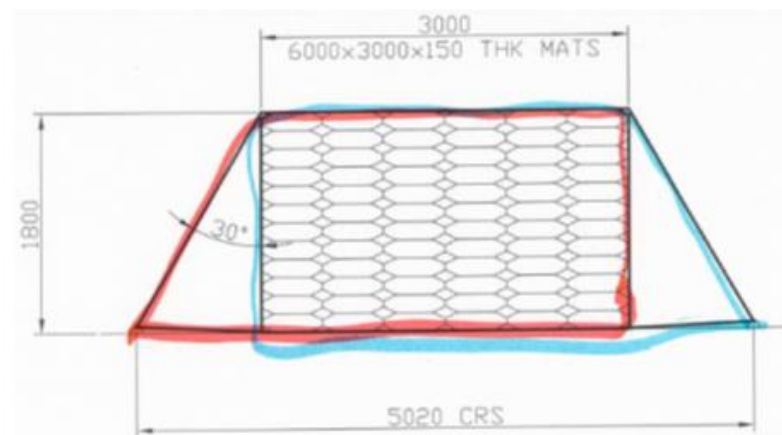


Figure 2.20: Typical seafastening of a concrete mattress stack with cargo straps attached to padeyes

The installation engineers of the vessel must check and approve the deck plans for the correct positioning and stability of the concrete mattress stacks. Special consideration should be given to the position of the stacks as they must not be above hatches, too close to the pedestals and higher than 2m off the deck. Adequate space should be ensured in the surroundings to allow safe access and working conditions for seafastening equipment, riggers and welders. One common method for seafastening the mattresses is by attaching cargo straps to a welded padeye which goes under the stack and over the full assembly before re-attaching to the same padeye, as illustrated in Figure 2.20. The transverse beams of the deck provide the ground for welding the padeyes. Another common solution is the use of steel stanchions which are welded above and in-line with the deck stiffeners or T-bars (depending on the type of the deck), and restrict the stack or the frame.

Next, when the vessel has set on the designated for its marine operations location, the deployment procedure starts. All involved personnel should be fully aware of the tasks and the execution methods that will be used, especially on safety rules. The deployment frame (or beam) is landed on the stack of mattresses where the top one is attached to it. The most critical point is lifting through the splash zone as great slamming forces may be exerted on the frame and the mattress. A relatively fast lowering could lead to load inverting or damage to rigging, due to snatch loading, so low to moderate speeds are preferred. Approaching the seabed, the ROVs' workover begins, as they monitor the lowering and finally release the mattress from the frame. In most cases ROVs assist in the accurate positioning of the mattress by giving a push on the handling device, although this is not recommended. In the newly designed frames there is usually a built-in docking point for the ROV, which should be utilized for locking in and manoeuvring. The ROVs use either levers or activate existing hydraulic handling mechanisms of the frame, for rigging detachment and afterwards for the recovery phase.

2.3.9 Examples of large scale projects

As discussed above, concrete mattresses have been used for more than 50 years in the offshore industry with a remarkable operating and safety record. Herein four sizeable projects will be presented to demonstrate the use of concrete mattresses in pipeline protection and foundation support works.

Scolty and Crathes oil fields [22]

EnQuest discovered the fields Scolty and Crathes in 2007 in the central North Sea sector of the UK Continental Shelf, 160km east of Aberdeen. It is also the operator of the field (40%) in partnership with MOL UK Facilities (50%) and Ithaca Energy (10%). The selected field architecture is two producing wells tied back over via a 25 km pipeline to the Kittiwake platform. Trenching and backfilling are used for pipeline protection, however concrete mattresses have been deployed to protect and stabilize pipelines when they are out of the trenches in the Kittiwake platform 500 m zone and at the field locations. According to the supplier, SPS, a total of 270 concrete mattresses were manufactured and delivered to the operator for installation in 2016.

Greater Gabbard wind farm

The wind farm is located east-south of England and consists of 140 Siemens 3.6 MW turbines with a total capacity of 504 MW. Electricity and telecommunication cables span 45 km and concrete mattresses were used for protection against trawling. As stated by RedS [23], that performed the installation activities, 65 mattresses were installed with diver intervention one-by-one in winter 2009/10.

Messina II Project, Gioia Tauro, Italy [24]

Prysmian Group was responsible for installing two electrical 380 kV AC cables to connect Sicily and Italy in a high importance project of a total value of €300 million. A total of 260 km of cables were installed of which 38 km were placed on the seabed. The company chose to use flexible concrete mattresses to protect the cables from falling objects, for crossing over existing pipeline infrastructure and soil stabilization purposes. Officine Maccaferri was the supplier and manufactured and delivered a total of 520 concrete mattresses with dimensions of 5x2x0.2 m.

Shah Deniz 2 [25]

The second field development phase of the gigantic gas field in the Caspian Sea about 70km off Azerbaijan included a \$24 billion investment, which reveals the great fabrication and engineering work done for the project. Among the broad subsea equipment that was used, such as subsea isolation valves, tie-in piping spools and anchors, around 1,000 concrete mattresses were deployed for seabed flattening and stabilization, so the subsea structures could be sited on, and for pipeline and umbilical protection purposes.

2.4 ROV tooling

2.4.1 Introduction to ROVs

ROVs are extensively used in the oil and gas industry in broad applications including rig support, field installation operations, survey applications and inspection, maintenance and repair tasks as well. Their specific area of work is to perform underwater tasks such as installation and removal of protective caps, operations with valves, cut hydraulic lines, remove small debris, perform tie-in operations and drilling support to name a few [14].

A ROV is comprised by the following elements:

- The control unit.
- The Launch and Recovery System (LARS).
- The umbilical.
- The Tether Management System (TMS).
- The vehicle.
- The tooling package.

The use of manipulator arms enhanced their capabilities and boosted their utilization, since the first ROV with arms was deployed for military purposes by the US Navy in the 1960s [26]. Usually, a ROV is equipped with a 7-function manipulator (see Figure 2.21) acting as a right arm, whereas the left arm is a 5-function grabber. Torque can be produced by the 7-function manipulator, and referring to Schilling Robotics Titan 4, which is in accordance to the industry standards, the nominal wrist torque output is 170 Nm [27]. This is far greater than a human arm can generate, and fairly adequate for certain “low torque” tasks. However, when “high torque” operations have to be performed, ROV torque tools are usually utilized. Furthermore, the 7-function manipulator has a maximum lift capacity of 122 kg, however this is not designed for

extensive work, as the standards set lower lift limits; for instance, 50 kg is defined as the lift figure by the API standard. Due to its high complexity this part costs around USD \$200,000, which is three times the cost of a 5-function grabber.

These sophisticated subsea robots are guided by a ROV controller, the pilot, located onboard a vessel, usually by a joystick similarly to a video game. The connection between the vehicle and the controller is established via an umbilical cable which supplies the necessary control, energy (electric, hydraulic) and chemicals.

The ROV deployment is done through the TMS in order to decouple its motion from the dynamic motion of the vessel due to sea conditions, whereas the TMS is lowered subsea from the LARS, as depicted in Figure 2.21. The main features of a typical ROV used during Subsea 7's operations are also illustrated in Figure 2.22.

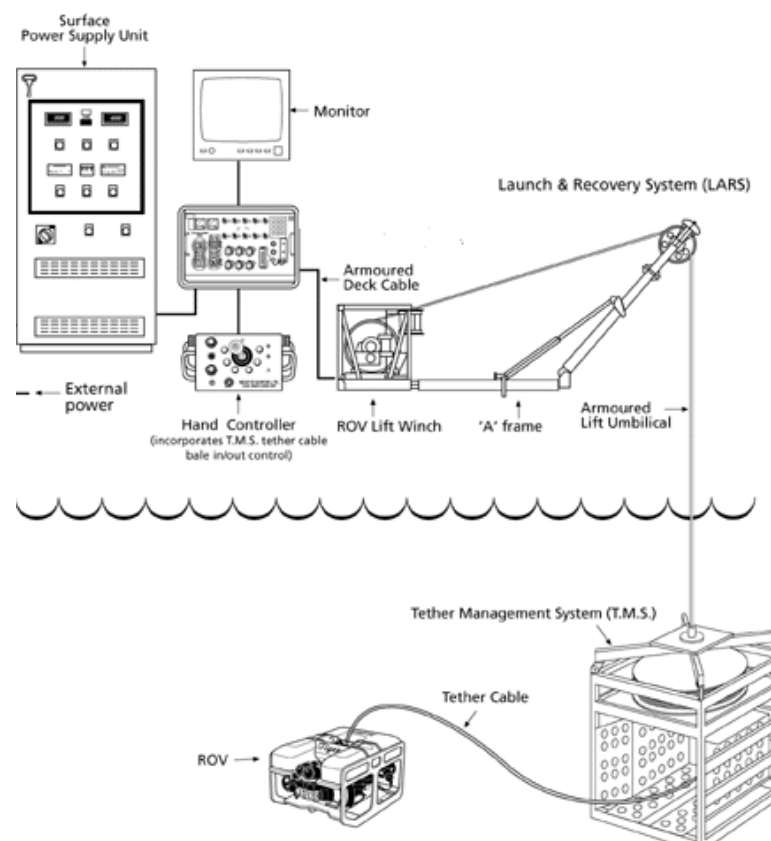


Figure 2.21: The process of ROV deployment (seaeye.com/tms.html)

The ROV tooling deployment methodologies can be categorized in the following groups:

- Small ROV deployed & manipulator carried tooling.
- ROV mounted, powered & operated tooling.
- Separately deployed, ROV powered and operated tooling.
- Surface powered, vessel-deployed ROV guided tools.

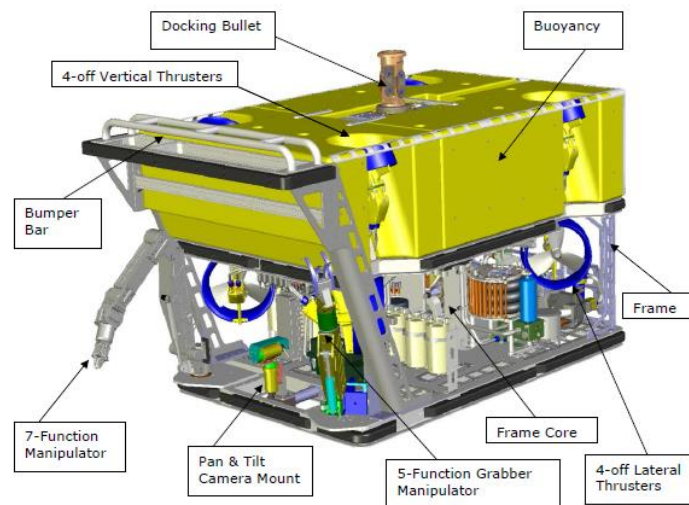


Figure 2.22: Key elements of a standard ROV (courtesy of Subsea 7)

2.4.2 ROV torque tools

The majority of the torque tools available on the market are hydraulic powered, although there are few manufacturers producing torque tools operating with electric motor with enhanced capabilities. However, the following context is relevant for whether the torque tool is hydraulically or electrically powered. The features presented below comprise the desirable requirements to be fulfilled by a torque tool:

- Delivers its full torque range without changing motors, operating a gear change lever, or disassembly. It is sometimes safer to have a “low” and a “high” torque tool than run the risk of forgetting to reconfigure a tool before producing the desired output torque with an over-powered torque tool.
- Clearly labelled hose connections and a very clear quick set-up schematic diagram in addition to a manual.
- Accurate and repeatable results.
- Turns and torque feedback sensors and remote display.
- LED display of turns and torque on the back of the torque tool.
- Latching lugs (with failsafe spring release).
- Easy to change sockets.
- Strong, but lightweight.
- Axial cushioning (shock absorber) of the Socket.
- Manipulator handle located at the tool’s centre of gravity.

2.4.3 Torque tool failures

One of the most common faults when setting up a torque tool is forgetting or neglecting to fit a case drain. All hydraulic motors allow a small flow of oil to leak past their pistons to lubricate them. This oil collects in the case of the motor before flowing back under low pressure to the hydraulic tank, or reservoir. If a drain hose is not fitted the pressure will soon build up in the motor's case. At best this will cause an 'O' Ring seal to blow out and, at worst, the internal pressure build-up will be high enough to crack the metal case of the motor. Both situations will result in uncontrolled loss of hydraulic oil. On the same basis, it is also essential to be verified that all hydraulic hoses are connected to the correct port on the hydraulic motor, before switching on the power pack.

In addition, special care should be taken when inserting the torque tool into the receptacle to avoid damage to either the stem, or the torque tool itself. A loose grip of a fishtail handle (which has no compliance) on the tool is usually attached. It may be necessary not to operate the torque tool until the socket lines-up with the stem. A torque tool must never be forced or dropped into a receptacle.

Consequently, there are many issues to consider when designing subsea torque interfaces to be operated by a ROV with, or without, a torque tool. As a precautionary measure, every torque tool system is supplied with a torque analyser also commonly known as a Torque Verification Unit, or a Test Jig. This consists of a torque tool receptacle fitted with a calibrated torque transducer on the end of a dummy square shaft and is used to calibrate the output of a torque tool. The calibration is usually valid for one year.

2.4.4 Torque tool controllers

A torque tool's output is normally controlled by either a three-stage control unit, or a proportional controller. The three-stage controller controls the flow of hydraulic oil to the tool to regulate the speed of rotation of the socket, a directional control valve selects the direction of rotation and three pressure reducers are used to select low, medium and high torque outputs. The speed and torque values are set-up on deck before the ROV is launched. The temperature of the oil is a very important aspect of the output torque and speed, as when its temperature increases, it becomes thicker (less viscous) and the rated torque decreases, and vice-versa.

On the other hand, proportional controllers introduced the remote control of direction and proportional control of both speed (hydraulic flow) and flow (hydraulic pressure) and have an upward trend of utilization in the offshore sector. In addition, the calibration of the torque has been automatized via the utilization of a subsea torque

verification unit, the torque analyser, where the torque output can be checked in place and accurately applied afterwards. Another advantage is that proportional controllers are supplied with surface control units, usually through a laptop application with a Graphical User Interface (GUI). The software is usually provided with the torque tool and displays both input and output parameters. The main input parameters are the hydraulic pressure and flow being supplied to the torque tool and the output parameters are the number of turns (rpm) and torque the tool is applying to the stem. Torque against time is usually displayed as a graph. All the data is logged and stored as file in the computer's memory for subsequent reporting and verification purposes. A typical interface of such software is illustrated in Figure 2.23.

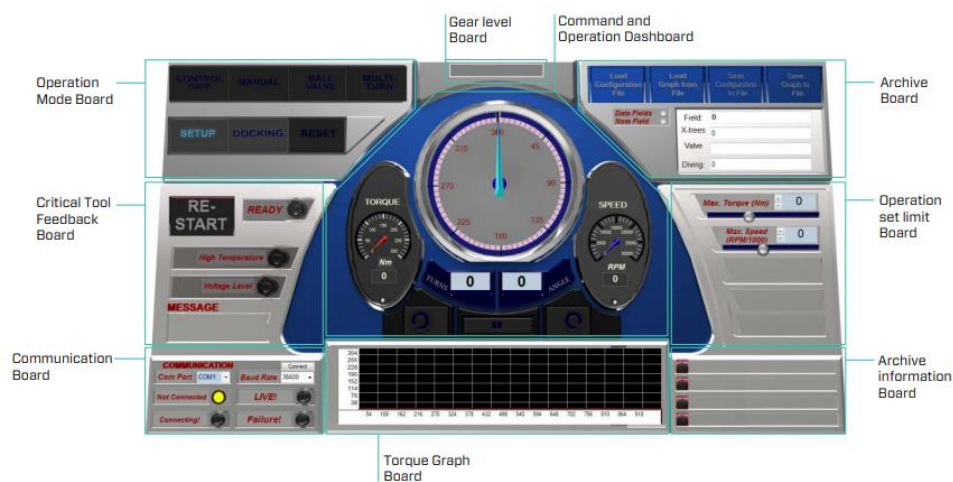


Figure 2.23: GUI main window overview (e-sea.bluelogic.no)

2.4.5 International standards for ROV interfaces

When deploying an ROV with tooling to actuate subsea valves by applying specific values of torque, aspects of space limitations, clear access, free space for the umbilical, matching interfaces and accurate calibration of the torque to be applied, usually arise. Consequently, ROV tooling must be standardized as well as interfaces mounted on the valves, manifolds, control systems, actuators etc., The standardization of subsea tools has made tremendous leaps in the recent years and has been expanded in the whole offshore industry. There are three international standards that provide essential information on the design of ROV interfaces:

- API 17D, *The Design and Operation of Subsea Production Systems – Subsea Wellhead and Tree Equipment*, Second Edition, September 2011.
- API 17H, *Remotely Operated Tools and Interfaces on Subsea Production Systems*, Second Edition, June 2013.
- ISO 13628: Part 8 (also adopted as API RP17H), *Remotely Operated Vehicle (ROV) interfaces on subsea production systems*, Corrected Edition 2006.

The two latter standards are more applicable to the scope of the present study. They are considered equivalent to each other and both are worldwide accepted and well-proven, albeit some minor differences do exist.

2.4.6 Torque tool interface

For the purposes of the current work the most relevant equipment is the rotary docking receptacle, which provides docking, torque reaction, alignment and socket mating for ROV torque tools [28]. The interface is shown in Appendix A.1 and usually comes with securing latches and tubular housing to facilitate the bearing of the rotating shaft.

The torque tool interfaces (or ROV buckets-Figure 2.24) are divided in seven classes, as per Table 2.3, in which all commercial torque tools are standardized, designed on and refer to the maximum allowable torque that can be produced and applied at the interface.

Table 2.3: Torque interface receptacle classification [28]

Class	Maximum design torque N·m (lbf·ft)
1	67 (50)
2	271 (200)
3	1,355 (1,000)
4	2,711 (2,000)
5	6,779 (5,000)
6	13,558 (10,000)
7	33,895 (25,000)



Figure 2.24: ROV bucket with (left) and without (right) stem (google.images.com)

Chapter 3

Gear theory

3.1 Introduction to gears

Gears are widely used for the transmission of motion (energy) from one axis to another - mostly between shafts. Gears are used since ancient times and are first introduced in the writings of Aristotle [29] around 330 BC, where they were used to build simple everyday structures such as compasses, clocks and water-lifting equipment. There are however indications and sketches that gears are used since 3,000 BC by Chinese, Babylonians, Romans and Greeks. The most remarkable example of the wide use of gear and the high level of complexity achieved during that time is the famous Antikythera mechanism (see Figure 3.1 for illustration) dated around the first century BC. It is believed (because scientists have not fully solved the riddle) to be the first analog computer and orrery, used to predict the movements of the planets, their orbits, eclipses and as a time-cycle tracker for the ancient Olympic Games taking place every four years [30]. It included at least 32 bronze gears manufactured with detailed engineering and accuracy, with its largest gear having a 140 mm diameter and 223 teeth.



Figure 3.1: Left-The Antikythera mechanism as kept at the National Archaeological Museum in Athens, Right-An artistic illustration of how it may look like (wikipedia.com)

There are various means of mechanical power transmission such as belts, chains and gears. The latter though have the largest market share in most industries, as have their durability and robustness has been tested and verified. The high efficiency ratios

naturally come with a cost, as gears are costlier than their counterparts, and as the need for precision increases so does the manufacturing costs.

Gears present some great advantages during the transmission of motion such as:

- High level of efficiency.
- Transmission of high power (up to 50,000 kW).
- Manipulation of torque and speed input and output.
- Reliable and long lifespan of safe operation,
- Transmission of power between parallel, non-parallel, intersecting and nonintersecting shafts.
- Relatively low maintenance.
- Exact ratio of transmission.
- The capability of overloading.
- Small size.

Yet, some drawbacks do exist:

- The high cost of manufacturing.
- The noisy operation.
- Power cannot be transmitted over long distances.
- Requirement for continuous lubrication.
- The sensitivity in tooth meshing.
- The non-elastic transmission of the loading.

Despite that, gears are the primary form of mechanical power transfer used in robotics, automobiles and even in the mechanism that opens the tray on a DVD player. The multiple mattress-handling mechanism will have a set of gears, with the purpose being that gears can increase the torque provided by the ROV torque tool, with a velocity decrease as counterbalance. In other words, the gearset is a device to exchange torque for velocity and vice-versa according to the mechanical advantage (or torque ratio m_T) m_A :

$$|m_A| = |m_T| = \frac{\omega_p}{\omega_g} = \frac{n_p}{n_g} = \frac{N_g}{N_p} = \frac{d_g}{d_p} \quad (3.1)$$

Where the subscript p and g refer to the pinion and gear, respectively onwards. Also:

- ω = angular velocity (rad/sec)
- n = rotational speed (rpm)
- N = number of teeth
- d = the pitch diameter (mm)

Therefore, a comprehensive study of gearing is deemed necessary for a good understanding of the related mechanics and gear design.

3.1.1 Type of gears

There are several different types of gears classified according to the direction of the power they transmit and to the type of the teeth. Figure 3.2 shows a broad classification of gears, with the most widely used ones being the spur gears, the helical gears, the worm gears and the bevel gears. Albeit, standard gears are massively manufactured and used in many industries, a tailor made gear design is preferred for particular applications in order to reduce the cost penalty involved with the assist of computer tools which decrease the requirements in engineering time.

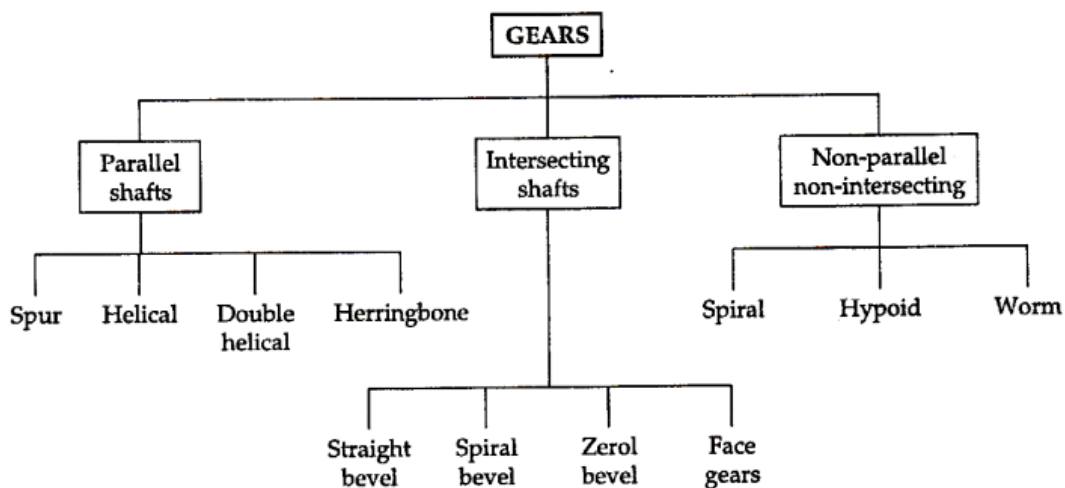
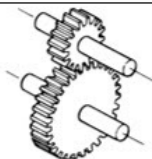

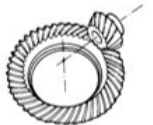
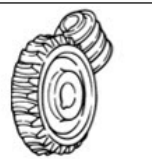
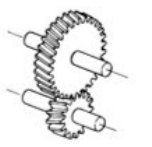


Figure 3.2: Classification of gears according to the orientation of the operating shafts [31]

In the following Table 3.1 a comparison between the different gear arrangements and features is attempted. A brief presentation of the gear types will follow alongside with the basic gear terminology and nomenclature.

Table 3.1: Comparison of the different type of gears and their characteristics [32]

Type	Spur	Bevel		Worm	Helical
		Straight Bevel	Spiral Bevel		
					
Shaft Arrangement	Parallel shaft	Intersecting shaft	Intersecting shaft	Non intersecting, non parallel shaft	Parallel shaft
Meshing	Same pitch & pressure angle	same pitch, pressure angle & face width	same pitch, pressure angle & face width	same thread, pitch & pressure angle	Same pitch, pressure angle & helix angle
Gear Ratio	1:1 to 6:1	3:2 to 5:1	3:2 to 4:1	5:1 to 75:1	3:2 to 10:1
Efficiency	94-98%	93-97%	95-99%	50-90%	94-98%
Features	Most common & cost-effective type of gear	Durable & ideal for high load applications	Highly durable & can handle high load than straight bevel	Can be used for special occupations	Higher strength and durable than spur gears
Noise and Vibration	Noisy	Less than spur gear	Less than straight Bevel	Quiet and Smooth	Less than spur gears
Application	Conveyors, Constant	Printing press, Differential gear	Tractors, final reduction gearing	Anti Reversing, Indexing devices	Automobile transmission

Spur gears [31]

Spur gears are the most used gears in many industries and they transmit power between two shafts being in parallel to each other and impose only radial loads on their support (or bearings).



Figure 3.3: Spur gears (science.howstuffworks.com)

Their unique characteristic is the straight teeth which run in parallel to the gear's axis of rotation enabling a rolling contact between the teeth, which produces less thermal energy than other teeth configurations. Because of the simultaneous contact of the same inner side of the teeth they are wearing out and make noise due to high vibrations. A proper lubrication of the gears can solve this issue, but it must be implemented on a frequent basis. An illustration of spur gears is shown in Figure 3.3

where the small gear is called *pinion* and the large one holds its term (name). In most cases, the pinion is the driving element (energy input in the system), whereas the gear is the driven component. The pinion is usually the component that has large angular velocity and low torque values, and through the transmission of motion to the gear the angular velocity decreases, while the output torque increases.

Helical gears [31]

Helical gears (see Figure 3.4) have the same concept with spur gears with one main difference; their teeth are curved in the shape of helix (helix angle varies from 15° to 30°), which might be right-handed on one gear and left-handed on the other one. Therefore, they act as a conduit of motion between parallel shafts, but they can also be used for transmission of motion between perpendicular non-intersecting axes of rotation. In addition to spur gears, they gradually start to take over the loading which results in a smoother teeth engagement and less noisy operation even at high rotating speeds (up to 50 m/s). In single helical gears both radial and thrust loads are created on the bearing, whilst only radial loads should be considered on double helical gears, as the imposed axial thrust loads act on opposite direction and thus they are self-neutralized.



Figure 3.4: Illustration of helical gear (<https://apps.autodesk.com/FUSION>)

Worm gears [31]

When there is small place available and a need for high-ratio speed reduction exists, the most appropriate set of gears to be utilized are the worm gears (see Figure 3.5).

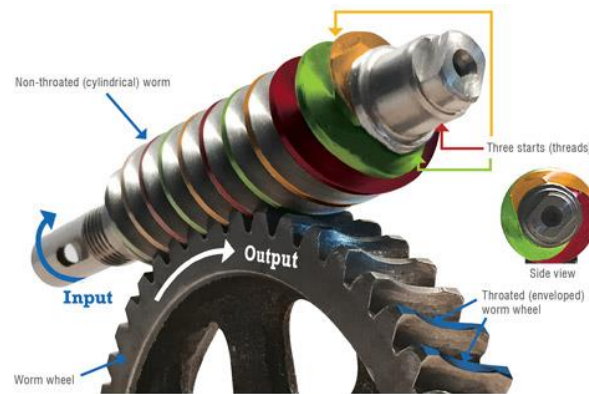


Figure 3.5: Single-enveloping worm gears (machinerylubrication.com)

The arrangement comprises a worm gear, which resembles a skew and a worm wheel (similar to a spur gear), which together transfer the motion between (usually) perpendicular shafts. The speed ratio may vary from 1:10 to 1:300 and worm gears can either greatly increase the torque or greatly decrease the speed. Some more advantages of this type of gear set are the smooth and silent operation and the provision for self-locking. The latter unique characteristic of worm gears allows the worm to easily turn the gear, but the gear cannot turn the worm. With proper design in regards the contact interface and the associated friction, and in conjunction with frequent lubrication, the worm will be kept in place and the mechanisms will not back-drive. However, some limitations do exist; worm gears have a low power transmission capacity up to 100 kW, the high speed ratio yields excessive heat which reduces the efficiency of transmission and requires constant lubrication.

Bevel gears [29]

This system of gears can transmit motion between shafts that have intersecting axes of motion and for nearly any angle of intersection, though usually used for perpendicular ones. It consists of conically shaped teeth, which may be straight or spiral as pictured in Figure 3.6.



Figure 3.6: Left- Bevel gears with straight teeth, Right-Bevel gears with spiral teeth (wikipedia.com)

Spiral bevel gears, likewise helical gears, have the feature of gradually engagement of the teeth and carrying out the loading, thus making their operation smoother and quieter. Bevel gears are usually chosen to carry a constant velocity ratio between axes

of motion and their unique feature is that their cones may roll together with complete absence of sliding motion. The main concern regarding bevel gears are the great thrust loads transmitted in the bearings as these forces may cause a bending to the shaft.

3.2 Gear standards, terminology and nomenclature

The standard that will be applied during the gear design is the metric edition of the American Gear Manufacturers Association: ANSI/AGMA 2101-D04 [33], with reference to the books of Childs [34], Juvinal [35] and Norton [31]. The standard suggests an empirically based analytical gear stress analysis approach for determining the root bending and contact stresses in involute spur gears. Moreover, the metric edition uses International Organization for Standardization (ISO) symbology and SI units and is closer to the European academic intuition. Furthermore, the AGMA standard corresponds to the majority of the citations in the bibliography as per gear design, and many reputable authors include a gear design analysis with the AGMA standard as reference.

Each set of gears has its unique characteristics and elements, but there is a common definition basis for the various peculiar gear terms. It would be in the benefit of the reader a presentation and explanation of the main terms and properties that make the gear function smoothly in energy transmission. Gaining a holistic view of the terminology and the nomenclature used in the literature can lead to a more sound gear design. Definitions are given with reference to Norton [31].

The nomenclature that is used is presented in Table 3.2 alongside with the respective fundamental unit.

Table 3.2: Variables used in the present chapter

Variable	Symbol	SI units
Addendum	α	m
Dedendum	b	m
Center distance	C	m
Surface finish factor	C_f	-
Hardness factor	C_H	-
Elastic coefficient	C_p	-
Pitch diameter	d	m
Face width	F	m
Brinell hardness	HB	-
AGMA surface geometry factor	I	-
AGMA bending geometry factor	J	-
Application factor	K_α, C_α	-
Rim bending factor	K_B	-

Idler factor	K_I	-
Life factor	K_L, C_L	-
Load distribution factor	K_m, C_m	-
Reliability factor	K_R, C_R	-
Size factor	K_s, C_s	-
Temperature factor	K_T, C_T	-
Dynamic factor	K_v, C_v'	-
Module	m	mm
Mechanical advantage	m_A	-
Gear ratio	m_G	-
Contact ratio	m_p	-
Angular velocity ratio	m_v	-
Number of teeth	N	-
Factors of safety-Bending and contact	k_n, k_f	-
Teeth number of pinion and gear	N_p, N_g	-
Number of revolutions per minute	n_{rpm}	-
Base pitch	p_b	m
Circular pitch	p_c	m
Diametral pitch	p_d	-
Gear quality index	Q_v	-
Pitch radius	r	m
Pitch line velocity	V_t	m/sec
Total force on gear teeth	W	N
Radial force on gear teeth	W_r	N
Tangential force on gear teeth	W_t	N
Lewis form factor	Y	-
Pressure angle	φ	deg
Radius of curvature	ρ	m
Bending stress	σ_b	Pa
Surface stress	σ_c	Pa
Angular velocity	ω	rad/sec

In addition, in the next table, Table 3.3, an attempt is made to provide all the necessary formulas and conversions of the various gear variables.

Table 3.3: Gear formulas and conversions

To obtain	From known	Formula
Pitch diameter	Module and number of teeth	$d = mN$
Mechanical advantage	Pitch radius or angular velocity	$m_A = \frac{\omega_{in}}{\omega_{out}} = \pm \frac{r_{out}}{r_{in}}$
Circular pitch	Module	$p_c = m\pi = \frac{\pi d}{N}$

Module	Diametral pitch	$m = \frac{25.4}{p_d}$
Diametral pitch	Number of teeth and pitch diameter	$p_d = \frac{N}{d}$
Number of teeth	Module and pitch diameter	$N = \frac{d}{m}$
Gear ratio	Number of teeth	$m_G = \frac{N_G}{N_P}$
Addendum	Module	$a = m$
Dedendum	Module	$b = 1.25m$
Outside diameter	Module and pitch diameter or number of teeth	$D_o = D + 2m = m(N + 2)$
Root diameter	Pitch diameter and module	$D_R = D - 2.5m$
Base circle diameter	Pitch diameter and pressure angle	$D_b = D \cos \phi$
Base pitch	Module and pressure angle	$p_b = m\pi \cos \phi$
Tooth thickness at standard pitch diameter	Module	$T_{std} = \frac{\pi m}{2}$
Center distance	Module and number of teeth	$C = \frac{m(N_1 + N_2)}{2}$
Minimum number for teeth for no undercutting	Pressure angle	$N_{min} = \frac{2}{\sin^2 \phi}$

Gears follow the same principles as two friction rolling cylinders that have no slip conditions on their contact point, and thus transmit motion from axis to another. The surfaces of these cylinders can theoretically be considered as two tangential circles, the *pitch circles*, where all calculations are based on. The diameter of the pitch circle is the *pitch diameter*, designed as d . Therefore, when teeth are added on the pitch circle expands both outside and inside the pitch circles.

The *circular pitch* p_c is the circular distance from a point on one gear tooth to a like point on the next tooth, taken along the pitch circle. Two gears must have the same circular pitch to mesh with each other. The *module*, m , is measure of tooth size in the metric system. In units, it is millimeters of pitch diameter per tooth. As the tooth size increases, the module also increases. Modules usually range from 1 to 25. The *diametral pitch*, denoted as p_d , is the ratio of the number of teeth on the gear to the pitch diameter the imperial units.

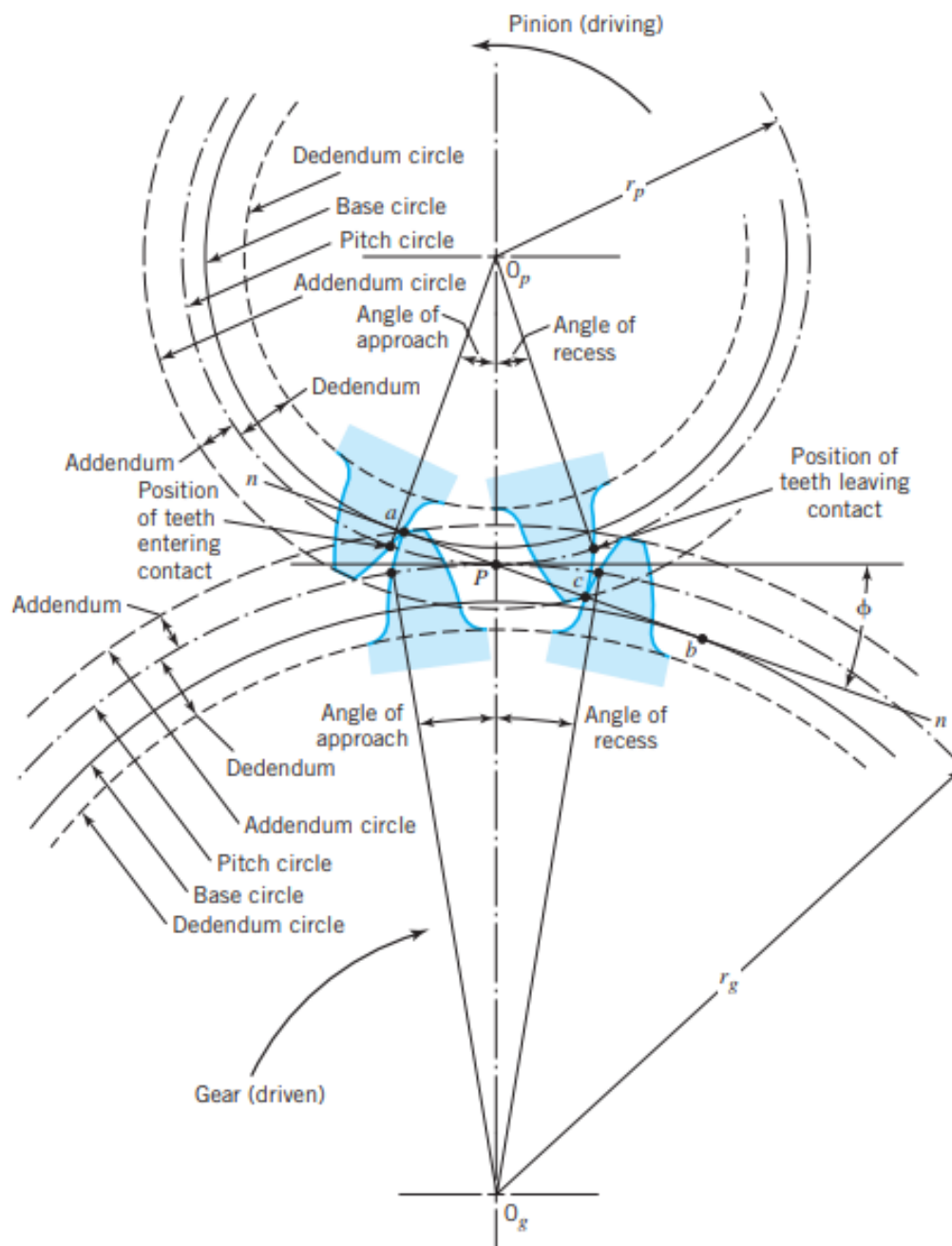


Figure 3.7: Basic gear terminology [35]

The most relevant teeth characteristics are presented below:

Addendum is the radial height of a gear tooth above the pitch circle, while *dedendum* is the radial height of a gear tooth below the pitch circle. Adding these parameters yields the *whole depth*, which is the total radial height of a gear tooth (whole depth = addendum + dedendum). *Pressure angle* is the slope of the gear tooth at the pitch-circle position and defines the plane of the induced force on the gear. The current

standard values of the pressure angle are 20° and 25° , with the former dominating the market.

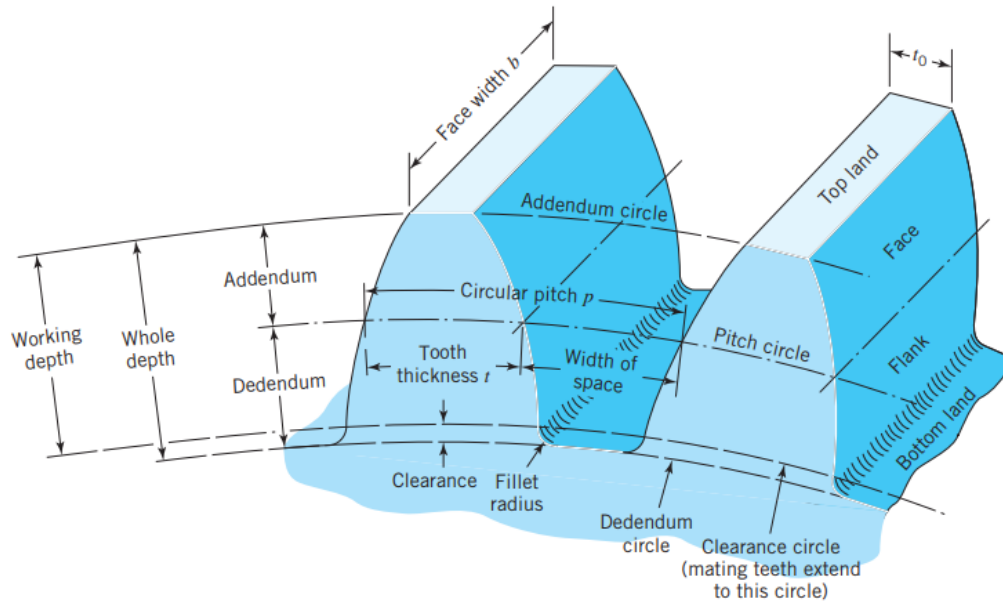


Figure 3.8: Gear tooth characteristics [35]

Helix angle is the inclination of the tooth in a lengthwise direction. (If the helix angle is 0° , the tooth is parallel to the axis of the gear—and is really a spur-gear tooth.) The *backlash* is the difference between the tooth thickness of one gear and the tooth space of the mating gear. *Clearance* accounts the difference of dedendum form the addendum of the mating gear and is required to prevent the tip of the tooth of on gear from riding on the bottom of the mating gear. *Center distance* is half-sum of the pitch diameters of two non-intersecting axes.

3.3 Forces on spur gears

When the pinion transfers a torque T_p to the gear, the gear teeth are in contact at the pitch point O and a force W is transmitted from one tooth to another in the direction of the pressure angle ϕ , as shown in Figure 3.9. This force is analyzed in two normal directions, W_t acting in the vertical direction whilst W_r acts in the radial direction.

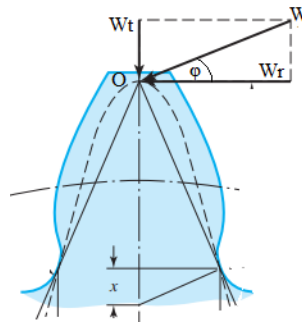


Figure 3.9: Forces on the gear tooth

The magnitude of the components is:

$$W_t = \frac{T_p}{r_p} = \frac{2T_p}{d_p} = \frac{2p_d T_p}{N_p} \quad (3.2)$$

$$W_r = W_t \tan \phi \quad (3.3)$$

$$W = \frac{W_t}{\cos \phi} \quad (3.4)$$

Where T_p is the torque on the pinion shaft, r_p is the pitch radius, d_p the pitch diameter, N_p the number of teeth and p_d the diametral pitch of the pinion. The force applied on the gear is exactly the same as the one on the pinion.

The tangential force can be associated with the power and the rotating speed of the shaft, which will later be an important aspect of the design. The mean pitch line velocity, V , is introduced for this purpose:

$$V = \frac{\pi \cdot d \cdot n}{60 \cdot 10^3} \quad (3.5)$$

Where d is in mm and n in revolutions per minute (rpm). The transmitted power P (W) is:

$$P = \frac{W_t}{V} \quad (3.6)$$

$$\Rightarrow P = \frac{\frac{2T}{d}}{\frac{\pi \cdot d \cdot n}{60 \cdot 10^3}} = 120 \cdot 10^3 \frac{T}{\pi d^2 n} \quad (3.7)$$

Where, T is the torque of the shaft in Nm.

Taking into account expression (3.7) the tangential force (in N) acting on the tooth can be viewed as:

$$W_t = \frac{60P}{\pi \cdot d \cdot n} \cdot 10^3 \quad (3.8)$$

Expression (3.8) relates the magnitude of the tangential force component with the transmitted power, the pitch diameter of the gear and the speed of the shaft.

3.4 Gear failures

The gear designer's main area of study is to choose the appropriate gear size, geometry and material to carry the required power. He should bear in mind the various stresses developed on the gear teeth and the several failure modes that can be developed and bring disastrous consequences.

Figure 3.10 aims to show the big list of gear failure modes, nevertheless the present piece of work will focus on two types of gear failures:

- Tooth bending fatigue leading to breakage (root cracking): The maximum bending stress occurs at the tooth root fillet, due to the fact that is considered as a cantilever beam rigidly fixed at its base. Therefore, the excessive bending results in highest magnitude of tensile stresses that can yield fracture and cracks at the root fillet [29].
- Tooth surface contact fatigue leading to pitting: Pitting occurs due to repeated cycling contact stress on the tooth surface, which Hertzian contact stresses exceed the surface fatigue strength of the material. In or in close proximity of the fatigue region craters are created and material is wearied, causing a stress concentration area. This imposes greater impact loads to an already weakened tooth and increases the probabilities of fracture. The failure pitting process is relatively slow and requires at least 10000 cycles of contact [29].

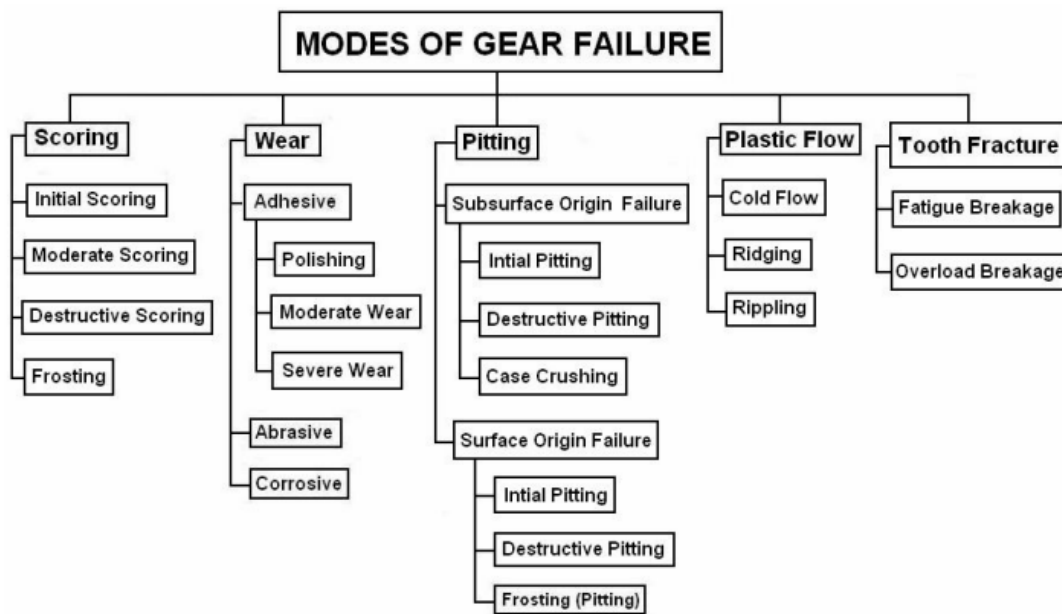


Figure 3.10: Different modes of gear failure

The above critical stress points can be viewed in Figure 3.11 where a photoelastic pattern of gear-tooth stresses is pictured. The photoelastic process is beyond the scopes of this thesis but is sufficient here to note that the highest stresses exist where the lines are bunched closest together. This occurs at two locations: (1) the point of contact with the mating gear, where force F is acting, and (2) in the fillet at the base of the tooth [35].

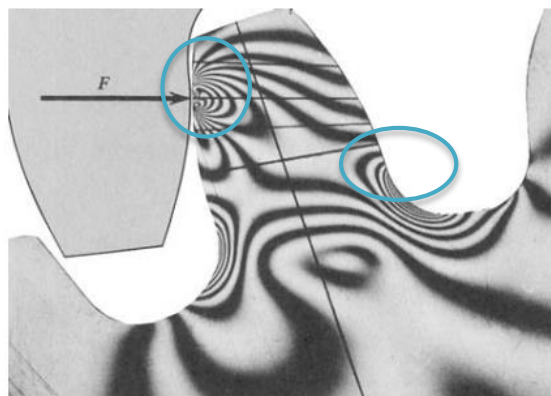


Figure 3.11: Contour lines of maximum spur gear stresses under an applied force on the tip of the tooth [35]

Fatigue fracture due to bending stresses can be controlled and endured during the lifetime of a gear with the selection of the proper material with higher allowable bending stresses. On the other hand, materials do not have a resistance upper boundary for cycling surface-contact stresses and thus is impossible to design gears with infinite lifecycle against surface failure. The two principal failure modes will be addressed in the paragraph in accordance to the AGMA standards and recommendations.

3.5 Gear tooth strength

3.5.1 Bending stresses

Lewis Equation [34]

Lewis was the first to describe the bending stresses of a gear tooth in 1892, and the AGMA standards still rely on the basic principles of his equation. Lewis assumed that the gear tooth behaves as a cantilever beam when a normal force is applied on its tip, resulting in highest values of bending stresses in the tooth root, and he delivered the following equation:

$$\sigma_b^{Lewis} = \frac{W_t}{m \cdot F \cdot Y} \quad (3.9)$$

Where:

- σ_b^{Lewis} = The Lewis bending stresses
- W_t = the tangential force on the tooth tip
- m = the normal metric module
- F = the face width
- Y = the Lewis form factor (dimensionless geometry factor)

The Lewis form factor Y was introduced by Lewis himself and takes into account the geometry of the tooth root to distribute the stresses. He published several tables for different pressure angles and tooth numbers. These tables can be replicated into a graph which is shown in Figure 3.12. The factor is different for the pinion and the gear resulting in different values of bending stresses.

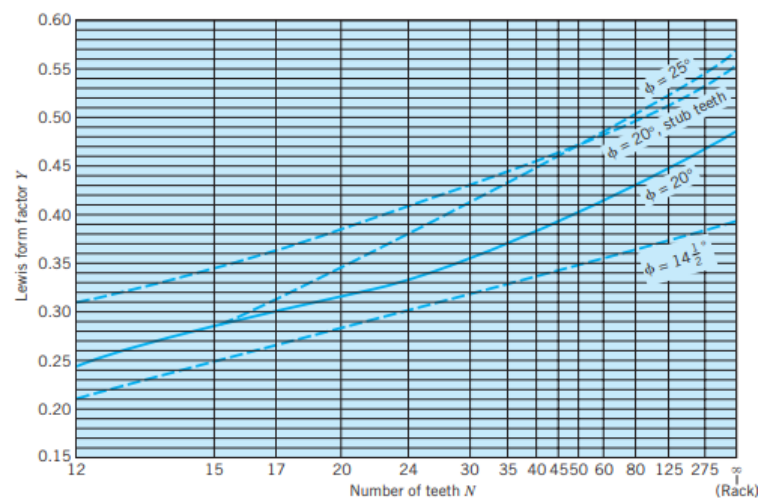


Figure 3.12: Values of Lewis form factor Y for standard spur gears [31]

AGMA equation for bending stress [34]

The AGMA standards use the Lewis equation as a basis and through reaffirmed and adding of more geometric and reliability factors propose the following equation for the calculation of the bending stresses of a gear tooth:

$$\sigma_b = W_t K_O K_v' K_s \frac{1}{F \cdot m} \frac{K_H K_B}{Y_J} \quad (3.10)$$

Where:

σ_b	= the bending stress (N/mm ²)
W_t	= the transmitted tangential load (N)
K_O	= the overload factor
K_v'	= the dynamic factor
K_s	= the size factor
F	= the face width (mm)
m	= the normal metric module for spur gears (mm)
K_H	= the load distribution factor
K_B	= the rim thickness factor
Y_J	= the geometry factor for bending strength

The overload factor takes into account any abnormal applied load in the excess of the nominal load W_t and in the current work will be taken as unity, as no shocks are anticipated.

The dynamic factor K_v' tries to capture the vibrations and dynamics in the tooth spacing due to misalignments and non-accurately meshing gears. AGMA provides empirical curves to calculate the dynamic factor in accordance to the pitch line velocity V .

The size factor K_s accounts the different material properties of the gears and for well-established materials as steel is taken as unity.

The load distribution factor, or face width factor, K_H accounts the uneven load distribution on the face width due to axial deviations of the tooth geometry and variations in the assembly of the gears, and therefore depends on the size of the face width. Its value it is defined by the characteristics of the gears according to graphs or analytical expressions provided by AGMA.

K_B , the rim thickness factor, examines if the rim thickness is sufficient to provide full support for the bearing and in the present work will be taken equal to 1.

The geometry factor Y_J is calculated from a complicated algorithm in the AGMA standards, but some cases are tabulated and can be found from graphs for certain number of teeth and pressure angles. Such graph is the one shown in Figure 3.13.

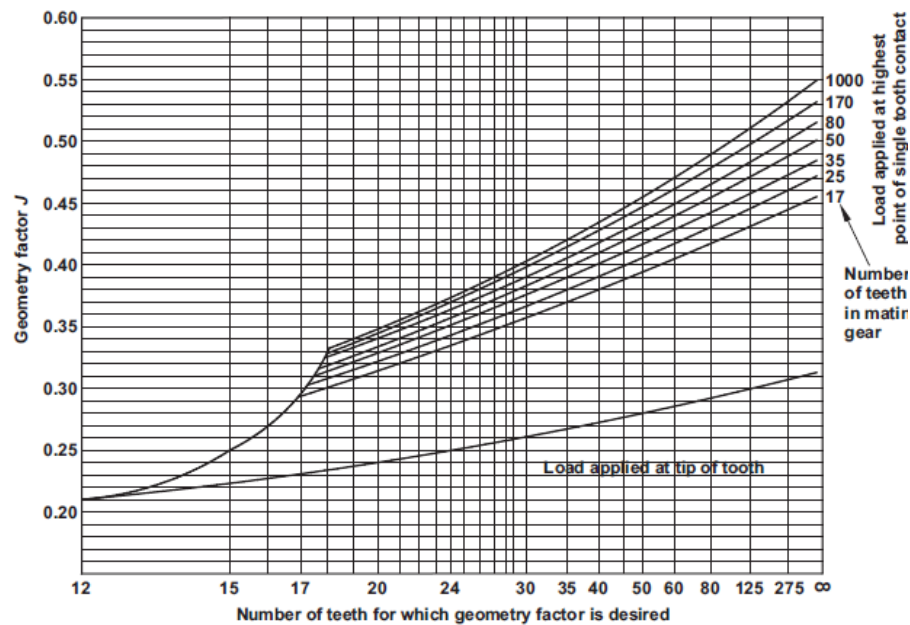


Figure 3.13: Bending strength geometry factor Y_J for 20° pressure angle [34]

AGMA equation for allowable bending stress [34]

The allowable bending strength according to AGMA is:

$$\sigma_b^{allowable} = \frac{\sigma_{FP} Y_N}{S_F Y_\theta Y_Z} \quad (3.11)$$

Where:

- σ_{FP} = the allowable bending stress of the material (N/mm^2)
- Y_N = the stress cycle factor for bending stress
- S_F = the AGMA factor of safety
- Y_θ = the temperature factor
- Y_Z = the reliability factor

The life factor Y_N accounts the differences in the lifecycle of the gears. The test data use 10^7 cycles of operation, so the factor modifies the AGMA strength taking into consideration the different number of load cycles. The pinion and the gear have different values, which can be extracted from the graph in Figure 3.14.

The temperature factor can be taken as unity for temperatures up to 120 °C. Above this value the factor should be increased to account the degradation of the lubricant.

The AGMA strength standards are based on statistical distributions of the fatigue failure of the material in 99% reliability. If this value is deemed satisfactory then the reliability factor is taken as unity, otherwise a linear interpolation should be used for any other case.

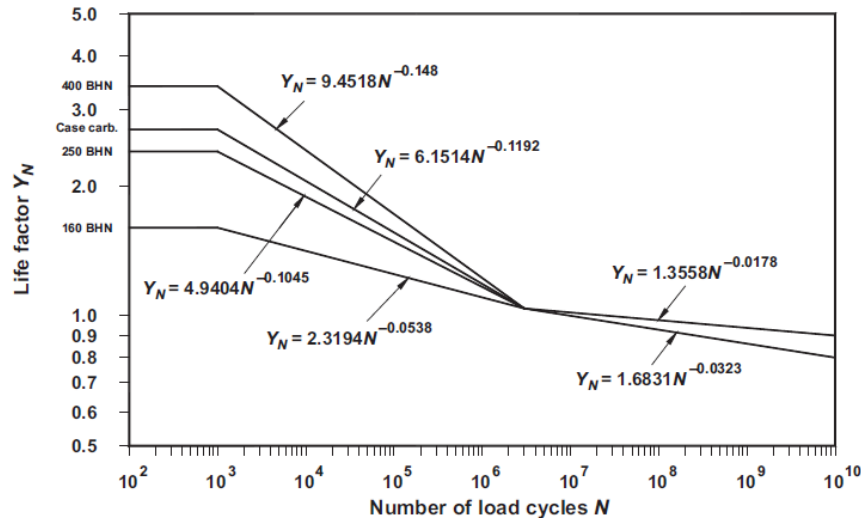


Figure 3.14: Bending strength life factor Y_N [34]

The allowable bending stress, σ_{FP} , is a material property and is given usually by the supplier. It can also be calculated as:

$$\sigma_{FP} = 0.533H_B + 88.3 \quad (\text{steel grade 1}) \quad (3.12)$$

$$\sigma_{FP} = 0.703H_B + 113 \quad (\text{steel grade 2}) \quad (3.13)$$

Moreover, values can be obtained from Table 3.4 below, which also contains allowable bending stresses for nitride through hardened steel grades 1 and 2. Alternatively, an estimate can be derived from:

$$\sigma_{FP} \approx 20.25 + 1.176H_B - 9.584 \cdot 10^{-4} H_B^2 \quad (3.14)$$

Table 3.4: Repeatedly applied allowable bending stress and allowable contact stress for a selection of iron and bronze gear materials at 10^7 cycles and 99% reliability [34]

Material	Designation	Heat treatment	Typical minimum surface hardness	Allowable bending stress (MPa)	Allowable contact stress (MPa)
ASTM A48 gray cast iron	Class 20	As cast	—	34	345–414
	Class 30	As cast	$174H_B$	59	448–517
	Class 40	As cast	$201H_B$	90	517–586
ASTM A536 ductile (nodular) iron	Grade 60-40-18	Annealed	$140H_B$	152–228	530–634
	Grade 80-55-06	Quenched and tempered	$179H_B$	152–228	530–634
	Grade 100-70-03	Quenched and tempered	$229H_B$	186–276	634–772
	Grade 120-90-02	Quenched and tempered	$269H_B$	214–303	710–869
Bronze	ASTM B-148 alloy 954	Sand cast	$\sigma_{\text{UTS min}} = 275 \text{ MPa}$	39	207
		Heat treated	$\sigma_{\text{UTS min}} = 620 \text{ MPa}$	163	448

Where H_B is the Brinell hardness.

3.5.2 Contact stresses

AGMA equation for contact stress [34]

AGMA proposes the following equation for pitting resistance, namely for repetitive high contact stresses:

$$\sigma_c = Z_E \sqrt{W_t K_o K'_v K_s \frac{K_H}{F \cdot d_w} \frac{Z_R}{Z_I}} \quad (3.15)$$

Where:

- σ_c = the absolute value of contact stress (N/mm^2)
- Z_E = elastic coefficient ($\sqrt{\text{N/mm}^2}$)
- W_t = the transmitted tangential load (N)
- K_o = the overload factor
- K'_v = the dynamic factor
- K_s = the size factor
- F = the face width (mm)
- d_w = operating pitch diameter of the pinion (mm)
- K_H = the load distribution factor
- Z_R = the surface condition factor for pitting resistance
- Z_I = the geometry factor for pitting resistance

The factors K_O , K_v' , K_s and K_H are the same as the ones used for defining the bending stresses in equation (3.10) and can be found from the relevant tables or graphs.

The elastic coefficient factor, Z_E , is related to the different material properties of the gears and is given by the following equation:

$$Z_E = \sqrt{\frac{1}{\pi \left[\left(\frac{1-\nu_p^2}{E_p} \right) + \left(\frac{1-\nu_g^2}{E_g} \right) \right]}} \quad (3.16)$$

Where:

ν_p and ν_g = the Poisson's ratio for the pinion and gear, respectively

E_p and E_g = the Young Modulus for the pinion and the gear, respectively (N/mm²)

The elastic coefficient factor can also be retrieved from tables, as Table 3.5 below.

Table 3.5: Values of the elastic coefficient Z_E [34]

Pinion material	E_{pinion} (GPa)	Gear material					
		Steel	Malleable iron	Nodular iron	Cast iron	Aluminum bronze	Tin bronze
Steel	200	191	181	179	174	162	158
Malleable iron	170	181	174	172	168	158	154
Nodular iron	170	179	172	170	166	156	152
Cast iron	150	174	168	166	163	154	149
Aluminum bronze	120	162	158	156	154	145	141
Tin bronze	110	158	154	152	149	141	137

The operating pitch diameter, d_w , is given by:

$$d_w = \frac{2C}{1+\nu} \quad (3.17)$$

Where ν is Poisson's ratio and C the center distance.

The surface condition factor, Z_R , accounts the residual stresses, the surface finish and plasticity effects (work hardening). If the appropriate surface condition is achieved the factor is taken as unity.

The geometry factor for pitting resistance involves the geometric characteristics of the involute tooth shape and evaluates their radii of the curvature and how the contact stresses are spread in the tooth flank. AGMA suggests the use of tables for standard tooth shapes in order to determine the value of the geometry factor. The following analytical expression can also be used:

$$Z_I = \frac{\cos \phi \sin \phi}{2} \frac{m_G}{m_G + 1} \quad (3.18)$$

Where:

ϕ = the pressure angle

m_G = the speed ratio (N_g/N_p - ratio of the number of teeth)

AGMA equation for the allowable contact stress [34]

The calculated contact stresses must be compared with the allowable contact stresses as defined in AGMA:

$$\sigma_c^{allowable} = \frac{\sigma_{HP}}{S_H} \frac{Z_N Z_W}{Y_\theta Y_Z} \quad (3.19)$$

Where:

σ_{HP} = the allowable contact stress of the material (N/mm^2)

Z_N = the stress cycle life factor

Z_W = the hardness ratio factor

S_H = the AGMA factor of safety

Y_θ = the temperature factor

Y_Z = the reliability factor

The stress cycle life factor, Z_N , is the respective Y_N factor that is used in the bending stresses in equation (3.11). It can be found from Figure 3.15.

The hardness ratio factor accounts the differences in the hardness of the materials, the gear ratio and the surface finish of the pinion, which can yield a work hardening effect. The factor can be calculated by the following equation:

$$Z_W = 1 + A(m_G - 1) \quad (3.20)$$

Where:

$$A = 8.98 \cdot 10^{-3} \left(\frac{H_{Bp}}{H_{Bg}} \right) - 8.29 \cdot 10^{-3} \quad (3.21)$$

H_{Bp} and H_{Bg} = the Brinell hardness of the pinion and gear, respectively.

m_G = the speed ratio (N_g/N_p - ratio of the number of teeth)

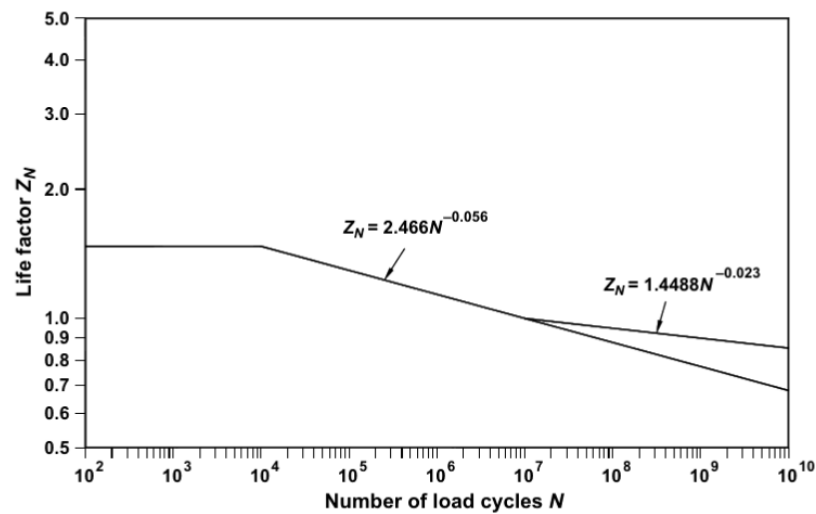


Figure 3.15: Pitting resistance life factor Z_N [34]

The temperature and reliability factors, Y_θ and Y_Z respectively, are similar to the ones defined in equation (3.11) for the bending stresses and are calculated in a similar way.

The allowable contact stress, σ_{HP} , is a material property and is also given by the supplier. It can also be calculated as:

$$\sigma_{HP} = 2.22H_B + 200 \text{ (steel grade 1)} \quad (3.22)$$

$$\sigma_{HP} = 2.41H_B + 237 \text{ (steel grade 2)} \quad (3.23)$$

Values can be drawn also from table 1.4; otherwise estimation can be made as:

$$\sigma_{HP} \approx 2.382H_B + 182.7 \quad (3.24)$$

3.6 Rotational work and power

In order to design a gearset of any kind some input is needed, with the torque, speed, power and gear size being the most dominant ones. In this section, these parameters will be presented.

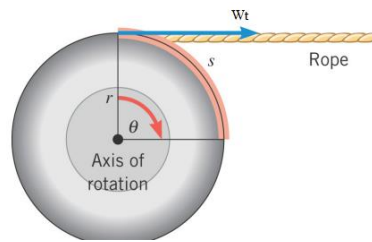


Figure 3.16: tangential force applied on a shaft (physics.ohio-state.edu)

The work done (WD) of a rotating shaft with a tangential force W_t by an angle θ is given as:

$$WD = W_t s = W_t r \theta \quad (3.25)$$

$$\Rightarrow WD = \overset{T=W_t r}{T} \theta \quad (3.26)$$

Power, P , is the amount of work done with respect to time, and for a constant force is defined as:

$$P = W/dt = \frac{T\theta}{dt} = T\omega \quad (3.27)$$

Where ω is the angular velocity in rad/sec, which can also be expressed as:

$$\omega = 2\pi \cdot n_{\text{rps}} = 2\pi \cdot \frac{n}{60} \quad (3.28)$$

Where:

n_{rps} = the number of rotations per second

n = the revolutions per minute

If we substitute ω from equation (3.28) to equation (3.27) the final expression of the power is extracted:

$$\begin{aligned}
 P &= T \cdot 2\pi \cdot \frac{n}{60} \\
 \Rightarrow P &= 0.1047T \cdot n
 \end{aligned} \quad (3.29)$$

Chapter 4

Concept presentation

The design of a steel frame capable of deploying multiple concrete mattresses in one lift will be based in the fulfillment of all the necessary operating and safety requirements. In this chapter, the proposed concept alongside with all the associated challenges will be presented and discussed. An attempt is made to address most of the identified design challenges with practical solutions and new ideas, in order to conclude to a simple and robust tool.

4.1 Challenges and requirements

Firstly, no such multi-handling tool exists in the market. A master thesis carried out five years ago within Subsea 7 [36], made a first attempt to design an installation frame for installing five concrete mattresses in a single lift. A concept design and detailed structural calculations were performed in some components of the frame. However, despite the good work done in that thesis, eventually the concept did not manage to get into further studies, as later on the proposed handling mechanism was re-examined and found to impose large forces on the frame. Therefore, the frame had to be relatively large, and thus heavy and impractical for subsea installation of concrete mattresses. Consequently, the deployment mechanism will need special consideration and detailed engineering as it will be consisted by small mechanical parts that require structural and mechanical modelling, calculations and checks.

A working basis was set with the company, which should meet certain requirements. These requirements can be summed up to the following:

1. The frame should handle as many as practically possible concrete mattresses in a single lift.
2. Ability to deploy one mattress at a time, while holding the rest in place.
3. Simple seafastening and rigger friendly.
4. ROV and diver friendly.
5. Reliable, safe and time-effective.

4.2 Multiple concrete mattress installation frame concept

Herein, the concept proposed by Subsea 7 will be thoroughly discussed and analyzed. Its backbone and key elements will be identified, so the detailed engineering can follow in the next chapters.

Firstly, the orientation of the mattresses in the frame is given in Figure 4.1; the mattresses will be positioned in the frame in their longitudinal axis ($x-x'$), while the transverse direction lays in the vertical axis ($y-y'$) and the mattress thickness defines the third axis ($z-z'$). The minimum dimensions of the main frame are derived by the ones of a typical concrete mattress, as they have been defined before and are shown in the drawing attached on Appendix A.2. Therefore, the length, height and width of the frame are based on the length, the width and the thickness of the mattresses, respectively.

Additionally, the frame will be consisted by cassettes where each mattress will be placed. Such configuration will restrict the large motions of the mattresses due to the dynamics involved in the marine operations, and also prevent the collision with each other, which could damage the product itself.

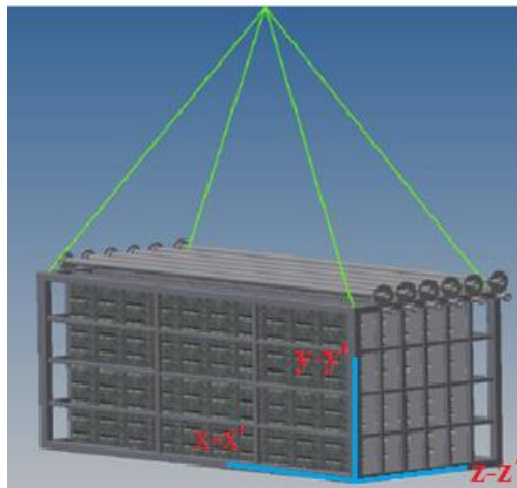


Figure 4.1: Illustration of the concept proposed by Subsea 7

A standardization of the deployment tool is desired, so practically it can be considered as a steel rectangular cage. In addition, one important aspect that will be taken into account regarding the geometry is the mobility of the frame. The idea is that the mattresses will be loaded in the frame at their manufacturing facilities and then transported with a regular size truck to quayside. As no special vehicles will be required, many frames can be produced and treated as single units loaded on trucks,

speeding up significantly the transportation time. Thereafter, the mobilization of the portable unit at quayside can be done with the vessel crane.

The rigging of the mattresses and the deployment mechanism are illustrated in Figure 4.2. As all cassettes of the frame are similar, a bottom up description of one only cassette is presented.

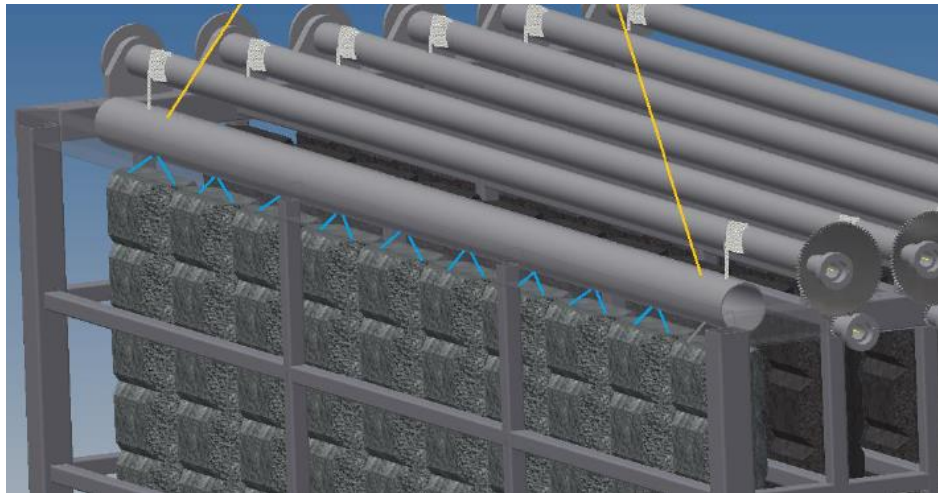


Figure 4.2: Illustration of the handling mechanism

The bottom of the deployment frame has no beams or any other restriction components to hold the selfweight of the mattresses, so they are entirely lifted by a spreader beam, called lower pipe from now onwards. The spreader beam acts as crosspiece to distribute the loading, and due to that, hooks will be mounted on its bottom. As described in section 2.3.2, the mattresses have rope loops on each side. The loops of the longitudinal side of the mattress will be attached to the hooks of the lower pipe, establishing several attachment points, as depicted on Figure 4.3. On the top side of the lower pipe, two padeyes with shackles will be attached close to each pipe-end, which will act as lifting points of the lower pipe and the mattress.

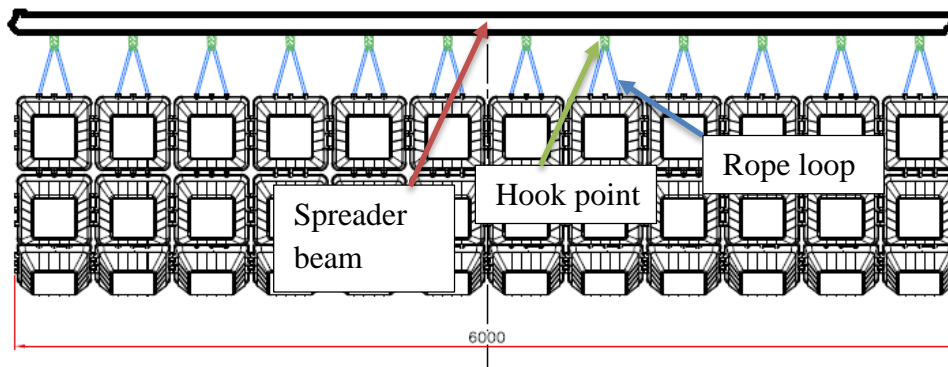


Figure 4.3: The attachment points of the mattress with the lower pipe

A cylindrical pipe, the upper pipe, is located above and holds the lower pipe. The connection is established with the use of steel wire slings that are attached to the shackles of the lower pipe and transmit vertically the load to the upper pipe (see Figure 4.2). The steel wires are reeled around the upper pipe between an arrangement of two circular flanges welded around the pipe. The flanges will keep the steel wires compactly reeled on the drum and simultaneously act as securing points of the wire ends. The upper pipe is restricted on both sides with padeyes attached on the frame. To prevent the pipe from getting out and falling off the padeye, a circular end-plate will be welded on each end, as shown in Figure 4.4. The diameter of the pipe is expected to be outside the pinhole diameter of padeyes available on the market, and thus a custom-made padeye design will be considered. The inner pinhole section will accommodate a thin layer of plastic or other polymer (e.g. polyoxymethylene or POM as its market name) material with very low value of friction coefficient, so the upper pipe can easily rotate. The rotation of the upper pipe is necessary in order to unreel the steel wires and lower the object close to the seabed.

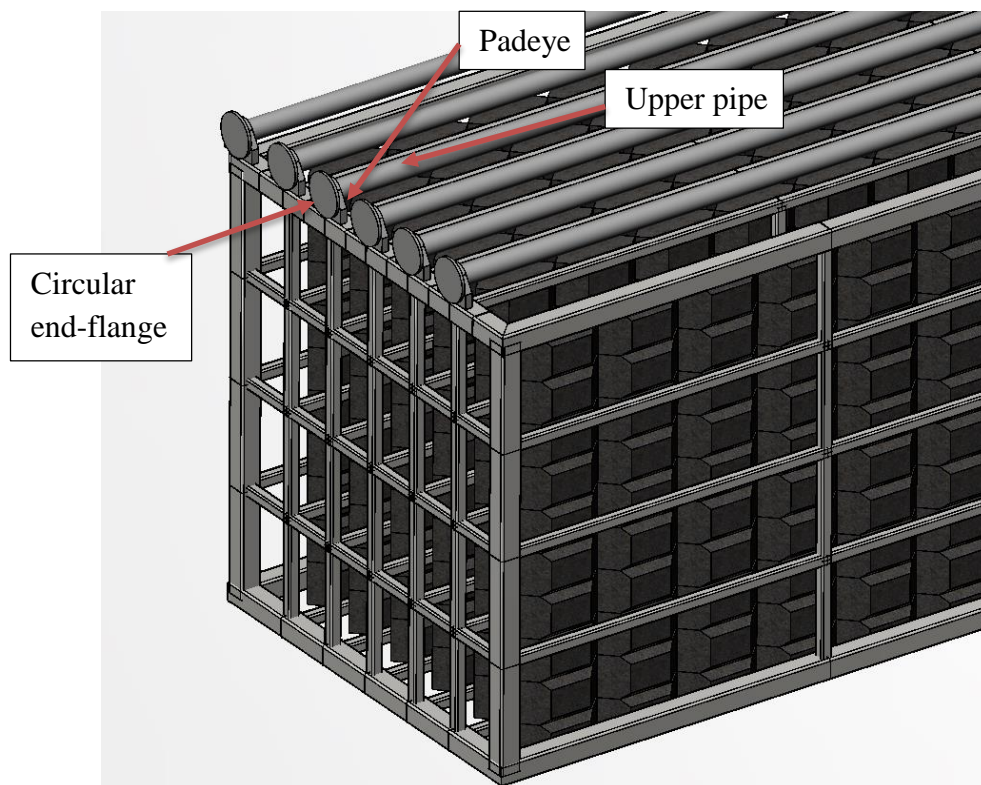


Figure 4.4: The support of the upper pipe to the padeye

However, the forces acting on the upper pipe through the steel wires due to the selfweight of the mattress will tend to constantly rotate the pipe, jeopardizing the whole installation procedure. A measure to counterbalance the produced torque on the pipe will be the introduction of locking pins in one of its side-ends. The pin (or pins)

will penetrate horizontally the circular end-plate and the padeye, establishing a locking-attachment against rotation of the pipe.

For the initiation of the deployment procedure, torque should be applied on the different direction of the torque produced by the concrete mattress selfweight. In this phase, the locking pin can be released, as the large forces acting on it are waived, and afterwards the lowering of the mattress can start by gradually reducing the input torque.

The concrete mattress is a relatively heavy object and is expected to impose quite large torque values on the upper pipe. The regular subsea ROV torque tools are expected to be inadequate to apply the required torque values to counterbalance the produced one. Hence, a gearset solution will be considered, in order to provide the desired torque increase. The gears will be located at the side where the locking pin is, as depicted in Figure 4.5. The larger gear should have a bore equal to the diameter of the end-flange, so it can be welded on it and provide the mechanical advantage to the upper pipe. The smaller gear can be attached to the steel frame with a bearing support, beneath the larger gear. A drive stem needs to be welded on the former gear for the rotary operation.

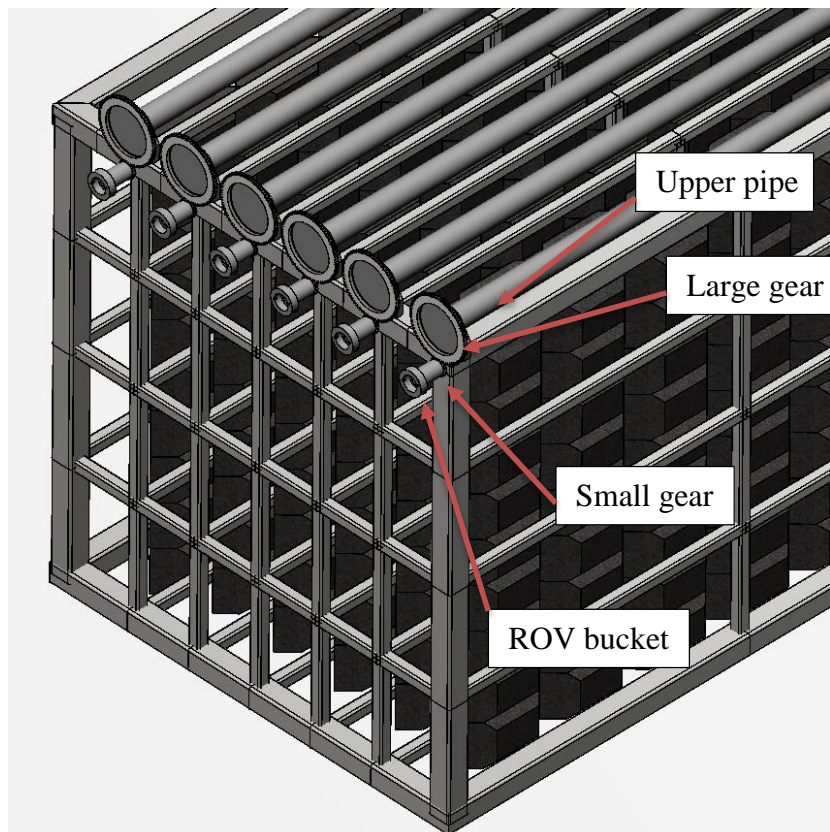


Figure 4.5: View of the frame with the incorporated gear set

The input torque to the mechanism will be provided by a ROV operated subsea torque tool. A ROV bucket will be incorporated with the bearing support in alignment with the small gear. The purpose of the bucket is to offer a socket where the torque tool can be latched and secured on. The drive stem needs to be extended inside the bucket, so it can be fitted in the tool's reception and transmit the torque to the system.

4.3 Deployment procedure

The hypothesis is based on the fact that the frame is located in the desired location and water depth, and is ready for deployment of the first concrete mattress. In addition, in the present procedure presentation is assumed that the selfweight of the concrete mattress tends to rotate the upper pipe in the anti-clockwise direction.

Step 1

The ROV approaches the frame towards the x-y plane (the plane is shown in Figure 4.2). It uses its thrusters to maneuver and carefully inserts the torque tool in the ROV bucket. When the stem is completely fitted in the socket of the tool, the tool is latched on the bucket and secured.

Step 2

The ROV is docked in the steel frame through the bucket. It starts incrementally applying torque on the stem connected with the small gear. The pinion starts rotating and transmitting the torque to the larger one, and with the present mechanical advantage the value of the torque is multiplied.

Step 3

The torque extracted from the large gear has reached the value of the produced torque due to the selfweight of the concrete mattress. The system is balanced. A slight increase is then produced by the torque tool, so the torque "reaching" to the large gear is greater now. Since this gear is welded on the end-pipe flange, the latter will slightly rotate the upper pipe in the clockwise direction.

Step 4

The transverse load acting on the locking pin(s) is eliminated with the slight clockwise rotation of the upper pipe. The ROV uses its 7-function arm to take out the locking pin(s) while simultaneously holding the lifting arrangement (lower, upper pipe and the mattress) by applying the same torque value.

Step 5

The ROV starts gradually decreasing the torque applied on the system. As result, the lower pipe with the mattress starts lowering towards the seabed. When the mattress has reached to the desired depth of deployment, the ROV applies the torque value needed to keep the mattress stable. Then the vessel (or the crane) moves the frame towards the desired direction of deployment, while at the same time the ROV reduces the produced torque in order to lay the mattress on the seabed. When the laying has been completed, the output torque of the tool should be zero and the rope loops of the mattress are released from the hooks of the lower pipe. It should be noted that at this point of the study, it is assumed that the releasement is done by a second ROV unit. Some recommendations and future work tasks in regards this topic, will be given in the last chapter.

Step 6

The ROV produces torque in the clockwise direction and the steel wires start reeling again onto the drum, and therefore lifting the spreader beam at the same time. When the spreader beam has been recovered to its initial position, the ROV inserts the locking pin in the end-flange and secures the system. Ultimately, it disengages the torque tool and is ready to move on to the next cassette.

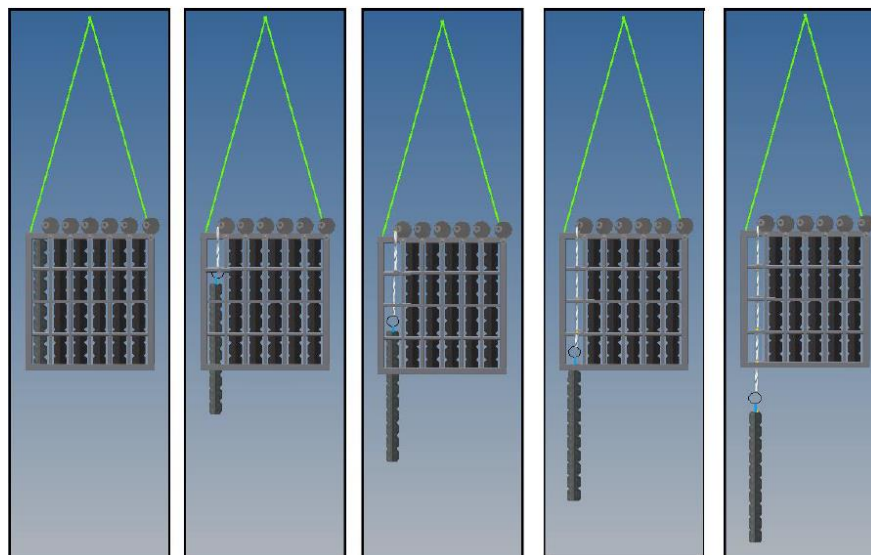


Figure 4.6: Procedure of lowering the mattress (only for illustration purposes)

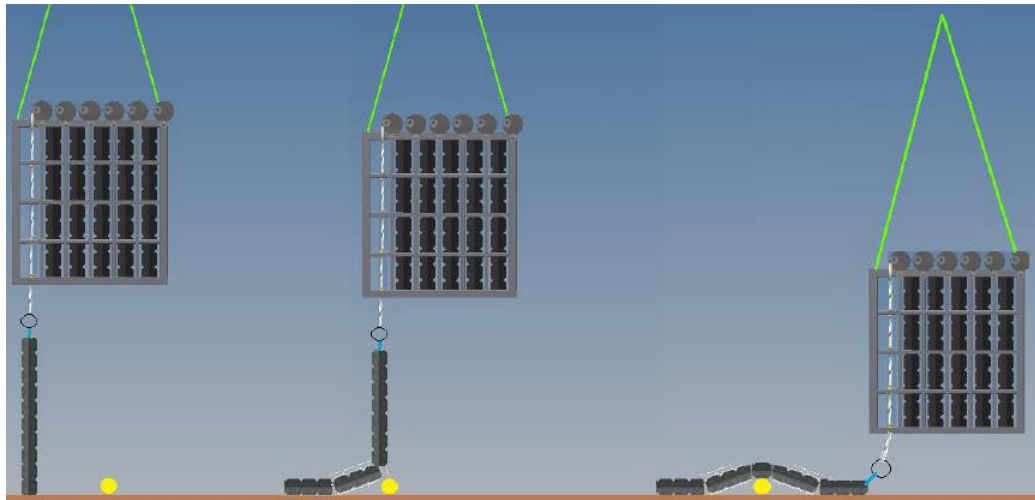


Figure 4.7: The process of laying the concrete mattresses on a pipeline (only for illustration purposes)

4.4 Selection of parameters and assumptions

Despite the fact that the multi-handling mechanism was thoroughly described, there are still several design and operational aspects that have to be studied further. However, these issues are addressed with rational assumptions due to the time limitations a thesis work has. Moreover, in this section some remaining critical parameters with respect to design will be selected, so the analyses can follow later on.

Selection of critical parameters

1. It is decided that the optimum number of mattresses to be handled is six. The operation should be rigger friendly and adding more pieces would result to a large and no easily manageable structure.
2. The selected dimensions of the concrete mattress are 6m x 3m x 0.30m, and the value of weight is 7.13 Te in air, whilst the submerged weight is 4.2 Te, as given by the supplier (Appendix A.2).
3. The minimum base-design dimensions for the frame are defined: height is expected to be 3m and the length (longitudinal directions) 6m, whereas the width is governed by the thickness of the mattresses, namely for six mattresses the width is $6 \times 0.30\text{m} = 1.80\text{m}$. Undoubtedly, these dimensions will be increased as the cassette sections and some necessary clearances need to be accounted.
4. The number of hook points in the lower pipe is 12, as the number of the rope loops of the concrete mattress are.

5. The maximum width of a regular size truck in Europe is 2.60 m [37]. Due to the desired mobility of the frame its maximum width is selected as 2.55 m.
6. In the present piece of work the ISO 13628-8:2006 ROV standard will be used as reference for determining the ROV torque tool and interface dimensions.
7. The class 4 ROV rotary torque receptacle will be the design scenario for the purposes of this thesis. After discussions with Subsea 7 installation engineers with high offshore experience in ROV work tasks and with engineers from the ROV department, it was decided to target a ROV torque tool with class 4 interface, for providing torque to the handling mechanism. The explanation is that class 4 ROVs torque tools are widely used in most of the subsea operations, and most vessels doing offshore campaigns have usually one or more on-board. They are relatively flexible and have a good balance of high operability and load carrying capacity. On the other hand, for instance, class 7 tools are used in specific project tasks, are rugged, heavier, take more time to be employed and naturally are costlier. The geometry of the class 4 interface is shown in Appendix A.3.
8. Through the comparison of the different type of gears in Chapter 3, it is decided to design a spur gearset for the purposes of the present thesis. Spur gears are the simplest type in gear manufacturing, have a great efficiency ratio and do not impose great radial forces on the bearings. Their main disadvantage is their noise while in operation. However, this is not an issue for the living marine environment as the frame is not a permanent subsea structure.

Assumptions

- The lift is assumed to be handled with an active heave compensation technique by the vessel crane, in order to minimize the dynamics loads transferred to the crane and keeping the frame as stable as possible.
- The distance between two consecutive rope loops of the mattress is assumed to approximately be 0.45 m. Each manufacturer sets its own values for this distance and a specific figure comprising the major suppliers cannot be provided.

- The clearance between the upper and the lower pipe is assumed to be 0.30 m. A relatively small figure is assumed in order to eliminate dynamic phenomena that would rise due to hanging effects.
- The upper pipe is longer than the lower pipe, as some clearance on each side is added. This clearance is assumed to be 0.10 m on each side.
- As long as the mattress has been lowered just out from the frame, the distance covered to that point is equal to its height, namely 3 m. For safety purposes a clearance is required between the mattress and the pipeline, where this distance is assumed to be 5 m. Consequently, it is extracted that prior to deployment the frame will be located at least $3+5=8$ m above the sea bottom. This figure is the total distance that needs to be covered by the steel wires reeled on the upper pipe.
- During deployment of the first mattress there will be a slight shift in the Center of Gravity (CoG) of the whole frame. It is assumed that because of the robust 4-point lifting arrangement lifting the whole structure, there is adequate structural integrity. In addition, the next mattress to be deployed will be the one in the opposite site, so the loading remains symmetric. The installation of the rest mattresses will be performed likewise. Therefore, the shift of CoG can be neglected.
- They exist similar steel frames performing other type of works tasks in the market, so a rough estimate can be done for the total weight of the frame loaded with six concrete mattresses.
The frame weight is around 10 and adding six mattresses, $6 \times 7.13 \text{ Te} = 42.78 \text{ Te}$, results in a total weight of $10 \text{ Te} + 42.78 \text{ Te} = 52.78 \text{ Te}$.
- In the spur gear design, a reasonable efficiency of $\eta=0.95$ is assumed in the power transmission.
- The gears are assumed to be accommodated in a casing arrangement, such as a template, in order to be protected by debris, fish etc. Also, lubrication and maintenance of the gears will not be discussed in the present work.

4.5 Potential savings by the multi-deployment frame

The frame geometry is intended to follow a standard container size and thus be capable of transported with regular size trucks from the manufacture facilities to the mobilization site. As result, the easy transportable unit can support global applications in a short amount of time.

Moreover, the load-in procedure followed to date, utilizes a special lifting component, the speed loader, which can lift 3-5 mattresses in a simple lift and stack them onboard. The maximum number of stacked mattresses is approximately 6-10 pieces. In contrary, the new concept eliminates the use of the speed loader, as the frame with its 6 mattresses is loaded directly onboard as a simple “cage”. According to installation engineers, the latter could reduce the mobilization time up to 20 minutes per mattress. Furthermore, many frames units can be stacked on top of other, saving both vessel space and time.

In addition, the seafastening of the object is expected to be a more standardized and time-effective procedure. Now, the most common ways of seafastening stacks of mattresses is with straps that end to padeyes, or bumper bars welded on the deck. Both operations are time consuming, require a lot of welding consumable and require large proportions of the deck space. With the new proposed concept deck space, vessel time and welding material can be saved.

The installation of concrete mattresses on the seabed is expected to be on high demand, and the single deployment tools available on the market will be inadequate to install large numbers of mattresses in a profitable time frame. For instance, let us consider a project that requires 24 concrete mattresses to be installed at 3,000 m water depth (ultra-deep water). Some rational assumptions are made:

- Only the lowering of the mattress and the recovery of the winch are considered. The detailed releasement of the mattress on the seabed is not accounted.
- The hoisting speed of the crane wire loaded with a single mattress is roughly 15 m per minute (deployment speed).
- The hoisting speed of the crane wire without lifting an object is roughly 50 m per minute (recovery speed).

Therefore, the approximate installation time of one mattress is:

$$\frac{3000m}{15m/\text{min}} + \frac{3000m}{50m/\text{min}} = 260 \text{ min or } 4.33 \text{ hours}$$

The total installation time for all products is hence 260 min x 24=6,240 min or 104 hours.

For the multi-deployment frame, the lowering and recovering speeds can be assumed half of the respective ones during installation of one mattress. Therefore:

$$\frac{3000m}{7.5m/\text{min}} + \frac{3000m}{25m/\text{min}} = 520\text{min or } 8.67 \text{ hours}$$

Nevertheless, since the frame lowers six mattresses it will take four lifts to transfer 24 mattresses at the seabed, resulting in a total deployment time of: 520 min x 4=2,080 min or 34.67 hours. This is a reduction of approximately 66% compared to single-lifting tools, interpreted in reduced vessel time. For a vessel with a daily book rate of USD \$150,000 [38], the first case would cost USD \$650,000, whereas with the multi-deployment frame it would cost USD \$216,680. So, it is obvious that lowering six mattresses instead of one will significantly decrease the installation time and increase the potential savings for the installation company.

In the course of deployment of the concrete mattresses on the seabed, most of the available on the market installation frames/beams rest on the concrete mattress after releasement so the ROV to cut the ropes for full detachment. In such operation, special attention should be given in the pipeline integrity with the added weight on top of it. However, with the proposed concept proposed, the installation will be done with the mattresses being in a vertical position and laid as the frame moves forwards. In such way, the frame will never be in contact with the released mattress and will not apply extra weight on the pipeline. Moreover, the mattress can be placed on the desired location with an extra accuracy. The latter enhances the capability of the mattresses to be used as foundation support of subsea structures and pipeline crossings. Consequently, the installation frame considered on the present thesis is deemed suitable for both pipeline protection and foundation support projects.

Chapter 5

Basis of design

The various engineering calculations and checks performed in the present thesis work are based on the principles from well-established standards and regulations, widely used across the oil and gas industry. The main standards used are Eurocode 3, ISO, the AGMA, NORSOK and DNV-GL standards. A continuous effort has been made to be consistent and simultaneously choose the right applicable standard on each engineering stage. Internal Subsea 7 engineering standards and technical documentation based on the international and national standards have been used in addition to them, as they offer a more practical point of view in some cases.

5.1 Units and material/sectional properties

The fundamental units that are used in the calculations and in the computer tools, are the following SI unites (or multiples of):

- Length: meter [m]
- Mass: kilogram [kg]
- Time: second [s]

The steel quality that is used is considered according to the yield and tensile strength values of table 3.1 in EN 1993-1-1:2005 [40] and the sections are chosen by European databases of cross sections. It is considered that the nominal thickness of all elements is below 40 mm, so the basic values of the material properties are:

- Steel grade: S355
- Yield strength: $f_y = 355 \text{ N/mm}^2$
- Ultimate strength: $f_u = 490 \text{ N/mm}^2$
- Density: $\rho = 7,850 \text{ kg/m}^3$
- Modulus of elasticity: $E = 210,000 \text{ N/mm}^2$
- Poisson ration: $\nu = 0.30$
- Shear modulus: $G = 81,000 \text{ N/mm}^2$

When a different steel grade, or material is used it will be mentioned accordingly, alongside with its properties.

5.2 LRFD method and limit state

The Load and Resistance Factor Design (LRFD) method is applied on the design of the structural members as defined in DNV-GL standards [41]. The LRFD method uses partial factors to measure the uncertainty both in the loads applied on the structure and the resistance of the materials. The characteristic expression that defines the method is:

$$S_d \leq R_d \quad (5.1)$$

Where:

S_d = The design load effect.

R_d = The design resistance.

When expression (5.1) is fulfilled, the level of safety is considered satisfactory. The design load is calculated if the characteristic load is multiplied with a load factor γ_f , while the characteristic resistance is divided by a material factor γ_M .

The equality $S_d = R_d$ defines a limit state, more specifically a condition where the structure or a part of it no longer fulfills its design criteria.

The design load effect (e.g. stress, mooring line load, sling load etc.) originates from the most unfavorable combination of design loads, so:

$$S_d = S(F_{d1} \dots F_{dn}) \quad (5.2)$$

Where:

S_d = design load effect

F_d = design load(s)

S = load effect function

According to DNV [41] there exist four limit states, which are presented in Table 5.1, with ULS being the design basis of the current work. Therefore, all members of the installation frame must meet the requirements set by the ULS limit state, namely maintain their level of safety without:

- Loss of structural resistance (excessive yielding and buckling).
- Failure of components due to brittle fracture.
- Loss of static equilibrium of the structure, or critical parts of the structure.
- Failure of critical components of the structure caused by exceeding the ultimate resistance (in some cases reduced by repeated loads) or the ultimate deformation of the components.

- Transformation of the structure into a mechanism (collapse or excessive deformation).

Table 5.1: Design limit states [42]

Limit State	Description
Ultimate Limit State (ULS)	Involves the structural integrity or strength, as such the structure is designed to have a very low probability of reaching this limit state since the consequences are severe
Fatigue Limit State (FLS)	Involves the fatigue damage resulting from cyclic dynamic loads accumulated throughout its life. The structure is designed such that its life, accounting for fatigue damage from all sources, meets or exceeds the design life
Accidental Limit State (ALS)	Relates the damage of the components due to an accidental event or operational failure
Serviceability Limit State (SLS)	Corresponds to the disruption of use of the structure as intended

5.3 Load and material factors

While performing an analysis of ULS, there are two sets of load combinations that shall be considered when designing under combined loads [41]. The condition resulting in the most unfavorable design load effect must be considered. The values of the load factors can be seen in Table 5.2.

The analyses carried out in this work are linear elastic analyses, unless otherwise specified. The permanent loads, namely the selfweight of the components, dominate the structural analysis. The environmental loads exerted on the structure, and chiefly the hydrodynamic forces, including dynamic effects and uncertainties, will be considered by introducing relevant load factors. These factors will multiply the static loads, and in such way a more realistic approach of the real loads induced in the structure is obtained. Consequently, the design combination of the present work will be the ULS (a), where the permanent loads (selfweight) are multiplied by a factor of 1.30

Table 5.2: Load factors γ_f for ULS [41]

Combination of design loads	Load categories			
	G	Q	E	D
(a)	1.30	1.30	0.70	1.00
(b)	1.00	1.00	1.30	1.00

The load categories are:

- G = permanent load
- Q = variable functional load
- E = environmental load
- D = deformation load

The material factor can be determined by both Eurocode 3 [40] and NORSOK N-004 [43], while DNV [44] suggests using the former for non-tubular steel members and the latter for tubular ones. A comparison of the values of the factors is shown in Table 5.3, with the presented partial factors of EN 1993-1-1:2005 taken in accordance to the Norwegian Annex.

NORSOK N-004 accounts the hydrostatic pressure differences which can buckle the structural components and therefore is considered more applicable to offshore steel structures. However, if perforated tubular sections are used and the water floods inside when subsea, the pressure difference is insignificant and can be ignored. Moreover, the basic formulas used in both codes are similar with only exception the interaction formulas for buckling (which will not be considered), Eurocode 3 may be considered equivalently applicable for the design that will follow.

Table 5.3: Material factors according to EC3 [40] and NORSOK N-004 [43]

		EC3 NA 6.1	NORSOK N-004: 6.3
Resistance of all cross sections	γ_{M0}	1.05	1.15
Resistance of members to instability	γ_{M1}	1.05	1.15
Axial tensile resistance to fracture	γ_{M2}	1.25	1.30

5.4 Load factors in marine lifting operations

The deployment of the frame and the releasement of the concrete mattresses involve lifting these objects and lowering them near the seabed. When planning an offshore lift there are some important aspects and load factors to be reviewed before the lifting is performed. In this piece of work the lifting involved in the handling mechanism will be the main area of concern with reference to DNV [44].

Dynamic Amplification Factor, DAF

DAF is a factor accounting for the global dynamic effects that naturally experienced during marine lifting operations. When an object is lifted through the splash zone it will experience hydrodynamic loads. The hydrodynamic loads will be a function of slamming impact forces, buoyancy forces, drag and inertia loads. The factor multiplies the deflections or stresses caused by static loading conditions to incorporate these dynamic phenomena experienced by the structural system.

$$\begin{aligned}
 F_{total} &= F_{static} \cdot DAF \\
 \Rightarrow DAF &= \frac{F_{total}}{F_{static}}
 \end{aligned}
 \tag{5.3}$$

Where: $F_{total} = F_{static} + F_{dyn}$

$F_{static} =$ Static loads

$F_{dyn} =$ Dynamic loads (such as hydrodynamic, snap loads etc.)

Therefore, in the present work, the total load applied on the members of the structure, incorporating hydrodynamic, inertia and static forces, it is assumed is the selfweight multiplied by DAF. The parameters influencing DAF could be [45]:

- Environmental conditions.
- Rigging arrangement.
- Type of crane vessel.
- Stiffness of crane-boom and lifting appliances.
- Type of cargo vessel.
- Weight and shape of lifted object.
- Lifting procedure.
- Whether the lift takes place in air, in water or through both.

The object should, as a general rule of thumb, not be installed in a sea state that will give snap loads in the main hoisting wire. The DAF value cannot be less than 1.0. For lifts where there is no slack in the main lifting wire the DAF cannot be higher than 2.0 (slack sling criteria) [45]. The DAF factors are drawn from the DNV standard and presented in Table 5.4.

Table 5.4: DAF values in air [44]

Static Hook Load (SHL) [Te]			DAF		
			Onshore	Inshore	Offshore
3	<SHL≤ 100	1.10	$1.07 + 0.05\sqrt{100/SHL}$	$1.07 + 0.25\sqrt{100/SHL}$	
100	<SHL≤ 300	1.05	1.12	1.25	
300	<SHL≤ 1000	1.05	1.10	1.20	
1000	<SHL≤ 2500	1.03	1.08	1.15	
	SHL>2500	1.03	1.05	1.10	

Where the SHL is defined as the static force exerted downwards on the hook by the lifted object [44]. More specifically:

$$SHL = W + W_{rigging} + F_{sp} \quad [\text{Te}] \quad (5.4)$$

Where:

W = The upper bound design weight of the lifted object [Te]

$W_{rigging}$ = The weight of the rigging equipment [Te]

F_{sp} = Forces due to special loads (e.g. friction loads) [Te]

The frame with the mattresses is approximated to weight 52.78 Te, whereas the weight of the rigging equipment and special loads can be neglected. So,

$$SHL_{frame} = 52.78 \text{ Te}$$

According to Table 5.4 the DAF values for this structure is:

$$\begin{aligned}
 DAF_{frame} &= 1.07 + 0.25\sqrt{100/SHL_{frame}} \\
 \Rightarrow DAF_{frame} &= 1.07 + 0.25\sqrt{100/52.78} \\
 \Rightarrow DAF_{frame} &= 1.41
 \end{aligned}$$

However, when a subsea lift is considered, according to DNV GL the worst realistic scenario, DAF should be taken, which proposes DAF=2. This value will be adopted during extreme design of the structural members.

Weight contingency factor, γ_{cont}

The weight of the concrete mattress is usually measured and provided by the manufacturer on site, as inaccuracies are possible. This issue is encountered in most of the objects as the exact weight is determined if and only if after the object has been constructed and tested. Therefore, in lifting application a factor that increases the weight due to the uncertainties is introduced. According to [45] the following values can be applied, unless otherwise specified:

Table 5.5: Values of γ_{cont} according to [45]

	Preliminary concept phase	Very detailed drawing	Detailed 3D model	Exact measured weight¹
γ_{cont}	1.15	1.07	1.05	1.03

Since, this work refers to a conceptual phase a weight contingency factor of 1.15 is selected.

CoG shift factor, γ_{CoG}

To have a level lift of an object the crane hook point is placed on top of the CoG of the structure. A flat lift is desired in order to avoid tilting or/and twisting of the lifting slings. However, in complex geometries there are uncertainties about the exact location of CoG position and thus one point of the sling arrangement may be in closer distance to CoG from another point. As result, these uncertainties are accounted with the CoG shift factor included in the design loads, which normally is greater or equal to 1.05 [44]. The latter figure is selected for the purposes of the current study.

Skew load factor, γ_{sk}

The skew load factor refers to additional loading caused by fabrication tolerances and inaccuracies of the slings and the lifted object, asymmetries, crane hook geometry, multi-hook lifting, differences in sling elongations and generally by unevenly distribution of the loads to the rigging arrangement [44]. Practically slings are fabricated within a tolerance. This tolerance on length has a direct impact on final geometry of the lift, tilt angle and load distribution in the slings. It should be noted that the mattress' polypropylene rope loops holding its selfweight, are attached to 12 hook points and the inaccuracies and uncertainties of the ropes can be neglected. As result, the skew load factor can be taken as unity.

¹ When the weight is measured this factor is acceptable as long as the inaccuracy is within 3%.

Load factor, γ_f

The load factor inserts the uncertainties involved with the various loads applied on the structure. The load factor is defined by the ULS limit state and will be 1.30 throughout the current work.

Consequence factor, γ_{cons}

The consequence factor measures the importance of the operation and the potential effects if a failure occurs. The members supporting the lifting should be considered under more severe loading as any loss of the lifting capacity will yield disastrous consequences for the whole structure. As a result, the lifting equipment has a high consequence factor of 1.30, the components carrying the lifting points a more moderate of 1.15 and the parts that do not participate in lifting have a unity consequence factor [44]. As the main scope of this work is the design of the components carrying the lifting points a consequence factor of 1.15 is sufficient.

5.5 Presentation of results

The demonstration of the structural integrity of the installation frame will be carried out with unity checks and presented as utilization ratios (UR), establishing an easy and simple way to directly depict if a component fails or not. The utilization ratio is defined as:

$$UR = \frac{\text{performance value of the load effect}}{\text{maximum allowable performance value}} \leq 1$$

The UR must always be lower than unity in order for the component to pass the check. For instance, if the bending moment of a component due to external loading is 100 kNm and the allowable bending moment is 200 kNm, then the member passes the check, as $UR=100/200=0.50 \leq 1$.

5.6 Structural checks

The assessment of the structural integrity of the components of the multi-deployment mechanism will be carried out in accordance to EN 1993-1-1:2005 [40], which evaluates the resistance of the cross-section. The standard states that: *“The design value of an action effect in each cross section shall not exceed the corresponding design resistance and if several action effects act simultaneously the combined effect shall not exceed the resistance for that combination”*, videlicet, it provides formulas to

calculate the cross-section resistance and compare it with the load effect(s). The comparison is performed with the unity check.

Initially, the standard categorizes the cross-sections in four classes depending on their rotation capacity, which enables them to form plastic hinges and redistribute the developed bending moments. The fraction of the rotation capacity and resistance is set by the local buckling resistance of the cross-section. The classification is done with reference to Table 15 of the standard, where the parts of the cross section subject to compression govern the class selection. In a simplified way, class 1 possess the higher rotation capacity, whilst as the class increases the capacity reduces.

Thereafter, clause 6.2 of EN 1993-1-1:2005 comprises the effective interaction equations to evaluate the resistance of the cross-section against particular action effects and combinations of them. The cross-sectional resistance due to the following effects is checked:

- Tension
- Compression
- Bending moment (and bi-axial bending)
- Shear
- Torsion
- Bending and shear
- Bending and axial force
- Bending, shear and axial force

Clause 6.2.7 studies the members subjected to torsion, and since the upper pipe of the handling arrangement exhibits torsional effects some discussion of the clause is needed. The code performs the unity check wherein accounts the summation of St. Venant torsion and warping torsional moments as the characteristic design torsion, which thereupon is compared with the torsional resistance of the cross section. However, the torsion effect is a complex phenomenon governed by the section properties, the boundary conditions at the supports and the load distribution along the component. The standards provides the option for an elastic (and more conservative) verification criterion:

$$\left(\frac{\sigma_{x,Ed}}{f_y / \gamma_{MO}} \right)^2 + \left(\frac{\sigma_{z,Ed}}{f_y / \gamma_{MO}} \right)^2 - \left(\frac{\sigma_{x,Ed}}{f_y / \gamma_{MO}} \right) \left(\frac{\sigma_{x,Ed}}{f_y / \gamma_{MO}} \right) + 3 \left(\frac{\tau_{Ed}}{f_y / \gamma_{MO}} \right)^2 \leq 1 \quad (5.5)$$

Where:

$\sigma_{x,Ed}$ = design value of the longitudinal stress at the point of consideration

$\sigma_{z,Ed}$ = design value of the transverse stress at the point of consideration

τ_{Ed} = design value of the shear stress at the point of consideration

The elastic criterion, and all structural checks mentioned above will be used in the design of the lower and upper pipe of the handling mechanism. If a member fails in any of the checks, a further investigation is conducted. It should be noted that since axial forces are not present in lifting arrangement, buckling effects will not be studied.

5.7 Software engineering and design tools

The structural checks are performed with the Finite Element software Staad.Pro V8i [46], which is a widely used structural engineering programme across the industry. The pipes that will lift on the concrete mattress can be designed in the software as no complicated geometry is involved. After the nodes of the components have been defined the various members are formed with beam elements, which are given section and material properties. Then, Staad.Pro can analyze the complex in static, dynamic, modal and various other analyses by calculating deformations, internal forces and stresses. One of the biggest advantages of the software is that performs the structural checks as per several international standards, including EN 1993-1-1:2005. So, the members are subjected to structural checks as they were described in section 5.5, and the programme visualizes if a member passes the check or no with the unity check.

Where complex geometry and nonlinearities are involved the mechanics of the structure need a more comprehensive analysis. For this purpose, the FE analysis software ANSYS Workbench [47] is utilized. ANSYS can simulate complex geometries and material nonlinearities and perform structural, dynamic, electromagnetic and various other analyses. It utilizes a wide range of powerful solvers based on the physics of the defined problem (ANSYS Manual). The advantage to design the components in Computer Aid Design (CAD) software and then import it to ANSYS makes it user friendly and time-effective. The output is usually stresses and deformations, which can be checked with the respective allowable ones from the standards.

As discussed before, the handling mechanism will incorporate a set of gear to increase the required torque of the ROV torque. Despite there are several different types of gears (which are discussed in Chapter 3), every gear set will have a challenging and complex geometry, especially in the case of involute teeth shape, such is the design case of the thesis. Therefore, the Autodesk Inventor 2015 [48] software is used to design the exact geometry of the gears, as the programme has a specific gear generator tool. Inventor is capable of 2D and 3D geometry integration in a single environment, allows the user to create a component and then validate its form, function and operation before manufacturing (Wikipedia, Inventor). The generated parts can be exported and used in other software for further analysis, such as ANSYS.

Chapter 6

Design phase

Static lift on air in combination with the load, material and lifting factors will be the ground of the analysis. The two main components of the multi-handling mechanism are the lower and upper pipe of each cassette section. The lower pipe lifts the concrete mattress, while the upper one supports the former through slings and is also free to rotate in order to perform the deployment. This section focuses on the design of the two pipes in the ULS condition, with the performed calculations executed on Staad.Pro, which are complemented with hand calculation where necessary. Two load cases will be in the sphere of interest of this thesis, which includes design and dimensioning due to extreme load conditions and the operational phase.

6.1 Input data

The global analysis and code check are done with reference to EN 1993-1-1:2005 [40] and with the Staad.Pro parameters as viewed in Table 6.1.

Table 6.1: Parameters used in STAAD.Pro

Parameter		Selection
Resistance of cross-sections - γ_{M0}	GM0	1.15
Resistance of cross-sections - γ_{M1}	GM1	1.15
Steel grade according to Table 3.1 of the EN 1993-1-1:2005	SGR	(2) - S355 grade steel
Torsion Check	TOR	(2) - Include torsion (detailed checks using warping effects)
Output details	TRACK	(2) – Output detailed results

The first two sections of Table 6.1 refer to material factors of the members. In the NA of the EN 1993-1-1:2005 the first partial factors are equal to 1.05, as shown on paragraph 5. However, this figure is lower than the value set by DNV ST-N001, and a value of 1.15 by enabling the GM0 and GM1 commands of the programme.

Additionally, the torsion check is important to be inserted, as it will allow the software to implement the elastic yield criterion in equation 5.5 of EN 1993-1-1:2005, on a critical point of the cross section. While selecting parameter 2 the programme will perform the elastic verification of cross sectional resistance regardless the existence or non-existence of torsion implementing equation (4.1), provided in section 5.5.

6.2 Load case 1: Lift in air

The weight of a typical concrete mattress is 7.13 Te and is distributed in 12 points. So:

$$F_{mat} = \frac{M_{mat} \cdot g}{12} = \frac{7.13 \cdot 9.81}{12}$$

$$\Rightarrow F_{mat} = 5.83 \text{ kN}$$

The following load factors are selected:

Load factor: $\gamma_f = 1.30$

DAF factor: $\gamma_{cons} = 2.00$

Weight contingency factor: $\gamma_{cont} = 1.15$

CoG shift factor: $\gamma_{COG} = 1.05$

Consequence factor: $\gamma_{cons} = 1.15$

Total load factor: $\gamma_{tot} = 3.62$

Therefore, the applied force on each hook point is:

$$F_{hook} = F_{mat} \cdot \gamma_{tot} = 5.83 \cdot 3.62 = 21.10 \text{ kN}$$

6.2.1 Lower pipe

The minimum dimensions of the frame are defined by the respective dimensions of the concrete mattress, namely 6m x 3m x 1.80m. The pipe is supported with slings reeled on the upper pipe through shackles attached to padeyes. The slings are considered pin-supported on the upper pipe and are modelled as truss members (axial-only members) with sufficient resistance to carry the loads, as the main interest is in dimensioning the pipe. Also, week springs with negligible effect on the structural response are inserted at both ends of the beam, in order to overcome any instability issues,

The mattress has 12 rope loops with maximum length of 0.30 m made of 20-25 mm thick polypropylene rope. According to these figures the hook points will be located as viewed in Figure 6.1. The total length of the lower pipe will be 6.11 m. Thereupon, the pipe is modelled in Staad.Pro according to the design basis of Chapter 5 hereof.

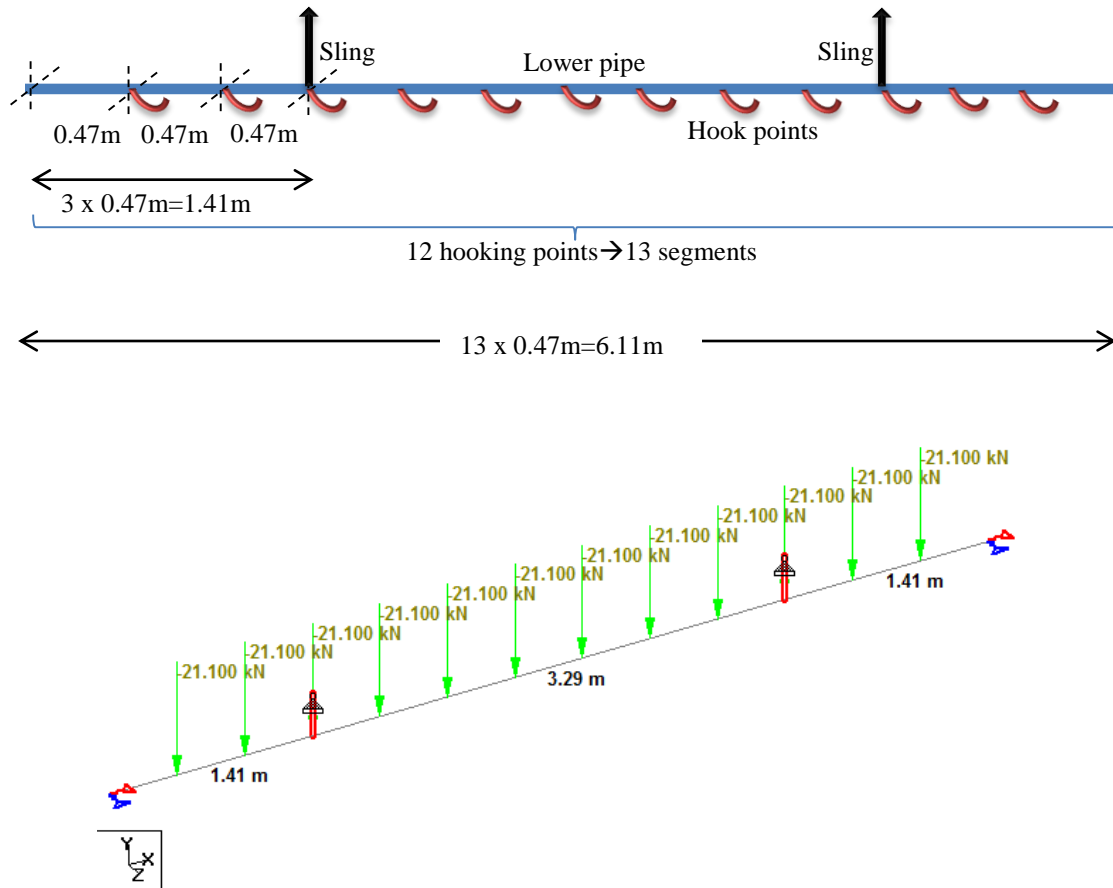
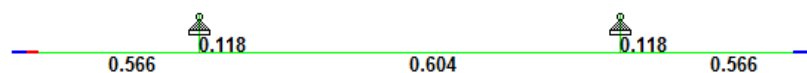
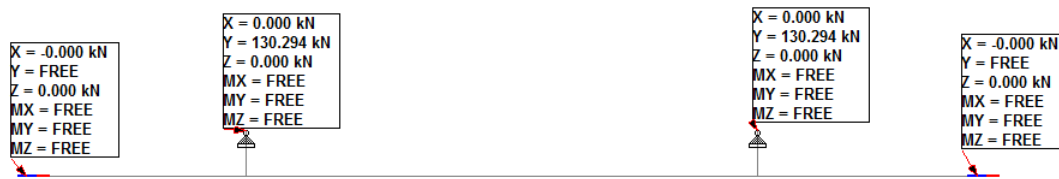


Figure 6.1: Geometry of the lower pipe and its model at Staad.Pro

With the trial and error method and an engineering intuition with respect to the structural checks done by Staad.Pro according to EN 1993-1-1:2005, a Circular Hollow Section CHS 139.7x8 is chosen with $UR_{max} = 0.61$, as shown in the below sketch.



The reaction sling forces are depicted in the next sketch and will be used for the design of the upper pipe.



6.2.2 Upper pipe

The external loading applied on the upper pipe will be the reaction forces of the slings, as obtained from the analysis of the lower pipe. The load and lift factors will not be multiplied with these forces as the associated uncertainties have already been involved, with the selfweight of the upper pipe being the only exception. The length of the rotating tube is equal to the length of the lower pipe in addition to some clearance on each side that will be added. This clearance has assumed to be 0.10 m on each side, and the pipe is considered as pinned connected to the padeye incorporated with the main frame, as revealed on Figure 6.2. The modelling and loads of this case are shown in next sketch. The forces are applied at the circumference of the pipe in a distance equal to the pipe radius, in order to adequately capture the torsion that is induced on the pipe by the slings.

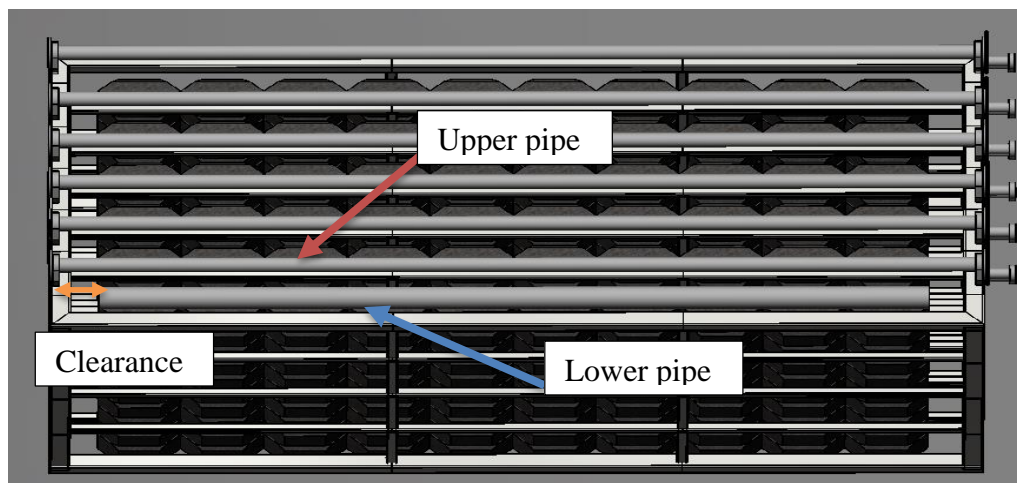
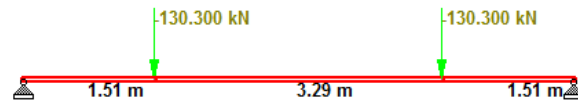


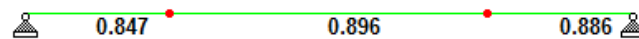
Figure 6.2: Illustration of different pipe lengths

Through the analysis is extracted that the use of a CHS 219.1x20 cross section that is initially selected has an $UR_{max} = 1.41$.

The aim is to keep the diameter of the pipe as low as possible in order to reduce the imposed torque. Therefore, it is decided to use a greater steel grade, namely S460 with the option SGR=4 in Staad.Pro. The selected steel grade has the following properties:

- Steel grade: S460
- Yield strength: $f_y = 460 \text{ N/mm}^2$
- Ultimate strength: $f_u = 540 \text{ N/mm}^2$

As result, the pipe demonstrates a better structural behavior and an $UR_{\max} = 0.90$, as pictured in the next sketch.



6.3 Load case 2: Subsea lift

The geometry and the cross sections of the pipes that will be used to lift and deploy the mattresses have been calculated in the previous sections. For the operational phase though, the loads should be reviewed in order to get the input for the design of the gears. During the operational phase the frame is located subsea and thus the submerged weight of the concrete mattress should be used for the calculations, namely 4.20 Te. Moreover, the DAF factor of 2.0 that was used during the design phase is quite an extreme approach and the more realistic value should be applied. The new loads and factors are presented below:

$$F_{mat,op} = \frac{M_{mat,sub} \cdot g}{12} = \frac{4.20 \cdot 9.81}{12} = 3.43 \text{ kN}$$

The following load factors are selected:

Load factor: $\gamma_{f,op} = 1.30$

DAF factor: $\gamma_{DAF,op} = 1.41$

Weight contingency factor: $\gamma_{con,op} = 1.15$

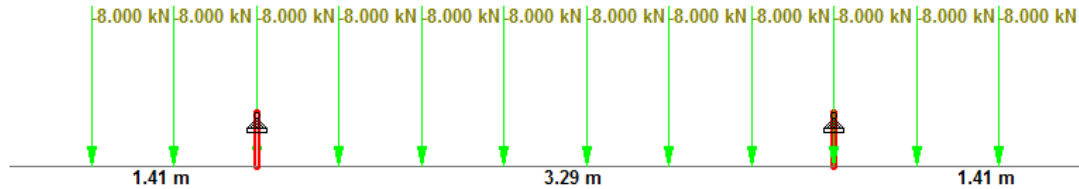
CoG shift factor: $\gamma_{COG,op} = 1.05$

Consequence factor: $\gamma_{cons,op} = 1.05$

Total load factor: $\gamma_{tot,op} = 2.33$

Hence, the new force to be applied on each hook point is:

$$F'_{mat,op} = F_{mat,op} \cdot \gamma_{tot,op} = 3.43 \cdot 2.33 = 7.989 \cong 8 \text{ kN}$$



The series of analyses is run again to get the sling forces during installation phase, and results to the reactions as presented in the next sketch (lower pipe-operational phase).



As obtained from the analysis, the sling forces that will tend to rotate the upper pipe while in operational phase are equal to $F_{sling,op} = 49.96 \text{ kN}$, and will be used as a design input for the torque introduced in the gearset. The design torque is calculated as:

$$T_{Ed} = 2 \cdot F_{sling,op} \cdot \frac{OD_{upper}}{2} \quad (5.6)$$

$$\Rightarrow T_{Ed} = 2 \cdot 49.62 \text{ kN} \cdot \frac{0.2191}{2} = 10.87 \text{ kNm}$$

Where: OD_{upper} = the diameter of the upper pipe

Chapter 7

Design of gears

7.1 Input data for the gear design

Herein, the input data will be presented, and additional parameters will be calculated based on the output of the problem of the handling mechanism and the requirements that have been set.

In the previous chapter it was calculated that the design torque of the handling mechanism is $T_{Ed} = 10.87$ kNm. The latter is produced by the selfweight of a single concrete mattress in the operational phase and thus will be induced in the gear that will be attached on the flange of the upper pipe. Therefore, the gear must have at least a torque output of the above magnitude, which will be denoted as T_2 from now onwards.

The ROV torque tool that will rotate the pinion to provide the required torque is a class 4 tool, as has been set in the requirements. This tool can produce up to 2.711 kNm of torque at a maximum speed of 40 rpm. These values are symbolized as T_1 and n_1 now onwards. It should be noted that the magnitude of the speed was provided by Subsea 7 ROV specialists.

The size of the gear governs the actual size of the gearset. The installation frame is set as requirement to be fitted on a standard truck size, in order to simplify and standardize the procedure. The length can be flexible, as commercial trucks can have long trailers up to 12 m. However, the maximum dimensions of height and width are 4 m and 2.55 m, respectively [37]. Therefore, it is set that the maximum gear size is 0.35 m and a clearance between the gears of 0.08 m, as pictures in Figure 7.1. The calculations result in a total width of: $6 \times 0.35\text{m} + 5 \times 0.08\text{m} = 2.50$ m, which is considered as a maximum boundary for the breadth of the structure.

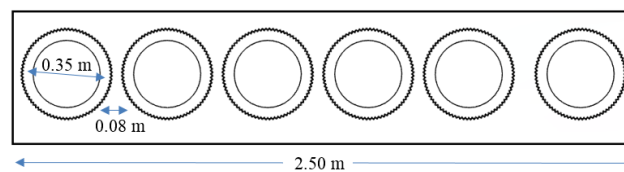


Figure 7.1: Dimensions for the spur gear design

The following table includes the input data.

Table 7.1: Input data for gear design

Parameter		Value	Units
Torque of ROV torque tool	T_1	2.711	kNm
Torque on the gear	T_2	10.87	kNm
Required torque ratio	$n_{T,req}$	$n_{T,req} = \frac{T_2}{T_1} = \frac{10.87}{2.711} = 4.01$	-
Speed of ROV torque tool	n_1	40	rpm
Maximum speed of the gear	$n_{2,max}$	$n_{2,max} = \frac{n_{rpm,1,max}}{n_T} = \frac{40}{4.01} = 9.88$	rpm
Maximum power on the pinion	$P_{1,max}$	$P_{1,max} = 0.1047 \cdot 40 \cdot 2.711 = 11.35$	kW
Maximum power on the gear	$P_{2,max}$	$P_{2,max} = 0.95 \cdot 11.35 = 10.78$	kW
Maximum outside gear diameter	$d_{a,max}$	0.35	m

7.2 Speed of deployment

The maximum speed of the gear can be 9.88 rpm, however as more conservative speed is considered, namely 9 rpm. In one rotation of the gear it is unreeled a length wire S :

$$S = 2\pi \frac{OD_{pipe}}{2} = 2\pi \frac{0.2191}{2} = 0.688m$$

The total deployment height is 8m (section 4.4), so the rotations needed to deploy the mattress, N_{depl} , are:

$$N_{depl} = \frac{8}{0.688} = 11.6 \text{ rpm}$$

Therefore, the lowering time of one mattress to the seabed, t_{depl} , is:

$$t_{depl} = \frac{N_{depl}}{9} = \frac{11.6}{9} = 1'17'' \text{ (1 min and 17 sec)}$$

The lowering speed is considered relatively high and is satisfactory to proceed in the design phase.

7.3 Generation of gears with Inventor

Autodesk Inventor is a 3D design, modelling and simulation tool, in which the user can design complex mechanical assemblies, and simultaneously test the prototype products with the software's build-in stress analysis and dynamic motion simulation tools. The key features of Inventor are its vast design capabilities, as it offers tabs to draft and calculate the strength of mechanical components such as bearings, shafts, gears (spur, bevel, worm), splines, keys, brakes and plenty more. The spur gear component generator (see Appendix C) will stand as the main gear design tool at the present thesis work, as it is capable of calculating the complex geometries, the various factors, applied forces, checking the dimensions and most significantly performs strength checks according to the available standards (ISO, AGMA).

Despite the fact Inventor 2015 uses ANSI/AGMA 2001-D04:2005 [33] standard for the gear design, the differences with the ANSI/AGMA 2101-D04 standard that was used to derive the stress equations, are negligible for the purposes of this study, and the strength calculations are considered valid and accurate.

The design is carried out on an assembly file where the 3D model will be generated, however the gears are also automatically separated in part files if they need special modifications. The spur gears generator design guide assists the user to input the desired geometric characteristics and based on them to calculate the remaining geometry and tooth profile. For instance, if the target of the generator is to calculate the module, m , and the number of teeth of the gears, N , the desired gear ratio (n_T) and center distance (C) must be inserted.

Also, the loads are identified by inserting the power and the speed of the pinion, and the software calculates the respective values of the gear and the induced tooth forces. Afterwards, the software offers a wide material library, with all desired properties on screen (allowable bending stress, allowable contact stress etc.), in accordance to the international standards, and the user can assign a material to both the pinion and the gear.

The required factors involved in the strength checks are either calculated or inserted by the user, and ultimately the allowable bending fatigue and contact stresses are calculated, with the programme indicating if the design is permissible or not.

A very significant feature is the precise generation of the tooth geometry in the separate part files, as the produced gearset is modelled without absolute accuracy of the teeth in favor of computational power. So, if the gear geometry is to be inserted and analyzed in a FE software this procedure should be followed. Furthermore, the strength checks and the various dimensions of the gears are extracted in an *html* file.

7.4 Spur gear design

In the current work the desired speed, torque, power, maximum gear size are known and will be the input to the generator tool. The inserted values are illustrated in Appendix C.1 alongside with the calculated forces and the safety factors on the left of the interface. In Appendix C.2, the geometric characteristics of the gear are viewed.

7.4.1 Material of spur gears

The strongest available material is selected, namely 14NiCr18, a carburizing structural steel, widely used in the automation, ship-building, aerospace industries, and especially in gear and shaft design. The material properties are:

- Carburizing structural steel: 14NiCr18
- Yield strength: $f_y = 885 \text{ N/mm}^2$
- Ultimate strength: $f_u = 1130 \text{ N/mm}^2$
- Density: $\rho = 7,850 \text{ kg/m}^3$
- Modulus of elasticity: $E = 206,000 \text{ N/mm}^2$
- Poisson ration: $\nu = 0.30$
- Allowable bending strength: $f_b^{\text{allowable}} = 483 \text{ N/mm}^2$
- Allowable contact stress: $f_c^{\text{allowable}} = 1550 \text{ N/mm}^2$

7.4.2 Geometry of spur gears

The input data for the geometry of the spur gears is:

- Outside diameter of gear: $d_{a,g} = 0.336 \text{ m}$
- Speed of pinion: $n_1 = 40 \text{ rpm}$
- Torque of pinion: $T_1 = 2.711 \text{ kNm}$
- Efficiency: $\eta = 0.95$
- Gear ratio: $n_T = 4.5$
- Face width: $F = 0.05 \text{ m}$

7.4.3 Strength of spur gears

All the geometric characteristics of the gears, the load factors and the results of the strength checks can be seen in the figures attached on Appendix C.2, as extracted from Inventor. Herein, the strength calculations will be performed with the use of the AGMA equations presented on Chapter 3. As the pinion is the most vulnerable part, all calculations refer to it.

AGMA rooting bending stresses

The tangential force and the factors for the calculation of the bending stress as extracted from Inventor are:

Table 7.2: AGMA factors for root bending stresses

Parameter	Value
W_t	75305 N
K_O	1
K_v	1.014
K_s	1
F	50 mm
m	4 mm
K_H	1.114
K_B	1
Y_J	0.485

So, the maximum root bending stress, $\sigma_{b,p}^{AGMA}$, of the pinion is:

$$\begin{aligned}
 \sigma_{b,p}^{AGMA} &= W_t K_O K_v' K_s \frac{1}{F \cdot m} \frac{K_H K_B}{Y_J} \\
 \Rightarrow \sigma_{b,p}^{AGMA} &= 75305 \cdot 1 \cdot 1.014 \cdot 1 \cdot \frac{1}{50 \cdot 4} \frac{1.114 \cdot 1}{0.485} \\
 \Rightarrow \sigma_{b,p}^{AGMA} &= 877 \text{ N/mm}^2
 \end{aligned}$$

The allowable bending stress for unity safety factor is:

$$\sigma_{b,p}^{allowable} = \frac{483 \cdot 0.972}{1 \cdot 1 \cdot 1} = 469.5 \text{ N/mm}^2$$

The utilization ratio due to bending stresses is:

$$UR_b^{AGMA} = \frac{\sigma_{b,p}^{AGMA}}{\sigma_{b,p}^{allowable}} = \frac{877}{469.5} = 1.87$$

AGMA surface contact stress

Table 7.3: AGMA factors for contact stresses

Parameter	Value
Z_E	$191.7 \text{ (N/mm}^2\text{)}^{-1}$
W_t	75305 N
K_O	1
K_V	1.014
K_S	1
F	50 mm
d_w	4 mm
K_H	1.114
Z_B	1
Z_I	0.485

The maximum contact stress, $\sigma_{c,p}^{AGMA}$, is:

$$\begin{aligned} \sigma_{c,p} &= Z_E \sqrt{W_t K_O K_V K_S \frac{K_H}{F \cdot d_w} \frac{Z_R}{Z_I}} \\ \Rightarrow \sigma_{c,p} &= 191.7 \sqrt{75305 \cdot 1 \cdot 1.014 \cdot 1 \cdot \frac{1.114}{50 \cdot 72} \cdot \frac{1}{0.109}} \\ \Rightarrow \sigma_{c,p} &= 2822.5 \text{ N/mm}^2 \end{aligned}$$

The allowable bending stress for unity safety factor is:

$$\begin{aligned} \sigma_{c,p}^{allowable} &= \frac{\sigma_{HP}}{S_H} \frac{Z_N Z_W}{Y_\theta Y_Z} = \frac{1550}{1} \frac{0.952 \cdot 1}{1 \cdot 1.1} \\ \Rightarrow \sigma_{c,p}^{allowable} &= 1475.6 \text{ N/mm}^2 \end{aligned}$$

The utilization ratio due to contact stresses is:

$$UR_b^{AGMA} = \frac{\sigma_{c,p}^{AGMA}}{\sigma_{c,p}^{allowable}} = \frac{2822.5}{1475.6} = 1.95$$

A first interpretation of the UR indicates that the designed gearset will fail, with the contact stresses on the pinion being the most severe response inducing possible pitting of the teeth. However, the gear analysis is a rather complex procedure due to the nature of the imposed loads on the teeth and the contact stresses, which involve high nonlinearities and large magnitudes. These issues are treated with load factors in the standards which use semi-empirical formulae. Nonetheless, estimating correct and accurate factors is not straight forward and some uncertainties are present. In addition, the involute tooth geometry is very complex and the standards make several assumptions; for instance, AGMA assumes that the load is distributed in the whole contact area of the face width, whereas ISO applies the load at the tooth tip. So, it becomes obvious that further investigation regarding the gear strength is needed. In the next chapter, Chapter 8, a numerical analysis is carried out, with purpose to draw a final conclusion about the gear design.

Chapter 8

Verification of spur gears strength via FEA

8.1 Introduction

Gear design and manufacturing is a relatively complex and rigorous science, as many load factors and geometrical design parameters are involved. Even experienced and skilled mechanical engineers find the process challenging, since the conventional office practice utilizes standards and practices to select (sometimes even assume) a large number of parameters, resulting to time demanding and repetitive job.

Despite the extensive ongoing research on gear design in aspects of their efficiency, operational quality and durability [49], still some obstacles do exist in the accurate calculation of root bending and contact stresses of the spur gears due to the semi-empirical nature of the formulas provided by the standards. Both type of stresses depend on the complex involute tooth geometry, with the contact of the teeth being also a highly nonlinear phenomenon that introduces a maybe not insoluble, yet laborious mathematical problem. Hence, the researchers' attempt to overcome these limitations is the utilization of the Finite Element Method (FEM), to accurately extract and assess the stress-state of gears [49-57]

8.2 Reasons requiring a verification via FEA

The AGMA standard is used in the present work to calculate the gear stresses, and the results revealed that the design conducted in Chapter 7 suggests failure. However, as has been discussed there are many complex geometry issues that the standard deals with empirical approaches, whereas the calculation of the various factors is rather challenging. The aforementioned amplify the conclusion that the strength calculations according to AGMA are rough estimations and not precise. The load in AGMA is assumed to be uniformly distributed along the line of contact, while this is not the real phenomenon as the meshing stiffness of the teeth pair dominates and defines the

critical load points [57]. The results for the equivalent bending stress at the tooth root are not satisfactory and a FEA should be considered. Most of the findings in the literature confirm that the FEM can be the most accurate and precise tool to establish the root bending stresses [52]. This is also enhanced by some authors [49, 50, 52, 57] that have observed big deviations in the contact stresses when compared to numerical ones.

Moreover, despite the indications for failure according to the standards, gear have been manufactured and do operate successfully. I should be also noted that there have been some mistakes in how Inventor calculates the provided factors and especially the geometry factor. The issue has been acknowledged by mechanical engineers in Autodesk and is under investigation till the time of writing this thesis [58].

Consequently, it is rational and legitimate to conduct a 3D FEA to calculate the correct stress-state of the gear design and conclude if this particular gear solution can proceed perhaps to the manufacturing phase.

8.3 Parameters of FEA

It has been discussed beforehand that when complex mechanics are involved the required FEA will be carried out in Ansys software, and in particular in Ansys Workbench R14.5. The steps of the numerical analysis have been developed in reference with relevant research papers [58-50] and are described in the following sections. The full report as extracted from Ansys is enclosed in Appendix D.

8.3.1 Model geometry

Traditionally, the design of the involute tooth shape by analytical means has been considered cumbersome and time-consuming. Even the main illustration of the gears by the Inventor spur gear generator yields some small interference, as seen in Figure 8.1.

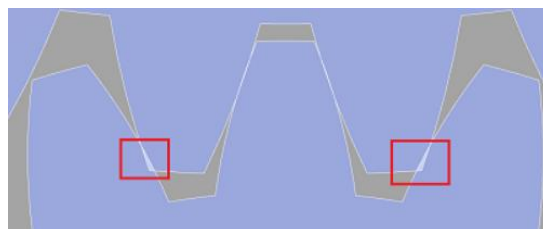


Figure 8.1: Interference observed in the output from Inventor spur gear generator

The main reason is that the precise geometry would require large computational resources and so a separate process has to be followed in order to get the desired tooth shape. This is achieved by enabling the option “Export tooth shape” and design accordingly the gear again. Afterwards, the inner rims of the gears are created to be able to apply the boundary conditions needed for the analysis. The final gear geometry and teeth shape are depicted in Figure 8.2. The file is saved with as *.stp* extension to be imported to Ansys.

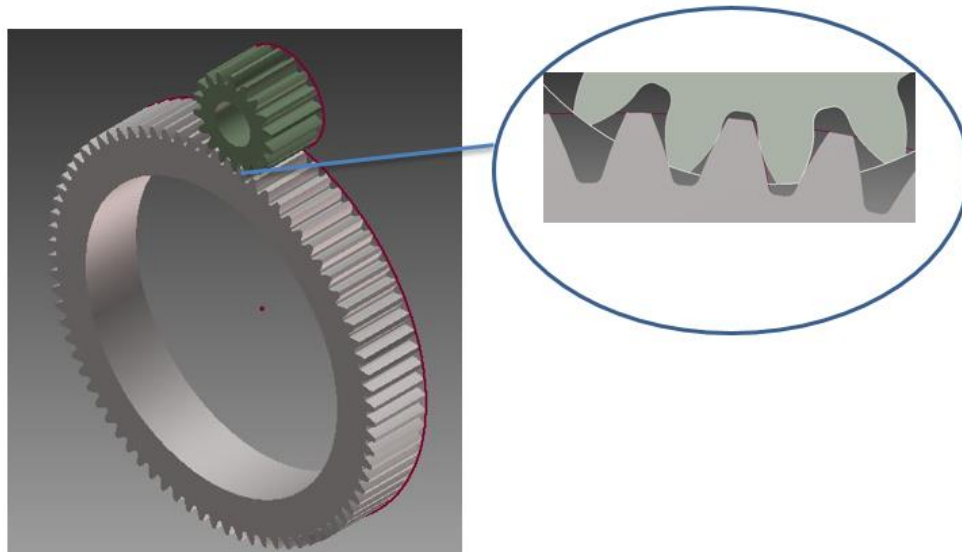


Figure 8.2: The final geometry of the spur gears and a zoom on the teeth shape

8.3.2 Mesh

Many series of analyses were carried out in order to set the right parameters that would produce sensible and valid results in a reasonable time frame. The mesh is a dominant parameter of the FEA, as the gear parts are relatively small mechanical parts and furthermore one of the desired outputs is the calculation of the highly nonlinear contact stress in the teeth. A balance should be found between accurate and valid results and computational resources. Herein, it is decided to have a general coarse mesh of the two bodies as the area of interest are the two teeth in contact. That being the case, it is decided to further refine the faces of the tooth in contact with the face sizing option of Ansys. The maximum elements size was set at 0.2 mm.

The type of elements forming the gears is the 20-node SOLID 186, which exhibits high order displacements of quadratic behavior. Each node has three transitional degrees of freedom in the x, y, and z direction. The good performance of this type of element comes with a cost in computational resources, as it composes a very large model. The final model is made of around 289k nodes and 64k elements, and the refined area is shown in Figure 8.3.

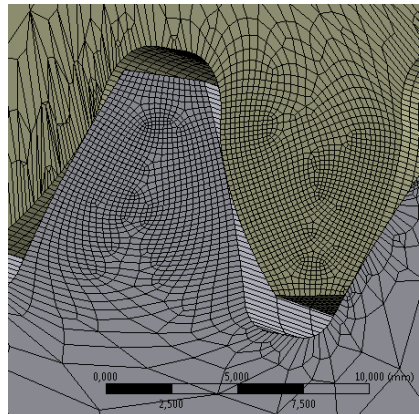


Figure 8.3: Refined mesh of the teeth in contact

8.3.3 Contact

The contact region is defined as frictionless and only one tooth pair is selected to be in contact, involving two faces (see Figure 8.3), as an analysis containing the study of more pairs would be impossible due to computational power restrictions. The contact elements of the pinion are CONTA 174 while the target face was assigned with TARGE 170 elements. The normal contact stiffness factor is set to unity while the penetrations tolerance is controlled by the software. The interface treatment is selected as Adjust to Touch to capture the initial touch of the contact points, while Augmented Lagrange is selected in order to reduce the sensitivity to the contact stiffness.

8.3.4 Boundary conditions

Torque with a value of 2.711 kNm (output from ROV torque tool) is applied in the inner rim of the pinion in conjunction with a frictionless support so it allows a tangential rotation, while the radial and axial deformations are restricted. The bore of the gear is fixed, and all movements are constrained. In addition, a remote displacement is applied on each side of both gears. The purpose to enable this remote boundary conditions is to constrain the translational motion of the gears, so the values of displacements in all three directions are set to zero, while the rotational direction is unrestricted and able to simulate the accurate phenomenon.

8.3.5 Analysis settings

The direct solver of the programme is utilized, as suggested by the programme, while all other parameters are set to default values.

8.3.6 Solution

The equivalent (Von Mises) stresses are extracted in order to calculate the root bending stresses, while the contact stresses are extracted as the pressure between the contact interfaces.

8.4 Results and discussion of FEA

Generally, the maximum bending stresses occur at the middle face width of the root, and the maximum contact stress is observed near the center of the contact curve. As has been discussed, if the gears are made from the same material (as in this case) the pinion will have the most critical response and will fail before the gear. Therefore, only the results regarding the response of the pinion are demonstrated.

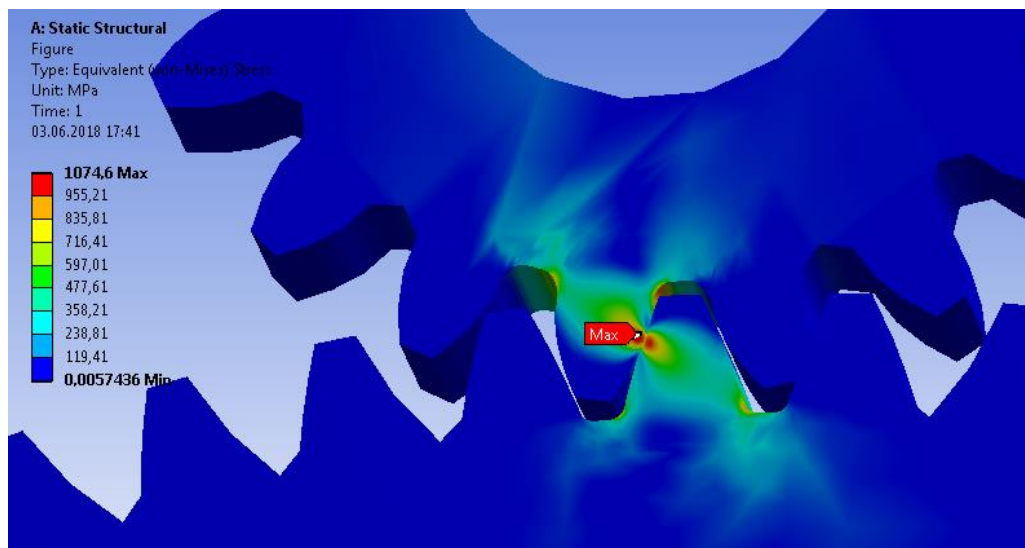


Figure 8.4: Equivalent stresses for torque value of 2.711 kNm on the pinion bore

Figure 8.4 illustrates the equivalent state of stress of both gears. The maximum equivalent stress occurs on the pinion and is equal to: $\sigma_{VM}=1075$ MPa. The FEM has a very good state stress distribution and manages to capture a valid response, similarly to findings of literature. The left side root fillet is under compression whilst the right side exhibits tensile stresses. The latter are the highest stresses on the tooth root, and thus are treated as the maximum root bending stresses of the pinion, and are equal to: $\sigma_{VM,b}=946$ MPa. If compared with the allowable nominal bending stress the UR is:

$$UR_b^{VM} = \frac{\sigma_{VM,b}}{\sigma_{FP}} = \frac{946}{483} = 1.96$$

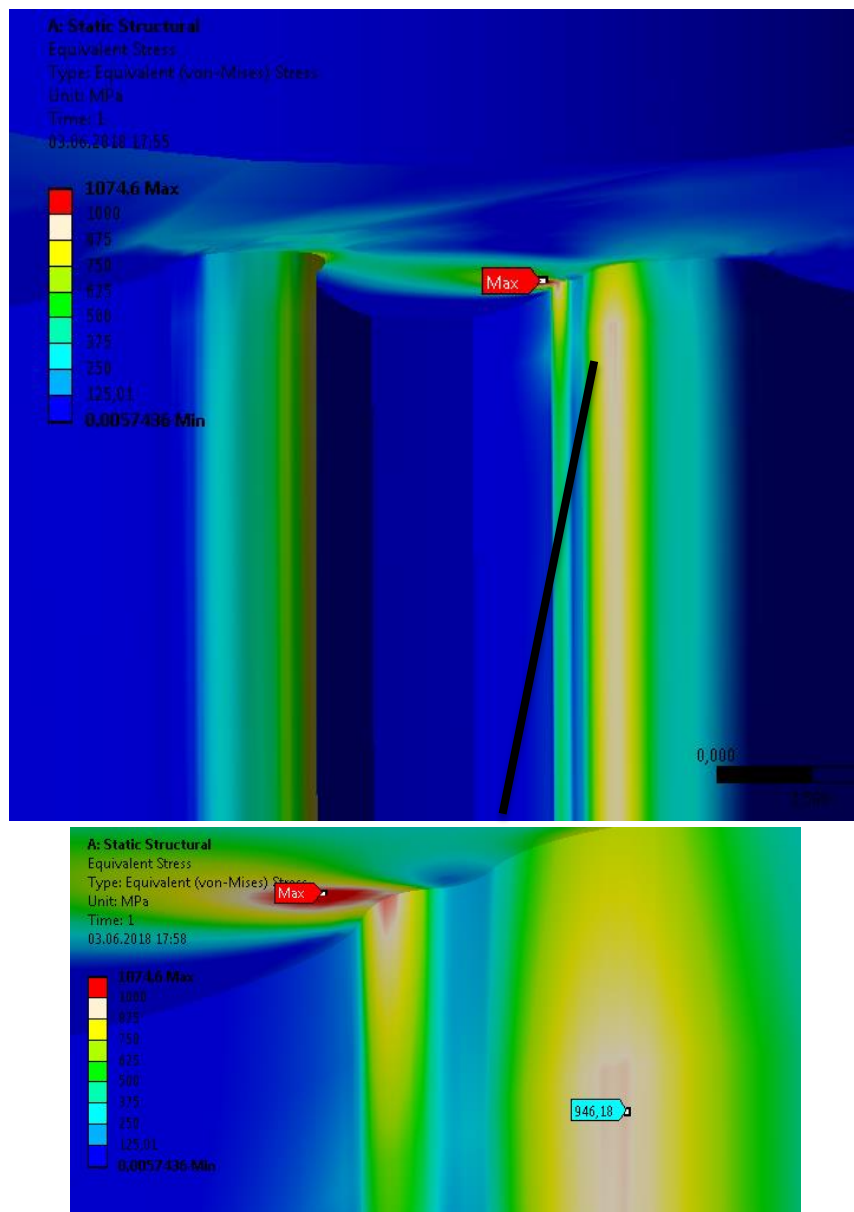


Figure 8.5: Above-The equivalent stresses on the root of the pinion, Below- A zoom in the maximum stresses at the root tooth

The compressive stresses are 6% lower. The produced results confirm that the failure due to bending stresses can lead to tearing of the root and finally to tooth breakage.

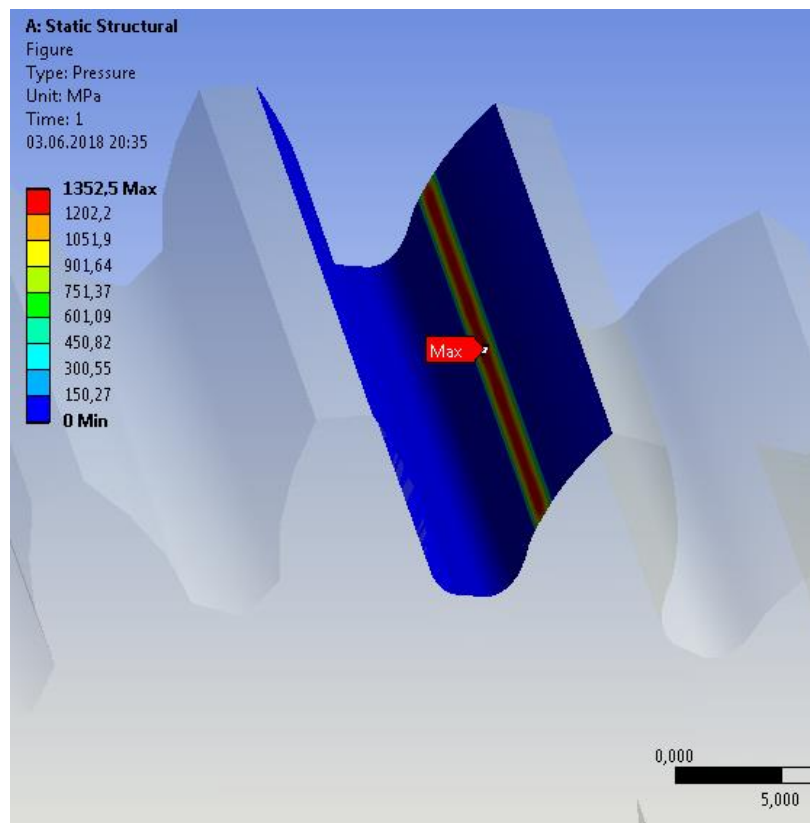


Figure 8.6: Contact stresses of the pinion according to FEA

The maximum contact stresses are located exactly on the area in the middle of the contact ellipse, as illustrated on Figure 8.6. This response is in good correspondence with the findings from the literature, and the thinner the area of contact is, the results are considered of higher quality. The maximum value is $\sigma_{c,FE}=1352.5$ MPa, and in contrary to the results of the bending stresses though, the produced magnitude of the contact stresses is considered unsatisfactory. This will be further elaborated in the discussion in the next paragraph.

8.5 Comparison of AGMA and FEM results

A comparison between the stresses calculated with AGMA [33] and the produced results from FEA is essential to extract a final conclusion. Table 8.1 summarizes the calculated stresses.

Table 8.1: Results of AGMA [33] calculations and FEA

Type of stress	Calculation based on	Value [MPa]	Allowable value	UR	Deviation
Root bending stresses	AGMA	877	469.5	1.87	7.5%
	FEA	946		2.01	
Contact stresses	AGMA	2882.5	1475.6	1.95	52.82%
	FEA	1352.5		0.92	

A very good correspondence is noted between the AGMA and the FEA root bending stresses, with the deviation being in acceptable limits. As shown, the solution according to AGMA underestimates the root bending stress, with the latter being in agreement with similar findings in the literature [52, 57]. The explanation is that AGMA is based on the Lewis equation where he considers the involute profile as a parabolic shaped beam in bending, and also neglects the stress concentration factors, which are present at the root fillet of the tooth. Overall, the FE analysis captured sufficiently the root bending stresses and can be considered as the most accurate technique for a precise calculation.

On the other hand, the numerical results of the contact stresses fail to be considered as valid. The value of FEA contact stress is very low and not in sensible engineering limits. Indeed, most researchers [49, 52, 53, 57] argue that obtaining exact results of contact stresses is practically unachievable due the vast computational resources that are required. The high nonlinear contact area needs a great level of mesh refinement, which was attempted in the present work, but failed because of the low computational power available. Nevertheless, the analyses managed to, at least, capture the impact phenomenon, as pictured in Figure 8.4.

In conclusion, the results of the AGMA equations and FEA, despite the fact that they are not in full agreement, both indicate that the designed gear configuration is not permissible. Both tooth breakage and pitting of the tooth material are possible due to URs greater of unity, and the design should not proceed under these conditions.

Chapter 9

New solution approach with the use of different ROV tooling

In the previous Chapter it was clearly demonstrated that the designed gear configuration will ultimately fail due to both excessive root bending and contact stresses. The considered design, though, fulfilled the torque, speed and space requirements. So, instead of consuming the majority of this work in the vast field of gear design, another application is proposed by the author.

9.1 ROV torque tool multiplier

One of the desired conditions is decided to be modified, in particular the class of the torque tool. After conducting a research on the market for ROV torque tools, it was found that when very high values of torque are required on a class 4 interface, torque tools multipliers are utilized. The torque multipliers usually incorporate an internal, sophisticated planetary gear system which can offer up to 15:1 mechanical advantage. The common practice is to use the multiplier alongside with class 4 tool, with the combined assembly having a tool range from 2.711 kNm to 34 kNm. So, while the input value is a class 4 interface, the multiplier provides outputs for class 5, 6 and 7. It is manufactured with light-weighted materials and weights around 75 kg in air and 55 in water, so it can be handled relatively easy by the ROV. However, the total payload of a ROV has limitations, so a good planning of the total tooling package it carries is essential. A torque tool multiplier with its full characteristics can be viewed in Appendix A.3, as provided by a ROV tooling company.

9.1.1 Lowering speed

Not all the capacity of the torque multiplier will be utilized. The required mechanical advantage for the deployment of the concrete mattress is $n_{T,req}=4.01$, so the lowering speed to the seabed of a single mattress is the same as calculated in section 7.2, namely 1 min and 17 sec.

9.2 New configuration of the handling mechanism

It is decided that the new interface will be a class 7 receptacle. In such way, both the combination of the class 4 torque tool with the multiplier and a standalone class 7 torque tool (up to 34 kNm available) can be utilized.

Within the new approach is also selected to design a common panel with bores that will act as the restriction support for all upper pipes, instead of designing six custom-made padeyes. The panel is easier and simpler to be manufactured and installed, and offers very good structural response.

The receptacle must be attached on a stable structure (the steel frame), in order to take over the reaction forces, which are produced during the rotation of the tool. Also, the ROV bucket needs to be in alignment with the longitudinal axis of the upper pipe in order to rotate the stem that will be welded on the center of the end-flange plate, and produce the required torque. This fixed support area will be another steel plate with six bores, so the stem is extended through it inside the receptacle. The final configuration of the multi-handling mechanism is shown in Figures 9.1 and 9.2.

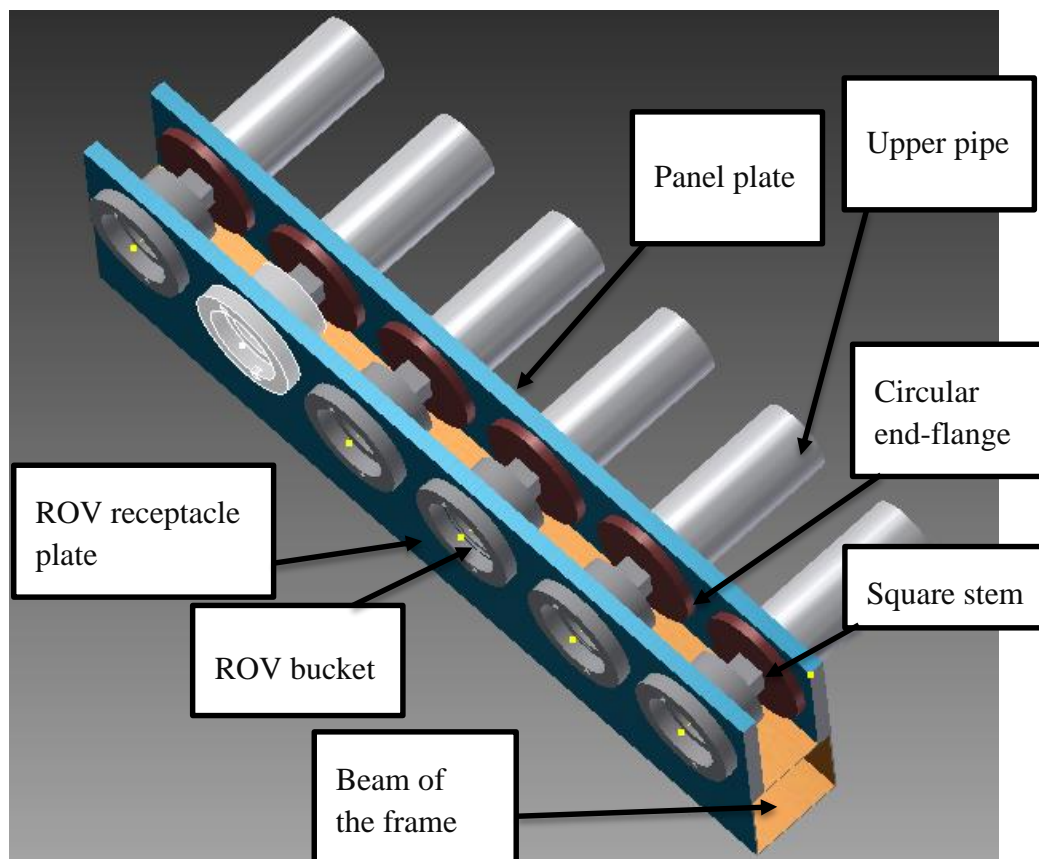


Figure 9.1: Final configuration of the multi-handling mechanism

The steps of the concrete mattress deployment are similar to the ones presented in Chapter 4, where the only difference is that the ROV torque tool rotates directly the stem. In the sequel, the latter as being mounted on the circular end-plate, will start rotating the upper pipe and initiate the unreeling of the sling wires.

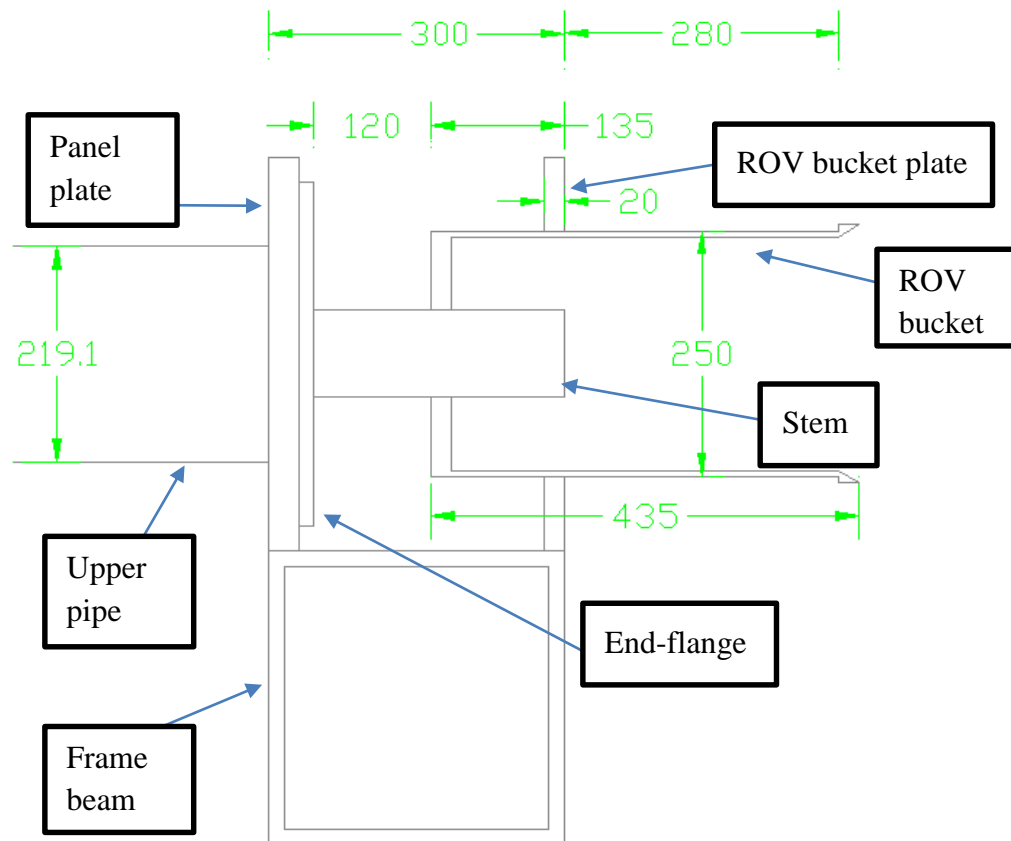


Figure 9.2: Side-view of the multi-handling mechanism

9.3 Locking mechanism

It is essential to design a robust and safe locking arrangement to prevent the rotation of the upper pipe due to the selfweight of the concrete mattress. In view of this, two alternative locking methods are proposed in the current section. The great importance of the locking approach deems necessary to conduct a thorough analysis of the arrangement, and therefore a future research is recommended.

Locking pin

The idea of utilizing a locking pin is discussed also in Chapter 4, as consisting part of the initial concept. According to that, the pin penetrates the end-flange and the panel plate, securing the upper pipe against unwanted rotation. In light of the new

configuration shown in Figure 9.1, the ROV bucket plate creates accessibility issues to the removal of the pin, as the access to this area will be limited. Therefore, the new design should penetrate also the ROV bucket plate and thus be secured in three components, considering the end-flange and the panel plate.

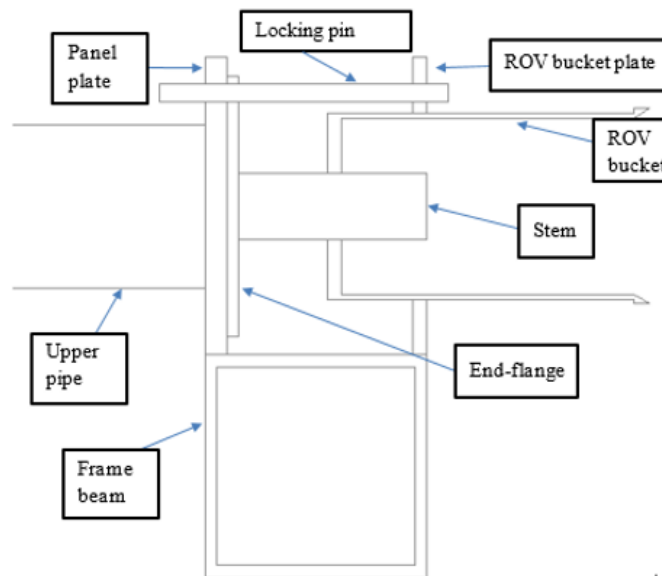


Figure 9.3: Side view of the handling mechanism depicting the locking pin

The locking pin can be similar to the one of a green pin ROV shackle with tapered pin and incorporate a fishtail-handle in the end, resulting in a ROV friendly component. An illustration of the green pin can be seen in Figure 9.4.



Figure 9.4: Green pin ROV shackle with tapered pin and fishtail-handle (vanbeest.nl)

Locking flaps

An alternative approach to secure the rotation of the upper pipe is to design a special end-flange. For the development of this proposal it is considered that the sling forces will tend to rotate the upper pipe in the counter-clockwise direction, as shown in Figure 9.5. In each side of the flange one piece of steel rod can be welded, protruding perpendicular to the plane of the paper. Similarly, the circular flange can have two protruding flap sections. On the left side, a small piece of steel bar can be bolted on its left end, but still be free to rotate with respect to this point. The bar is also supported

by the rod, as it stands on top of it. The left flange flap is supported by the bar, which restricts its rotation. A similar arrangement is made on the right side, with the difference that the bar is located below the rod, to restrict the upward motion of the right flange flap.

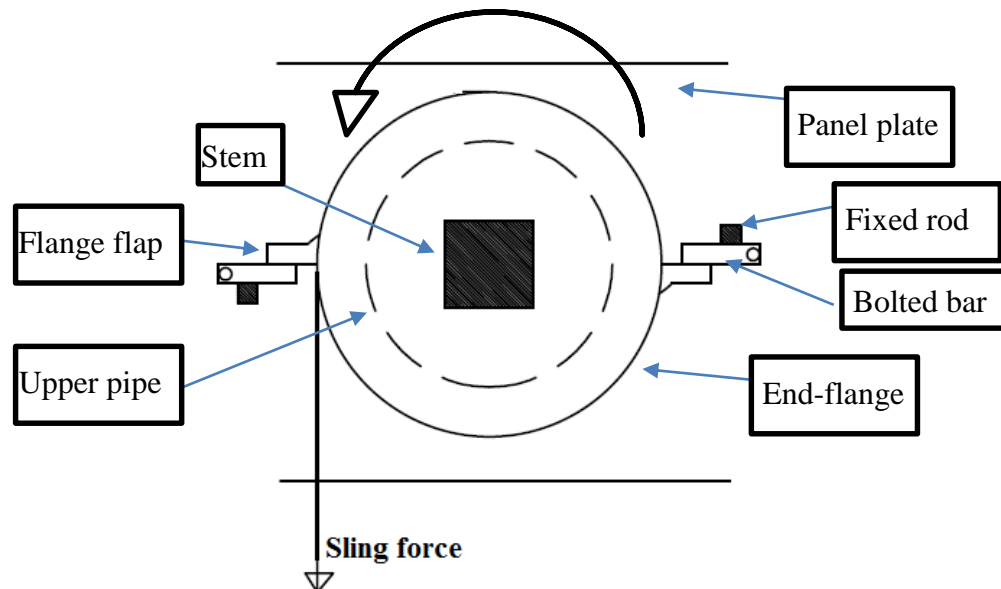


Figure 9.5: Front view of the panel plate depicting the protruding-locking flaps

In order to unlock this mechanism, the ROV torque tool should produce torque in the clockwise direction, in which the upper pipe is free to rotate. The angle of rotation should be at least 180° , so the flaps rotate the bolted bars to the vertical position shown in Figure 9.6. Ultimately, the ROV torque tool should generate torque towards the counter-clockwise direction, as the flange (and the upper pipe) is free to rotate now.

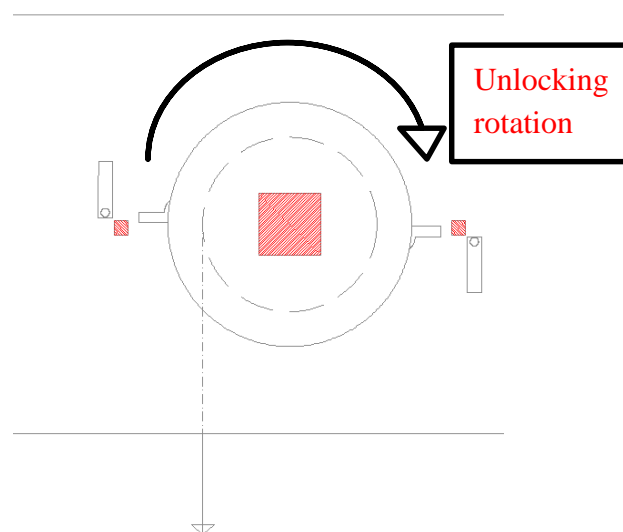


Figure 9.6: Direction of the unlocking rotation for the flap-locking mechanism

9.4 Design of the new setup

9.4.1 ROV Buckets

The new class 7 ROV bucket for the rotary operation is depicted on the drawing on Appendix A.1, and its structural integrity is satisfactory as it is a standard product according to ISO [28]. The bucket is bolted with four bolts on the plate and acts as a docking and securing point for the ROV, and thus docking loads are imposed to the plate bore. ISO [28] recommends the interface of the structure, the plate in this particular case, withstands the typical ROV intervention forces and loads, as shown in Figure 9.7.

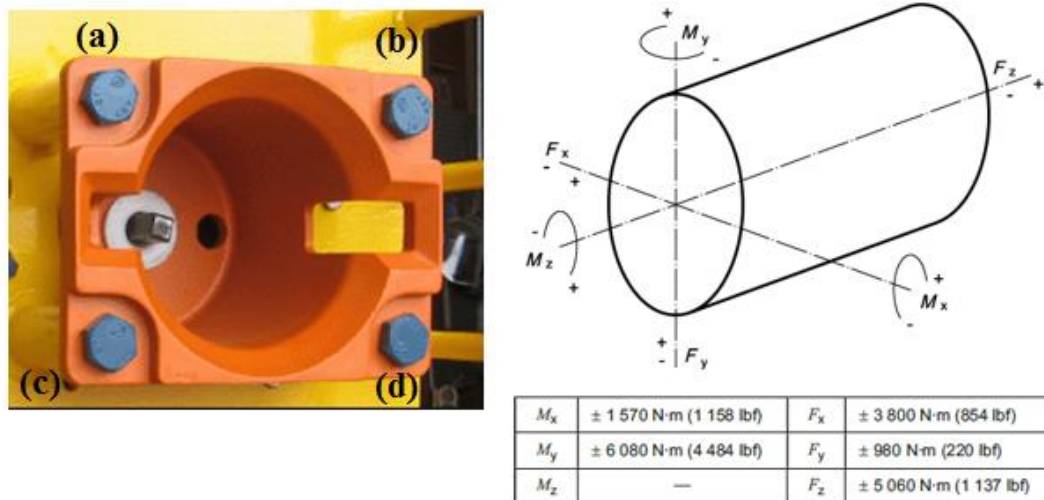


Figure 9.7: ROV bucket bolted on a plate panel (left) and the related intervention loads imposed on the ROV interface [28]

The loads of Figure 9.7 are considered for the selection and check of the bolts, which is performed in Appendix E. Additionally, the moment induced by the rotary operation of the torque tool is taken into account, namely $T_{Ed}=10.86\text{ kNm}$. The most severe load case scenario is used as basis for the design, where all loads are acting simultaneously and their effects are combined. The performed checks regarding the structural integrity of the bolts are due to tension, shear, slip resistance and bearing resistance. The view of the ROV bucket is depicted on Figure 9.8, while the all six ROV buckets bolted on the support plate are shown in Figure 9.9.

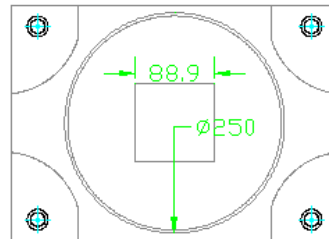


Figure 9.8: ROV bucket front view

Four preload M20 class 8.8 bolts are found to be adequate in securing each bucket on the plate.

9.4.2 Plate incorporating the ROV buckets

The plate where the ROV interfaces are bolted spans 2.55 m with 0.40 m height, and is welded (fixed) on the outer width-side of the frame. Six ROV buckets will be mounted on the plate, so the plate has six bores with their middle point in alignment with the respective center of the stem. The diameter of the bore is slightly larger than the diameter of the ROV tubular housing (243 mm), namely 250 mm in order to compensate the tolerances of the bucket dimensions or other deviations (e.g. painting). A simple FE stress check (see Appendix E) is performed in the plate subjected to the loading of Figure 9.7, with Inventor's stress analysis feature. The thickness of the plate is selected to be 20 mm, and in the analysis the bore located nearest to the outer side is examined. To reduce the computational power needed only one adjacent bore is included, as shown in Figure 9.10 (with yellow colors the applied loads as per Figure 9.7).

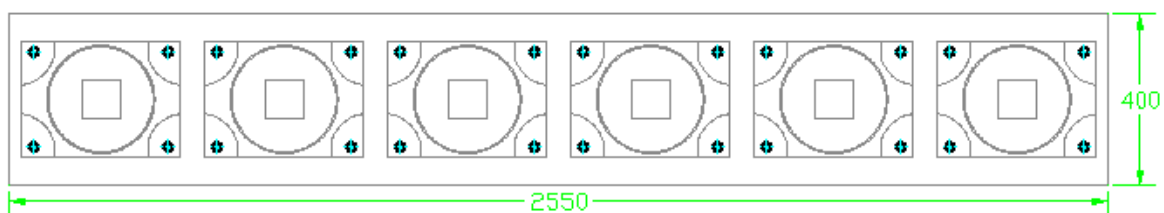


Figure 9.9: Plate incorporating the ROV buckets

The equivalent (Von-Mises) stresses are extracted, with the maximum value being equal to: $\sigma_{VM,ROV,pl}=0.52$ MPa, resulting to a negligible UR (less than 0.01).

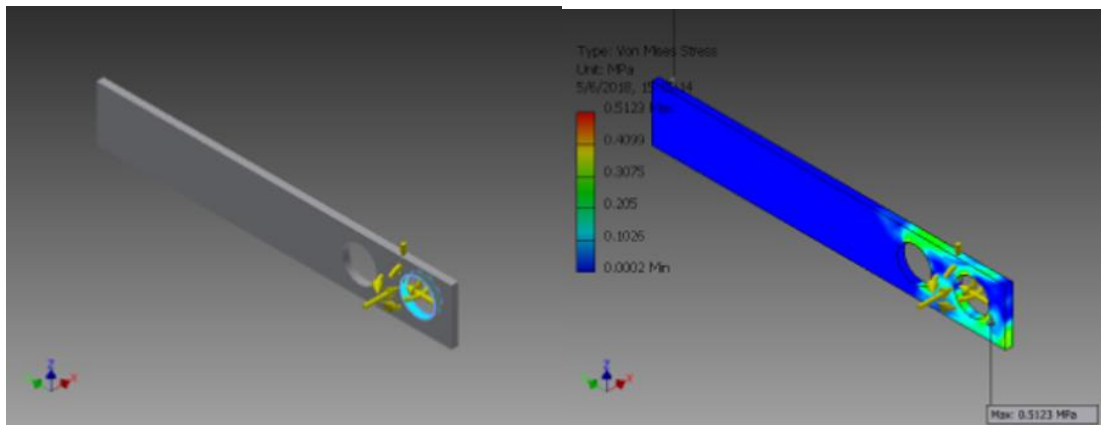


Figure 9.10: Left- The ROV plate model with the applied forces, Right- The equivalent stresses

9.4.3 Panel plate

Similarly to the plate which embodies the ROV interfaces, the panel plate has a length of 2.55 m and a chosen height of 0.40 m. The geometry of the panel plate is pictured in Figure 9.11 and the selected thickness is 30 mm. The panel has six bores where the upper pipes are stabilized and connected with the end-flanges to create a solid support. The reaction forces on the supports consist the design values for the plate, as taken from Staad.Pro. The bore has a diameter of 250 mm, despite the upper pipe's different diameter of 219.1 mm. This is due to the existence of a layer of a polymer material with low friction, so the pipe can easily rotate.

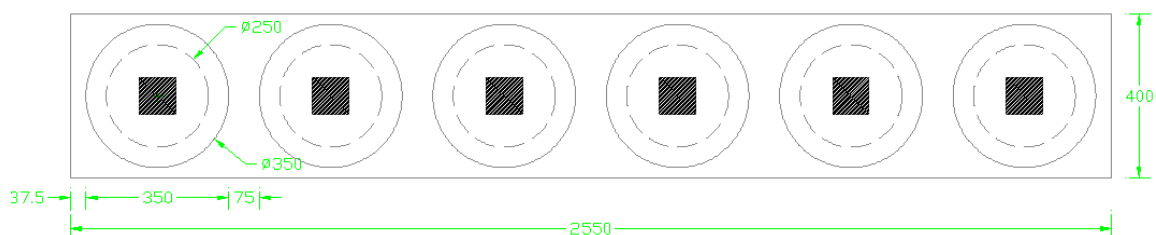


Figure 9.11: Panel plate geometry

The selected polymer material is POM and has the following characteristics [59]:

- Yield strength: $f_y = 67 \text{ N/mm}^2$
- Modulus of elasticity: $E = 2,300\text{-}2,800 \text{ N/mm}^2$
- Shear modulus: $G = 852\text{-}1,037 \text{ N/mm}^2$
- Poisson ration: $\nu = 0.35$
- Friction coefficient $\mu = 0.14$

The contact stresses exerted on the POM interface are analytically calculated on Appendix E. The compression resistance check is also performed. In each case, the URs are found to be below unity (see also Table 9.1).

9.4.4 Stem

The square stem is designed in accordance to ISO [28] specifications and can be seen in Figure 9.2. It has a length of 255 mm and width 88.9 mm and is welded on the end-flange. The stem is subjected to torsion due to the torque input from the ROV torque tool, namely $T_{Ed}=10.86$ kNm. Due to the fact that it is designed in accordance to ISO [28] dimensions, only a weld check is carried out. The resultant UR is found to be in acceptable limits (see also Table 9.1).

9.5 Results of the new design

The components of the new configuration are checked individually according to the most unfavorable load state. The analyses showed a satisfactory structural integrity of all items, and the detailed calculations can be found in Appendix E. Table 9.2 summarizes the results, and shows the highest UR of each component.

Table 9.1: Summarized results of the components of the new configuration resulting to highest UR

Component	Structural Check	UR _{max}
POM cross-section	Cross sectional resistance	0.88
Panel plate	Bore cross-section resistance	OK, due to POM check
ROV interface plate	Cross section resistance at the bore	≤ 0.01
Bolts	Bolting resistance	0.99
Stem	Weld check	0.54

In conclusion, the examined parts and the performed checks allow the fabrication of the new setup. However, they do exist some areas and more specifically some geometrical and space limitations aspects that need to be studied before fabricating the whole frame structure.

Chapter 10

Conclusions

10.1 Concluding remarks

A concept for an installation tool that will deploy multiple concrete mattresses in a single lift was proposed by Subsea 7. A handling mechanism that controls the lowering of each mattress on the seabed is the key feature of this tool. The primary objective has been to resolve the concept under certain requirements, elaborate on its operational and installation aspects, and assess the structural integrity of the finalized proposal.

Initially, the concept is thoroughly elaborated and all its components are presented alongside with their functionality. All installation steps are discussed under rational assumptions and the final framework for the design is set.

A static analysis is performed during design phase of the spreader beam (lower pipe) and the upper pipe with the LRFD approach. The cross sectional characteristics were defined through series of analyses that were carried out in Staad.Pro under ULS limit state. All load factors associated with marine and subsea lifting operations are included, in conjunction with the dynamic amplification factor (DAF) which accounts the dynamic loading in the static analysis. Both the lower and upper pipe have circular hollow sections, namely CHS139.7x10 and CHS219.1x20 respectively. These members are prone to forming air pockets and therefore drainage holes should be considered. The elastic verification criterion shown in equation (5.5) governs the design, whilst the second highest utilization ratio (UR) for both sections is due to the bending moments caused by the dead weight of the concrete mattress and the selfweight of the components. The maximum URs are 0.61 and 0.90 for the lower and upper pipe, respectively. It should be noted that the steel grade of the upper pipe is S460, as the goal is to increase its strength while having the lowest possible pipe diameter. A pipe with a larger diameter would create a longer lever arm for the acting sling forces and thus impose higher torque requirements for the handling mechanism. Afterwards, an in-place static analysis is conducted to get the required torque input for the operation of the mechanism, where the load factors were reduced accordingly. The resultant torque value is 10.87 kNm.

A class 4 ROV torque tool is utilized for the operation, with maximum output torque of 2.711 kNm and 40 rpm speed. In order to achieve the required torque value of 10.87 kNm, a gearset is considered, in order to increase the mechanical advantage of the torque tool. The gear design is performed with an Autodesk Inventor feature, as forming a detailed gear geometry is rather laborious. The two dominant gear failures

are examined, namely tooth breakage due to excessive bending stresses and pitting due to fatigue contact stresses, with reference to AGMA standard. The strength checks showed URs greater than unity under the input requirements of torque (2.711 kNm), speed (40 rpm) and gear dimensions (outside diameter of 0.35 m with 50 mm face width). The series of analyses showed that the designed gearset would be in an acceptable strength state in four different cases. In each case, only one parameter is modified:

- Input torque value of 0.76 kNm to the pinion from the ROV torque tool. This would result to a 3.17 kNm torque output, which is inadequate to handle the operation.
- Lowering the mechanical advantage ratio (torque ratio n_T) to 1.6:1. This modification would create a smaller gear (0.25 m outside diameter) with 4.12 kNm torque output, which is insufficient, similarly to the above case.
- Increase the face width from 50 mm to 250 mm. This would provide the desired torque output, but it is impractical to design such huge gears.
- Increase the outside gear diameter from 0.35 m to 0.65 m. However, the space limits that have been set prevent such design.

However, the AGMA semi-empirical equations that were used for the strength checks are deemed inadequate to calculate the accurate stress state of the gears by some researchers in the literature [49, 52-55]. Accounting the highly nonlinear contact tooth stresses and the complex involute tooth geometry a finite element analysis (FEA) is recommended. The FEA is performed in Ansys Workbench where the detailed geometry from Inventor is inserted, alongside with the defined boundary conditions. The mesh of the gear teeth is a key parameter of the numerical analysis; the right balance between computational power and quality of results should be found. In this thesis, the teeth contact area was refined by elements with a 0.2 mm maximum size, generating 289k nodes and 64k elements.

The numerical analysis manages to capture adequately the phenomenon where a tooth of the pinion meshes with a gear tooth. The highest bending stresses are developed at the root fillet, which is under tension, and can lead to tearing and breakage of the tooth. The latter finding is also acknowledged by observations in the literature. Moreover, the FE bending stresses are in very good agreement with the AGMA results, as a deviation of 7.9% is noted. Despite the good approach achieved in the bending stresses, the FEM was insufficient to provide a valid magnitude of the contact stresses. The numerical results reveal a significant deviation with the ones calculated by AGMA. The reasons are that the contact phenomenon is highly nonlinear and needs further mesh refinement, a fact noted by other authors as well. Ultimately, both analytical and numerical strength calculations suggest that the current gear design is not permissible and should be abandoned.

Under the new circumstances, a modified configuration for the handling mechanism is proposed by the author. In the new concept, a ROV intervention tool is utilized, more

specifically, a torque tool multiplier will be used in combination with the class 4 torque tool. The input of the multiplier is a class 4 interface and 2.711 kNm torque, while the output is a class 7 interface with a maximum output up to 32 kNm. Therefore, a class 7 ROV bucket should be incorporated in the new setup. The latter offers an extra advantage as the mechanism can be also operated by a class 7 ROV torque tool. The rest components of the mechanism are evaluated, and their structural integrity is found to be within acceptable limits.

10.2 Recommendations for future work

Despite a huge effort has been made to address the most critical points of the design of the handling mechanism, there are still areas that need further research and a more comprehensive study before a potential fabrication. Herein, an attempt has been made to include these areas and present the associated challenges.

Design of the steel frame

The focus on the present work has been kept in the handling mechanism that is utilized to deploy the mattress to the seabed. However, the steel frame that will facilitate the handling mechanism needs to be engineered and take into account the geometric restrictions set by the current design. In addition, a hydrodynamic analysis is essential especially when lowering through the splash zone, as it can induce higher dynamic loads to the structure and the mechanism. Since the operation of the frame requires ROV intervention, a ROV impact analysis with the frame and the mechanism should be also considered.

Lifting points and arrangement

Twelve hooks welded on the bottom of the lower pipe lift the concrete mattress. Two steel wire slings are reeled on each side of the upper pipe, while the other ends are attached on a padeye-shackle arrangement mounted on the upper part of the lower pipe. A lifting report should be made that will examine the lifting capacity of the above-mentioned lifting points and slings. Moreover, the rigging design of the four point lifting should be incorporated.

Bearing supports

In this thesis, a polymer material with low friction value and its required area are the only elements to be addressed in regards the bearing support. However, a more in-depth analysis of the bearing is required with respect to its geometry, functionality and maintenance.

Corrosion protection

A design case addressing the corrosion protection of the installation tool is necessary, as frame is intended for subsea application. This yields the need for protection against the corrosive offshore environment. The various components can be coated along with proper markings and labelling as set by the standards.

REFERENCES

- [1] Norwegian Petroleum Directorate. (2018). *Norwegian Petroleum*. Available: <https://www.norskpetroleum.no/en/>
- [2] Subsea Production Systems, "Concrete Mattresses", 2018, Available: <http://www.subseaprotectionsystems.co.uk/images/downloads/Concrete%20Mattresses.pdf>.
- [3] Oil & Gas UK, "Decommissioning of pipelines in the North Sea Region", 2013, Available: <https://oilandgasuk.co.uk/wp-content/uploads/2015/05/OP083.pdf>.
- [4] Submar. (2018). *Offshore Mats*. Available: <https://submar.com/products/offshore-mats/>
- [5] Wikipedia. (2018). *Submarine communications cable*. Available: https://en.wikipedia.org/wiki/Submarine_communications_cable#Importance_of_submarine_cables
- [6] DNV GL, "DNV-RP-F107 Risk Assessment of Pipeline Protection," Oslo, Norway, 2017.
- [7] Subsea 7, "ST-GL-ENG-RP-017-Engineering Standard: Rigid Pipelines-Subsea Pipeline Mechanical Protection Philosophy," 2015.
- [8] DNV GL, "DNV-RP-F111 Interference between trawl gear and pipelines," Oslo, Norway, 2010.
- [9] K. Gormley, F. Murray, and J. M. Roberts, "INSITE Data Roadmap and documentation," 2018.
- [10] X.-j. Yang, Z.-x. Xiu, X.-z. Yan, and Y.-x. Feng, "3D simulation of submarine pipeline impacted by dropped objects [J]," *Journal of Vibration and Shock*, vol. 11, p. 012, 2009.
- [11] M. Braestrup, J. B. Andersen, L. W. Andersen, M. B. Bryndum, and N.-J. R. Nielsen, *Design and installation of marine pipelines*. John Wiley & Sons, 2009.
- [12] UK Health & Safety Executive, "Guidelines for pipeline operators on pipeline anchor hazards," UK HSE2009, Available: <http://www.hse.gov.uk/pipelines/pipeline-anchor-hazards.pdf>.
- [13] H. K. Endresen and A. Tørum, "Wave forces on a pipeline through the surf zone," *Coastal Engineering*, vol. 18, no. 3, pp. 267-281, 1992/12/01/ 1992.
- [14] P. Barrette, "Offshore pipeline protection against seabed gouging by ice: An overview," *Cold Regions Science and Technology*, vol. 69, no. 1, pp. 3-20, 2011.
- [15] WeSubsea, "Concrete Mattresses", 2018, Available: <https://wesubsea.no/subsea-tooling/concrete-mattresses/>.
- [16] Submat. (2018). *Pipeline protection and stabilization systems*. Available: http://www.slp-projects.com/downloads/Submat_Brochure.pdf

- [17] International Marine Contractors Association, "Guidelines for Diver and ROV Based Concrete Mattress Handling, Deployment, Installation, Repositioning and Decommissioning," IMCA D042, 2011, Available: <http://www.subseasa.com/documents/mattress%20handeling.pdf>.
- [18] S. P. Musarra (2013) Concrete mattresses offer more than just pipeline protection. *Offshore Engineer Digital Edition*. Available: <http://www.oedigital.com/subsea/item/3882-concrete-mattresses-offer-more-than-just-pipeline-protection>
- [19] DeepOcean, "*Intelligent mattress frame*", 2014, Available: <https://deepoceangroup.com/wp-content/uploads/2015/11/54ec2e15a17fc.pdf>.
- [20] Offshore Marine Management, "*Multi-mattress deployment system MDS3*", 2016, Available: http://offshoremm.com/wp-content/uploads/2016/09/mds_spec_sheet_english.pdf.
- [21] Subsea 7, "ST-GL-ENG-RI-013 Engineering Standard: Remote Intervention Concrete Mattress Installation by ROV," 2013.
- [22] Offshore Technology, "*Scolty and Crathes Field Development, North Sea*". Available: <https://www.offshore-technology.com/projects/scolty-and-crathes-field-development-north-sea/>
- [23] Red-Services, "*Concrete mattress installation*". Available: http://www.red-services.co.uk/pdf/Case_Studies_GG_&_Thanet.pdf
- [24] Maccaferri Middle East. *Articulated Concrete Block Mattresses (ACBM)*. Available: <https://www.maccaferri.com/ae/products/articulated-concrete-block-mattresses-acbm/>
- [25] S. P. Musarra. (2014) Shah Deniz 2 takes off. *OE Digital*. Available: <http://www.oedigital.com/component/k2/item/5486-shah-deniz-2-takes-off>
- [26] AquaBotix. (2016). *Uses of Grabber Arms with ROVs*. Available: <https://www.aquabotix.com/news/uses-of-grabber-arms-with-rovs>
- [27] FMC Technologies. (2013). *Schilling Robotics TITAN 4 Manipulator*. Available: https://www.f-e-t.com/images/uploads/Schilling_Titan_4_with_Spares_Kit.pdf
- [28] ISO, *ISO 13628-6:2006: Petroleum and natural gas industries- Design and operation of subsea production systems - Part 6: Subsea production control systems*, Geneva, Switzerland, 2006.
- [29] S. P. Radzevich, *Dudley's handbook of practical gear design and manufacture*. CRC Press, 2012.
- [30] T. Freeth *et al.*, "Decoding the ancient Greek astronomical calculator known as the Antikythera Mechanism," *Nature*, vol. 444, no. 7119, p. 587, 2006.
- [31] R. L. Norton, *Machine design : an integrated approach*, 5th ed. ed. Boston, Mass: Prentice Hall, 2014.
- [32] D. Hans. (2018). *Introduction to Machine Design & Transmission Systems*. Available: <https://sites.google.com/site/designoftransmissionsystems>
- [33] AGMA, "*ANSI/AGMA 2101-D04:Fundamental rating factors and calculation methods for involute spur and helical gear teeth*," Alexanria, Virginia, USA, 2005.
- [34] P. R. N. Childs, *Mechanical Design Engineering Handbook*. Burlington: Elsevier Science, 2013.

- [35] R. C. Juvinall and K. M. Marshek, *Fundamentals of machine component design*, 4th ed. ed. New York: Wiley, 2006.
- [36] J. I. Jóhannsson, "Single-deployment frame for multiple concrete mattresses," Master Thesis, Department of Offshore and Dredging Engineering, TU Delft, Delft, Netherlands, 2014.
- [37] European Commission. (2015). *Road weights and dimensions*. Available: https://ec.europa.eu/transport/modes/road/weights-and-dimensions_en
- [38] Y. Dalgic, I. Lazakis, and O. Turan, *Vessel charter rate estimation for offshore wind O&M activity*. 2013.
- [39] C. KGaA, "Risk management programme gas dispersion", 2010. Available: <https://www.draeger.com/Library/Content/9046434-sab-gas-dispersion-engl-11.pdf>
- [40] European Committee for Standardisation, *Eurocode 3: Design of steel structures. Part 1-1: General rules and rules for buildings*. Lysaker: Standard Norge, 2008.
- [41] DNV GL, "DNVGL-OS-C101: Design of offshore steel structures, general-LRFD method," April 2016.
- [42] D. Karunakaran, "Lecture notes on pipelines and risers," University of Stavanger, Stavanger, 2017.
- [43] NORSOK, *Design of steel structures*, Rev. 3, February 2013. ed. (NORSOK standard). Oslo: Standard Norge, 2013.
- [44] DNV GL, "DNVGL-ST-N001: Marine operations and marine warranty," Oslo, 2016.
- [45] Subsea 7, "ST-GL-ENG-LR-001 Engineering Standard: Lifting and rigging design," 2016.
- [46] Bentley Systems, "StaadPro v8i Technical Reference Manual," 2012, Available: https://communities.bentley.com/cfs-file/_key/telligent-evolution-components-attachments/13-275895-00-00-00-24-18-4/Technical_5F00_Reference_5F00_V8i.pdf.
- [47] ANSYS, "Ansys Workbench user's guide," 2009.
- [48] Autodesk. (2015). *Inventor Online Help*. Available: <http://help.autodesk.com/view/INVNTOR/2019/ENU/>
- [49] A. Marciniak and A. Pawłowicz, "The bending and contact stress analysis of spur gears," *Journal of KONES*, vol. 16, pp. 243-250, 2009.
- [50] M. Guingand, J.-P. de Vaujany, and C.-Y. Jacquin, "Quasi-static analysis of a face gear under torque," *Computer Methods in Applied Mechanics and Engineering*, vol. 194, no. 39, pp. 4301-4318, 2005/10/01/ 2005.
- [51] S.-C. Hwang, J.-H. Lee, D.-H. Lee, S.-H. Han, and K.-H. Lee, "Contact stress analysis for a pair of mating gears," *Mathematical and Computer Modelling*, vol. 57, no. 1, pp. 40-49, 2013/01/01/ 2013.
- [52] T. J. Lisle, B. A. Shaw, and R. C. Frazer, "External spur gear root bending stress: A comparison of ISO 6336:2006, AGMA 2101-D04, ANSYS finite element analysis and strain gauge techniques," *Mechanism and Machine Theory*, vol. 111, pp. 1-9, 2017/05/01/ 2017.
- [53] J. I. Pedrero, M. Pleguezuelos, and M. Muñoz, "Critical stress and load conditions for pitting calculations of involute spur and helical gear teeth," *Mechanism and Machine Theory*, vol. 46, no. 4, pp. 425-437, 2011/04/01/ 2011.

- [54] V. G. Sfakiotakis, J. P. Vaitis, and N. K. Anifantis, "Numerical simulation of conjugate spur gear action," *Computers & Structures*, vol. 79, no. 12, pp. 1153-1160, 2001/05/01/ 2001.
- [55] P. Silori, A. Shaikh, K. C. N. Kumar, and T. Tandon, "Finite Element Analysis of Traction Gear Using ANSYS," *Materials Today: Proceedings*, vol. 2, no. 4, pp. 2236-2245, 2015/01/01/ 2015.
- [56] E. Trubachev, A. Kuznetsov, and A. Sannikov, "Model of Loaded Contact in Multi-pair Gears," in *Advanced Gear Engineering*, V. Goldfarb, E. Trubachev, and N. Barmina, Eds. Cham: Springer International Publishing, 2018, pp. 45-72.
- [57] J. Zhan, M. Fard, and R. Jazar, "A quasi-static FEM for estimating gear load capacity," *Measurement*, vol. 75, pp. 40-49, 2015/11/01/ 2015.
- [58] Autodesk Inventor Forum. (2018). *Geometry Factor Spur Gears Design Accelerator*. Available: <https://forums.autodesk.com/t5/inventor-forum/geometry-factor-spur-gears-design-accelerator/m-p/8040929>
- [59] GoodFellow. (2018). *Polyoxymethylene-Copolymer (Acetal-Copolymer POMC)*. Available: [https:// www.goodfellow.com/E/Polyoxymethylene-Copolymer.html](https://www.goodfellow.com/E/Polyoxymethylene-Copolymer.html)

APPENDIX A:

Drawings and information sheets

A1. Drawing and geometry of ROV receptacle [28]

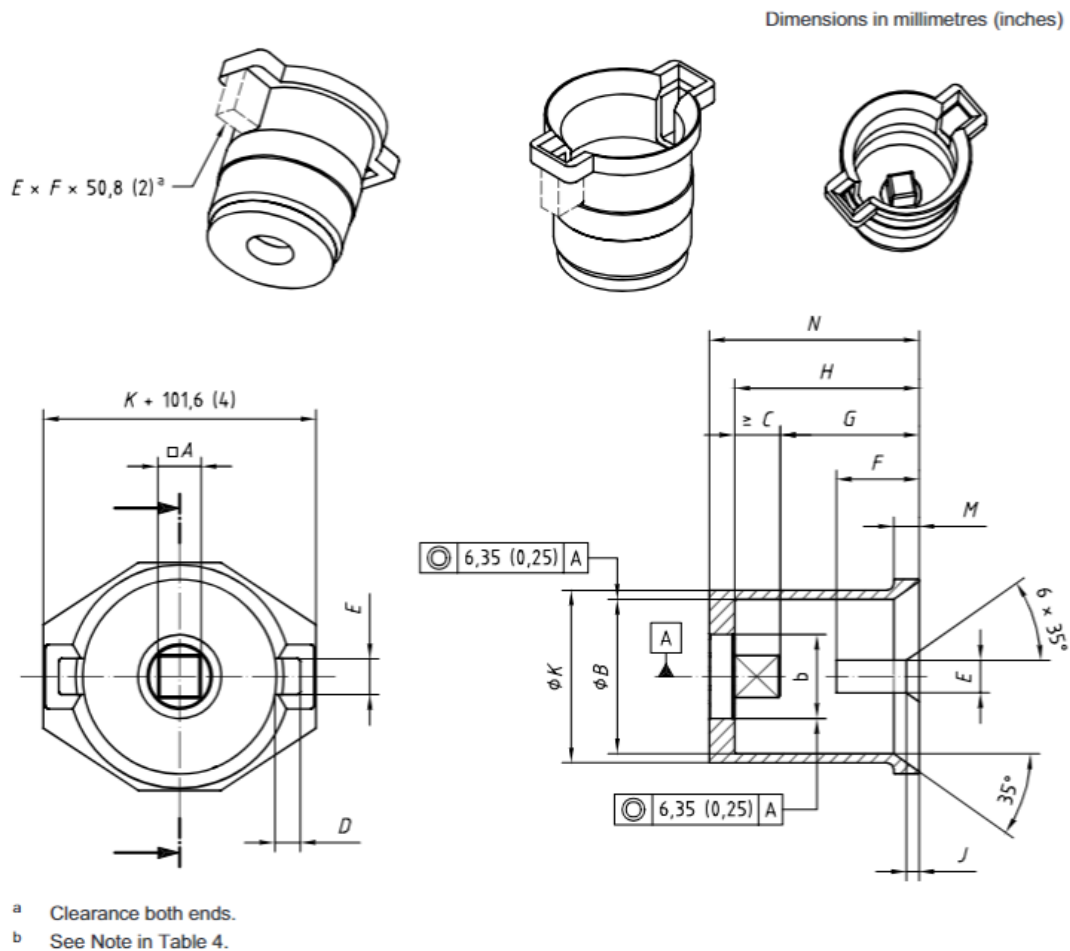


Figure 18 — Rotary torque receptacle

Table 4 — Dimensions for receptacle classes 1 to 7 (see Figure 18)

Dimensions in millimetres (inches)

Dimension	Class						
	1	2	3	4	5	6	7
<i>A</i> square	17,50 (0,687)	17,50 (0,687)	28,60 (1,125)	38,10 (1,50)	50,80 (2,00)	66,67 (2,625)	88,90 (3,50)
<i>B</i>	154,0 (6,06)	154,0 (6,06)	154,0 (6,06)	154,0 (6,06)	190,5 (7,50)	243,0 (9,56)	243,0 (9,56)
<i>C</i> min.	41,0 (1,62)	41,0 (1,62)	41,0 (1,62)	41,0 (1,62)	63,5 (2,50)	89,0 (3,50)	89,0 (3,50)
<i>D</i>	38,0 (1,50)	38,0 (1,50)	38,0 (1,50)	38,0 (1,50)	57,0 (2,25)	82,25 (3,25)	82,25 (3,25)
<i>E</i>	32,0 (1,25)	32,0 (1,25)	32,0 (1,25)	32,0 (1,25)	38,0 (1,50)	44,5 (1,75)	44,5 (1,75)
<i>F</i>	82,5 (3,25)	82,5 (3,25)	82,5 (3,25)	82,5 (3,25)	127,0 (5,00)	178,0 (7,00)	178,0 (7,00)
<i>G</i> min.	140,0 (5,51)	140,0 (5,51)	140,0 (5,51)	140,0 (5,51)	140,0 (5,51)	222,0 (8,75)	435,0 (17,13)
<i>G</i> max.	146,0 (5,75)	146,0 (5,75)	146,0 (5,75)	146,0 (5,75)	146,0 (5,75)	228,0 (9,00)	441,0 (17,38)
<i>H</i>	181,0 (7,12)	181,0 (7,12)	181,0 (7,12)	181,0 (7,12)	206,0 (8,12)	—	—
<i>J</i>	12,7 (0,50)	12,7 (0,50)	12,7 (0,50)	12,7 (0,50)	—	—	—
<i>K</i>	168,5 (6,63)	168,5 (6,63)	168,5 (6,63)	168,5 (6,63)	—	—	—
<i>M</i>	25,4 (1,00)	25,4 (1,00)	25,4 (1,00)	25,4 (1,00)	—	—	—
<i>N</i>	194,0 (7,63)	194,0 (7,63)	194,0 (7,63)	194,0 (7,63)	—	—	—

As an alternative to dimension *A*, end effector shapes as found in Annex D for the appropriate torque range may be used.

All dimension tolerances are as follows:

$0_{,x} \pm 0,5$ (0,020)

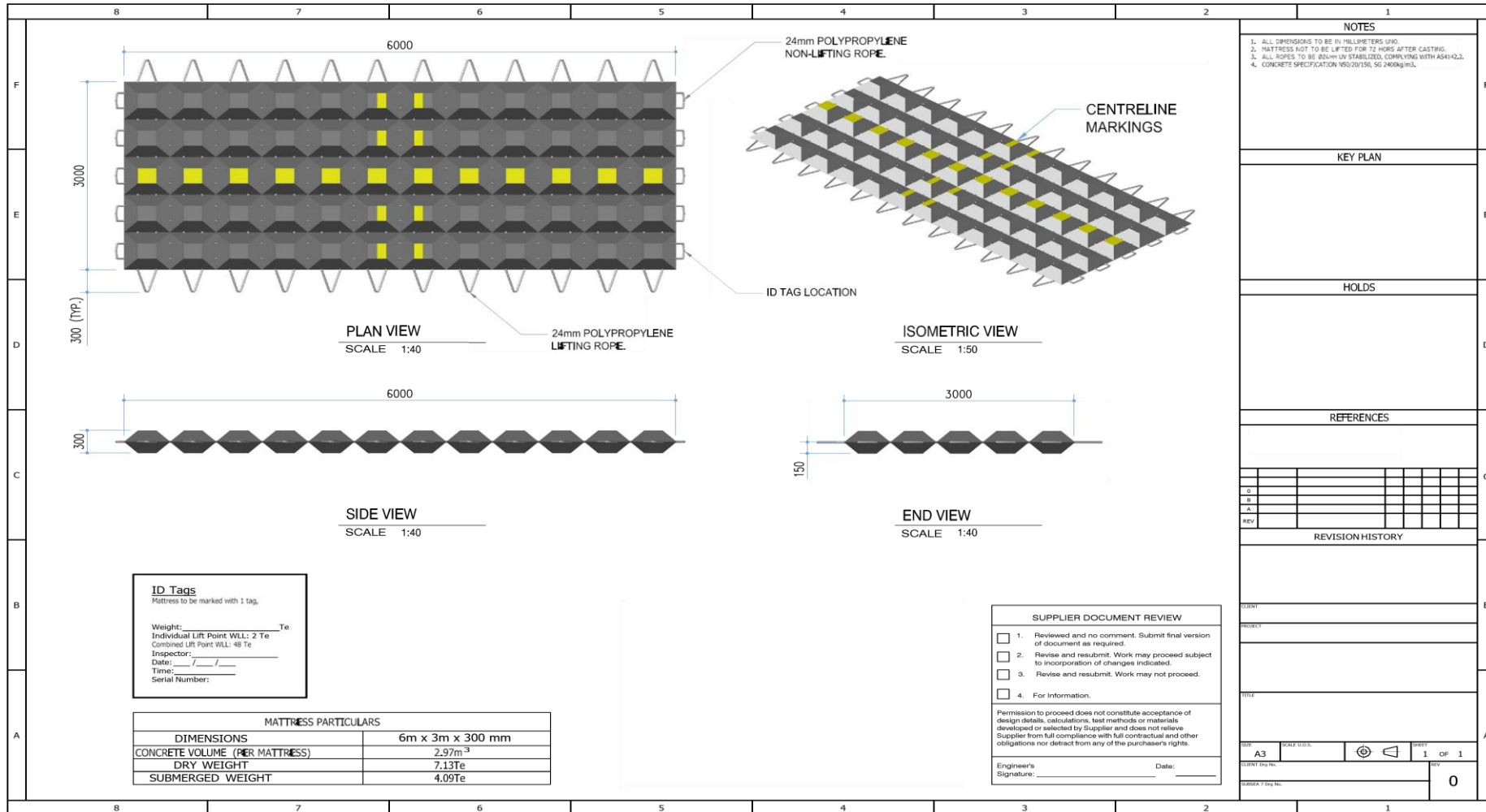
$0_{,xx} \pm 0,25$ (0,010)

$C: \begin{matrix} +1,27 \\ 0 \end{matrix} \left(\begin{matrix} +0,05 \\ 0 \end{matrix} \right)$

NOTE 1 Chamfer on the end of the end effector profile is $45^\circ \times 1,65$ (0,06) max.

NOTE 2 Clearance behind anti-rotation slots [*E* × *F* × 50,8 (2)] is to allow for locking feature option provided by some tools.

A2. Drawing of concrete mattress



A3. ROV tooling

FMC Technologies

We put you first.
And keep you ahead.

Schilling Robotics TITAN 4 Manipulator

Thousands of FMC Schilling manipulator systems are in use worldwide every day. TITAN manipulators are the highest quality system on the market for the dexterity and strength needed to withstand the industry's harsh and repetitive needs day after day.

- » Acute Precision Control
- » Durable Through the Harshes Conditions
- » Reliability Through the Harshes Conditions
- » Large Operating Envelope
- » High Lift-to-Weight Ratio
- » Depth Rating up to 7,000msw
- » Titanium Construction

The TITAN 4 is widely regarded as the world's premier servo-hydraulic remote manipulator system. Since 1987, these systems have been the industry standard for dexterous manipulator systems used in subsea applications, and are extensively used on ultra-heavy work class ROVs.

The TITAN 4 has the dexterity and accuracy necessary to perform the fine movements needed for complex tasks. When this ability is combined with the manipulator's reach (1,922mm), payload capacity (122kg at full extension), and large operating envelope, the TITAN 4 offers unequalled performance in a wide range of subsea applications.





In-arm electronics are located in the forearm, increasing system reliability and minimizing electrical connections.

Acute Precision Control

The TITAN 4 manipulator's accuracy is limited only by the pilot's eye. The master controller includes a six-degree-of-freedom replica master arm that ensures comfortable, intuitive manipulator operation. Its movements are just as sharp whether it's moving a 5lb. object or moving a 250lb object.

The controller also contains function keys for selecting menu options and a display for viewing diagnostic and status information. The controller's advanced operational features are individual joint freeze, position scaling (altering the ratio of master arm movement to manipulator arm movement), password security, programmable stow/deploy routines, individual joint movement limits, incremental gripper movement, individual joint diagnostics, and automatic error checking.



The replica master arm ensures comfortable, intuitive operation.

www.fmctechnologies.com

© 2013 FMC Technologies Schilling Robotics. All rights reserved.

SPECIFICATIONS

Reach:	1.92 meter
Type:	Position Controlled
Functions:	7
Material:	Primarily Titanium

- * Arm Specifications
 - Standard Depth: 4,000 msw
 - Extended Depth: 7,000 msw
 - Weight in air: 100kg
 - Weight in water: 78kg
 - Lift at full extension: 122kg
 - Maximum lift, nominal: 454kg
 - Standard Gripper Opening: 99mm
 - Grip Force, nominal: 4,092N
 - Wrist torque, nominal: 170Nm
 - Wrist rotate, cont.: 6-35rpm
- * Master Controller Specifications
 - Length: 470mm
 - Width: 177mm
 - Height: 67mm
 - Weight: 3.7kg
- * Electrical and Telemetry
 - Input Power, Controller: 90-260VAC
 - Input Power, Arm: 24 VDC
 - Power, Controller: 6W start, 3W run
 - Power, Arm: 6W start, 45W run
 - Telemetry: RS-232 or RS-422/485
- * Hydraulic Requirements
 - Fluid: Mineral, Glycol, or Synthetic
 - Viscosity: 10-200 cSt
 - Available Flow: 5.7 - 19 lpm
 - Max. Pressure: 3,000 psi
 - Max. Fluid Temperature: 54°C
 - Fluid Cleanliness: ISO 4406 14/11

Rotary Docking Class 1-4 Torque Tool



REMOTE TECHNOLOGY
SERIES

i-Tech⁷



The Class 1-4 Rotary Docking Torque Tool provides a means of developing torque for actuation of valves and lockdown clamps, throughout a subsea production system over a torque range of 27Nm to 2710Nm (20 to 2000ft-lb).

The torque reaction lugs on each side of the tool include an integral latching mechanism that anchors the tool into the ISO 13628-8 Figure 18 interfacet. This provides a means of stabilising the ROV during valve operations and allows for secure handling of fly-to-place electro-hydraulic flying leads.

Summary of Rotary Docking Class 1-4 Torque Tool:

- Combines functions of Class 1-4 torque tools in a single unit
- Single 5.1 torque multiplier
- Torque reacted locally within front single spring loaded multi end effectors for classes 1-4 torque tools: includes 1.50"/1.66" for class 4
- Signals from torque transducer and turns counter relayed back to continuous surface readout via ROV umbilical
- Hydraulic control achieved from ROV through hydraulics manifold or separate Hydraulic Control Panel
- Torque control achieved through closed loop proportional control system or can be manually pre-set at surface and selected from topside control console
- Tool assembly contained in aluminium housing for corrosion and environmental protection

Deeper Challenges, Wider Horizons

Specifications

Materials

Housing - aluminium alloy
Spring loaded socket - stainless steel

Hydraulic Supply

85 bar (1230 psi) for maximum tool output

Supply Fluid

Mineral Oil

Torque Output

27Nm to 2710Nm (20 to 2000ft-lb)

Output Speed

8 rpm @ 24 l/min (6.3 g/min)

Turns Counter

Accurate to ± 0.125 turns

Torque Feed-Back

Continuous

Depth Rating

Limited to ROV hydraulic compensation system

Weight In Air

52kg (115lbs)

Interfaces

ISO 13628-8 Figure 18 Rotary Docking Class 1-4 compatible

Deployment

Subsea 7's Alignment Tool, Tool Deployment Unit (TDU) or by manipulator

Auxiliary Equipment

Surface calibration Torque Analyser unit available

Class 4 to 7 Torque Tool Adaptor

VALVE MANIPULATION TOOLS

Product Number:
AUS-11024-0001



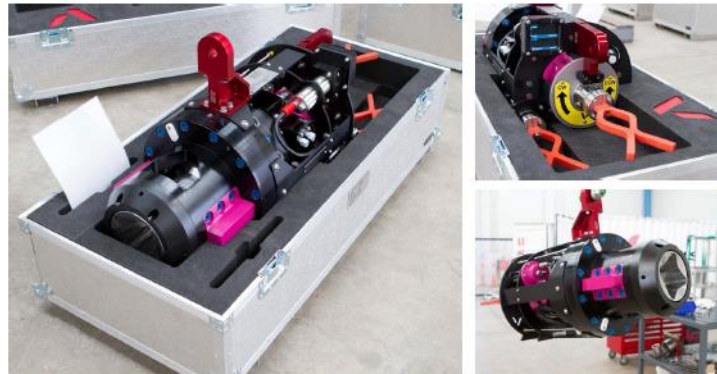
The class 4 to 7 torque tool adaptor is designed to handle class 7 valves and connectors through a standard class 4 torque tool. The adaptor is pressure compensated and has a mechanical latch mechanism activated through the vertical grab handle.

- Constructed from aluminium and stainless steel
- Pressure compensated housing
- Mechanical latching mechanism
- Max output torque 34,000 Nm (25,077 ft.lb)
- Gear ratio 14.1:1

Class 4 to 7 Torque Tool Adaptor

Product Number	AUS-11024-0001
Materials	Stainless Steel, Aluminium and Acetal
Depth Rating	3000msw (9,842ft)
Max Output Torque	34,000 Nm (25,077 ft.lb)
Hydraulic Power Requirement	N/A
Weight in Air	150 kg (330 lbs)
Weight in Seawater	120 kg (265 lbs)

DATA SHEET
DS-0070



Class 7 (Modified) Torque Tool

The Class 7 (Modified) Torque Tool is designed and built by Velocious and recommended for all high torque operations. The tool interfaces with a shortened form of a ISO 13628-8 Class 7 torque receptacle with a 3.5" square drive. This robust subsea unit is the product of a detailed design process that affords the appropriate level of respect to the integrity critical tasks being carried out.

This tool incorporates an integrated electronic display at the rear so that torque output and turns count can be continuously monitored. The tool also incorporates a visual turns indicator through 8 view ports on the main body housing and an indicator to verify that the tool is completely engaged with the torque bucket.

The Tool is typically supplied in a fully calibrated condition together with a Velocious calibrated torque analyser unit and delivers the highest level of torque repeatability across its entire supply pressure range. A maximum output torque of 40,000 Nm is available and the tool is rated to 3,000 m water depth as standard. This tool should be used in conjunction with a Subsea Control System for full proportional control and data logging of operations.

Technical Specifications - Torque Tool:

Weight in Air	140 kg (309 lbs) without buoyancy	
Weight in Water	45 kg (99 lbs) with buoyancy	
	109 kg (240 lbs) without buoyancy	
Depth Rating	3,000 meters	
Interface	Modified ISO 13628-8 Class 7	
Torque output	5,000 to 40,000 Nm (3688 to 29502 ft lbs)	
Operation Temperature Range	-15°C to 45°C (5°F to 113°F)	See sheet 2 for more

Unit 3, 115
Belmont Avenue
Belmont WA 6104

PO Box 247
Belmont
WA 6084

P +61 8 9373 1300
F +61 8 9373 1333
E info@velocious.com.au

www.velocious.com.au

DATA SHEET
DS-0070



Technical Specifications - Subsea LED Display & Electronics:

Dual simultaneous display of torque / turn count
Fixed character height (14.2 mm)
Torque readout w/rotational sign (+/-) in Nm or ft-lb, incremented to 0.1 kNm
Number of turns w/rotational sign (+/-), incremented to 0.1 turns
Light activated display
Low battery warning
Automated sleep mode (programmable)
Bi-directional RS-232 communications with topside
110 - 240 V, 50 - 60 Hz external power supply for charging
Torque readout accuracy +/- 10%
Rechargeable battery: 1 x D-Cell NiMH, 7 days battery life (display on); 6 months battery life (standby)

APPENDIX B:

Staad.Pro analysis

B.1 Spreader beam (lower pipe)

```
Thursday, June 07, 2018, 12:45 PM
PAGE NO. 1

*****
*
*          STAAD.Pro V8i SELECTseries3          *
*          Version 20.07.08.20                  *
*          Proprietary Program of              *
*          Bentley Systems, Inc.               *
*          Date= JUN 7, 2018                   *
*          Time= 12:45: 4                      *
*
*          USER ID: Subsea 7                   *
*****

1. STAAD PLANE
INPUT FILE: lower pipe final with slings operational.STD
2. START JOB INFORMATION
3. ENGINEER DATE 23-MAR-18
4. JOB NAME MASTER THESIS
5. JOB CLIENT UIS
6. JOB NO 3
7. ENGINEER NAME E.CHATZILL
8. END JOB INFORMATION
9. INPUT WIDTH 79
10. UNIT METER KN
11. JOINT COORDINATES
12. 5 1.38462 0 0; 8 2.79462 0 0; 15 6.08462 0 0; 18 7.49462 0 0; 19 2.79462 0.3 0
13. 20 6.08462 0.3 0
14. MEMBER INCIDENCES
15. 3 18 15; 4 15 8; 5 8 5; 6 8 19; 7 15 20
16. DEFINE MATERIAL START
17. ISOTROPIC STEEL
18. E 2.1E+008
19. POISSON 0.3
20. DENSITY 76.8195
21. ALPHA 1.2E-005
22. DAMP 0.03
23. TYPE STEEL
24. STRENGTH FY 365000 FU 490000 RY 1.5 RT 1.2
25. END DEFINE MATERIAL
26. MEMBER PROPERTY EUROPEAN
27. 3 TO 5 TABLE ST 139.7X8CHS
28. 6 7 TABLE ST PIPE OD 0.06 ID 0
29. CONSTANTS
30. MATERIAL STEEL ALL
31. SUPPORTS
32. 19 20 PINNED
33. 5 18 FIXED BUT FY MX MY MZ KFX 1 KFZ 1
34. MEMBER TRUSS
35. 6
36. MEMBER TRUSS
37. 7
38. LOAD 1 LOADTYPE DEAD TITLE DESIGN LOAD CASE
39. SELFWEIGHT Y -3.62
40. MEMBER LOAD

C:\Users\ss7n1827\Desktop\Offshore Technology\4th Semester\MSc Thesis\Calculations\Offshore Lift\Upper Pipe\lower p
```

Thursday, June 07, 2018, 12:45 PM

STAAD PLANE

-- PAGE NO. 2

41. 5 CON Y -21.1 0.94
 42. 5 CON Y -21.1 0.47
 43. 4 CON Y -21.1 0.94
 44. 4 CON Y -21.1 0
 45. 4 CON Y -21.1 0.47
 46. 4 CON Y -21.1 1.41
 47. 4 CON Y -21.1 1.88
 48. 4 CON Y -21.1 2.35
 49. 4 CON Y -21.1 2.82
 50. 4 CON Y -21.1 3.29
 51. 3 CON Y -21.1 0.94
 52. 3 CON Y -21.1 0.47
 53. LOAD 2 LOADTYPE DEAD TITLE OPERATIONAL LOAD CASE
 54. SELFWEIGHT Y -2.33
 55. MEMBER LOAD
 56. 5 CON Y -8 0.94
 57. 5 CON Y -8 0.47
 58. 4 CON Y -8 0.94
 59. 4 CON Y -8 0
 60. 4 CON Y -8 0.47
 61. 4 CON Y -8 1.41
 62. 4 CON Y -8 1.88
 63. 4 CON Y -8 2.35
 64. 4 CON Y -8 2.82
 65. 4 CON Y -8 3.29
 66. 3 CON Y -8 0.94
 67. 3 CON Y -8 0.47
 68. PERFORM ANALYSIS

PROBLEM STATISTICS

NUMBER OF JOINTS/MEMBER+ELEMENTS/SUPPORTS = 6/ 5/ 4

SOLVER USED IS THE OUT-OF-CORE BASIC SOLVER

ORIGINAL/FINAL BAND-WIDTH= 3/ 3/ 10 DOF
 TOTAL PRIMARY LOAD CASES = 2, TOTAL DEGREES OF FREEDOM = 14
 SIZE OF STIFFNESS MATRIX = 1 DOUBLE KILO-WORDS
 REQD/AVAIL. DISK SPACE = 12.0/ 22203.9 MB

ZERO STIFFNESS IN DIRECTION 6 AT JOINT 19 EQN.NO. 13
 LOADS APPLIED OR DISTRIBUTED HERE FROM ELEMENTS WILL BE IGNORED.
 THIS MAY BE DUE TO ALL MEMBERS AT THIS JOINT BEING RELEASED OR
 EFFECTIVELY RELEASED IN THIS DIRECTION.
 ZERO STIFFNESS IN DIRECTION 6 AT JOINT 20 EQN.NO. 14

69. PARAMETER 3
 70. CODE EN 1993-1-1:2005
 71. SGR 4 ALL
 72. TORSION 2 ALL

C:\Users\ss7n1827\Desktop\Offshore Technology\4th Semester\MSc Thesis\Calculations\Offshore Lift\Upper Pipe\lower p

Thursday, June 07, 2018, 12:45 PM

STAAD PLANE -- PAGE NO. 4

ALL UNITS ARE - KN METE (UNLESS OTHERWISE NOTED)

MEMBER	TABLE	RESULT/ FX	CRITICAL COND/ MY	RATIO/ MZ	LOADING/ LOCATION
3 ST	139.7X8CHS	(EUROPEAN SECTIONS)			
		PASS	EC-6.2.7(5)	0.566	1
		0.00	0.00	30.67	1.41

MATERIAL DATA

Grade of steel = S 460
 Modulus of elasticity = 210 kN/mm2
 Design Strength (py) = 460 N/mm2

SECTION PROPERTIES (units - cm)

Member Length = 141.00
 Gross Area = 33.10 Net Area = 33.10

	z-axis	y-axis
Moment of inertia	720.000	720.000
Plastic modulus	139.000	139.000
Elastic modulus	103.078	103.078
Shear Area	21.072	21.072
Radius of gyration	4.664	4.664
Effective Length	141.000	141.000

DESIGN DATA (units - kN,m) EUROCODE NO.3 /2005

Section Class : CLASS 1
 Squash Load : 1522.60
 Axial force/Squash load : 0.000
 GM0 : 1.15 GM1 : 1.15 GM2 : 1.25

	z-axis	y-axis
Slenderness ratio (KL/r)	30.2	30.2
Compression Capacity	1243.2	1243.2
Tension Capacity	1286.9	1286.9
Moment Capacity	55.6	55.6
Reduced Moment Capacity	55.6	55.6
Shear Capacity	486.6	486.6

BUCKLING CALCULATIONS (units - kN,m)

Lateral Torsional Buckling Moment MB = 63.9
 co-efficients C1_K : C1 =1.000 K =1.0, Effective Length= 1.410

TORSION CALCULATIONS (units - kN,m)

Total Torsional Load T = 0.0
 Effective Length for Torsion = 1.410
 END1: Torsion Fixed, Warping Fixed END2: Torsion Fixed, Warping Fixed

Max. section forces _capacities: [@ x = 0.000](units - kN,m)
 Torsion at section = 0.0
 Pure Torsion Component = 0.0
 Warping Torsion Component = 0.0
 Pure Torsion Capacity = 0.0
 Warping Torsion Capacity = 0.0

C:\Users\ss7n1827\Desktop\Offshore Technology\4th Semester\MSc Thesis\Calculations\Offshore Lift\Upper Pipe\lower p

Thursday, June 07, 2018, 12:45 PM

STAAD PLANE

-- PAGE NO. 5

ALL UNITS ARE - KN METE (UNLESS OTHERWISE NOTED)

MEMBER	TABLE	RESULT/ FX	CRITICAL COND/ MY	RATIO/ MZ	LOADING/ LOCATION
--------	-------	---------------	----------------------	--------------	----------------------

CRITICAL LOADS FOR EACH CLAUSE CHECK (units- kN,m):

CLAUSE	RATIO	LOAD	FX	VY	VZ	MZ	MY
EC-6.2.5	0.552	1	0.0	43.5	0.0	30.7	0.0
EC-6.2.6-(Y)	0.089	1	0.0	43.5	0.0	30.7	0.0
EC-6.3.2 LTB	0.480	1	0.0	43.5	0.0	30.7	0.0

ADDITIONAL CLAUSE CHECKS FOR TORSION (units- kN,m):

CLAUSE	RATIO	LOAD	DIST	FX	VY	VZ	MZ	MY	MX
EC-6.2.7(9)	0.089	1	1.4	0.0	43.5	0.0	30.7	0.0	0.0
EC-6.2.7(5)	0.566	1	1.4	0.0	43.5	0.0	30.7	0.0	0.0

C:\Users\ss7n1827\Desktop\Offshore Technology\4th Semester\MSc Thesis\Calculations\Offshore Lift\Upper Pipe\lower p

Thursday, June 07, 2018, 12:45 PM

STAAD PLANE -- PAGE NO. 6

ALL UNITS ARE - KN METE (UNLESS OTHERWISE NOTED)

MEMBER	TABLE	RESULT/ FX	CRITICAL COND/ MY	RATIO/ MZ	LOADING/ LOCATION
4 ST	139.7X8CHS	(EUROPEAN SECTIONS)			
		PASS	EC-6.2.7(5)	0.604	1
		0.00	0.00	30.67	3.29

MATERIAL DATA

Grade of steel = S 460
 Modulus of elasticity = 210 kN/mm2
 Design Strength (py) = 460 N/mm2

SECTION PROPERTIES (units - cm)

Member Length = 329.00
 Gross Area = 33.10 Net Area = 33.10

	z-axis	y-axis
Moment of inertia	: 720.000	720.000
Plastic modulus	: 139.000	139.000
Elastic modulus	: 103.078	103.078
Shear Area	: 21.072	21.072
Radius of gyration	: 4.664	4.664
Effective Length	: 329.000	329.000

DESIGN DATA (units - kN,m) EUROCODE NO.3 /2005

Section Class : CLASS 1
 Squash Load : 1522.60
 Axial force/Squash load : 0.000
 GM0 : 1.15 GM1 : 1.15 GM2 : 1.25

	z-axis	y-axis
Slenderness ratio (KL/r)	: 70.5	70.5
Compression Capacity	: 834.0	834.0
Tension Capacity	: 1286.9	1286.9
Moment Capacity	: 55.6	55.6
Reduced Moment Capacity	: 55.6	55.6
Shear Capacity	: 486.6	486.6

BUCKLING CALCULATIONS (units - kN,m)

Lateral Torsional Buckling Moment MB = 63.9
 co-efficients C1_K : C1 =1.000 K =1.0, Effective Length= 3.290

TORSION CALCULATIONS (units - kN,m)

Total Torsional Load T = 0.0
 Effective Length for Torsion = 3.290
 END1: Torsion Fixed, Warping Fixed END2: Torsion Fixed, Warping Fixed

Max. section forces _capacities: [@ x = 0.000] (units - kN,m)
 Torsion at section = 0.0
 Pure Torsion Component = 0.0
 Warping Torsion Component = 0.0
 Pure Torsion Capacity = 0.0
 Warping Torsion Capacity = 0.0

C:\Users\ss7n1827\Desktop\Offshore Technology\4th Semester\MSc Thesis\Calculations\Offshore Lift\Upper Pipe\lower p

Thursday, June 07, 2018, 12:45 PM

STAAD PLANE

-- PAGE NO. 7

ALL UNITS ARE - KN METE (UNLESS OTHERWISE NOTED)

MEMBER	TABLE	RESULT/ FX	CRITICAL COND/ MY	RATIO/ MZ	LOADING/ LOCATION
--------	-------	---------------	----------------------	--------------	----------------------

CRITICAL LOADS FOR EACH CLAUSE CHECK (units- kN,m):

CLAUSE	RATIO	LOAD	FX	VY	VZ	MZ	MY
EC-6.2.5	0.552	1	0.0	85.9	0.0	30.7	0.0
EC-6.2.6-(Y)	0.177	1	0.0	85.9	0.0	30.7	0.0
EC-6.3.2 LTB	0.480	1	0.0	85.9	0.0	30.7	0.0

ADDITIONAL CLAUSE CHECKS FOR TORSION (units- kN,m):

CLAUSE	RATIO	LOAD	DIST	FX	VY	VZ	MZ	MY	MX
EC-6.2.7(9)	0.177	1	3.3	0.0	85.9	0.0	30.7	0.0	0.0
EC-6.2.7(5)	0.604	1	3.3	0.0	85.9	0.0	30.7	0.0	0.0

C:\Users\ss7n1827\Desktop\Offshore Technology\4th Semester\MSc Thesis\Calculations\Offshore Lift\Upper Pipe\lower p

Thursday, June 07, 2018, 12:45 PM

STAAD PLANE -- PAGE NO. 8

ALL UNITS ARE - KN METE (UNLESS OTHERWISE NOTED)

MEMBER	TABLE	RESULT/ FX	CRITICAL COND/ MY	RATIO/ MZ	LOADING/ LOCATION
S ST	139.7X8CHS	(EUROPEAN SECTIONS)			
		PASS	EC-6.2.7(5)	0.566	1
		0.00	0.00	30.67	0.00

MATERIAL DATA

Grade of steel = S 460
 Modulus of elasticity = 210 kN/mm2
 Design Strength (py) = 460 N/mm2

SECTION PROPERTIES (units - cm)

Member Length = 141.00
 Gross Area = 33.10 Net Area = 33.10

	z-axis	y-axis
Moment of inertia	720.000	720.000
Plastic modulus	139.000	139.000
Elastic modulus	103.078	103.078
Shear Area	21.072	21.072
Radius of gyration	4.664	4.664
Effective Length	141.000	141.000

DESIGN DATA (units - kN,m) EUROCODE NO.3 /2005

Section Class : CLASS 1
 Squash Load : 1522.60
 Axial force/Squash load : 0.000
 GM0 : 1.15 GM1 : 1.15 GM2 : 1.25

	z-axis	y-axis
Slenderness ratio (KL/r)	30.2	30.2
Compression Capacity	1243.2	1243.2
Tension Capacity	1286.9	1286.9
Moment Capacity	55.6	55.6
Reduced Moment Capacity	55.6	55.6
Shear Capacity	486.6	486.6

BUCKLING CALCULATIONS (units - kN,m)

Lateral Torsional Buckling Moment MB = 63.9
 co-efficients C1_K : C1 =1.000 K =1.0, Effective Length= 1.410

TORSION CALCULATIONS (units - kN,m)

Total Torsional Load T = 0.0
 Effective Length for Torsion = 1.410
 END1: Torsion Fixed, Warping Fixed END2: Torsion Fixed, Warping Fixed

Max. section forces _capacities: [@ x = 0.000](units - kN,m)
 Torsion at section = 0.0
 Pure Torsion Component = 0.0
 Warping Torsion Component = 0.0
 Pure Torsion Capacity = 0.0
 Warping Torsion Capacity = 0.0

C:\Users\ss7n1827\Desktop\Offshore Technology\4th Semester\MSc Thesis\Calculations\Offshore Lift\Upper Pipe\lower p

Thursday, June 07, 2018, 12:45 PM

STAAD PLANE

-- PAGE NO. 9

ALL UNITS ARE - KN METE (UNLESS OTHERWISE NOTED)

MEMBER	TABLE	RESULT/ FX	CRITICAL COND/ MY	RATIO/ MZ	LOADING/ LOCATION
--------	-------	---------------	----------------------	--------------	----------------------

CRITICAL LOADS FOR EACH CLAUSE CHECK (units- kN,m):

CLAUSE	RATIO	LOAD	FX	VY	VZ	MZ	MY
EC-6.2.5	0.552	1	0.0	43.5	0.0	30.7	0.0
EC-6.2.6-(Y)	0.089	1	0.0	43.5	0.0	30.7	0.0
EC-6.3.2 LTB	0.480	1	0.0	43.5	0.0	30.7	0.0

ADDITIONAL CLAUSE CHECKS FOR TORSION (units- kN,m):

CLAUSE	RATIO	LOAD	DIST	FX	VY	VZ	MZ	MY	MX
EC-6.2.7(9)	0.089	1	0.0	0.0	43.5	0.0	30.7	0.0	0.0
EC-6.2.7(5)	0.566	1	0.0	0.0	43.5	0.0	30.7	0.0	0.0

C:\Users\ss7n1827\Desktop\Offshore Technology\4th Semester\MSc Thesis\Calculations\Offshore Lift\Upper Pipe\lower p

Thursday, June 07, 2018, 12:45 PM

STAAD PLANE -- PAGE NO. 10

ALL UNITS ARE - KN METE (UNLESS OTHERWISE NOTED)

MEMBER	TABLE	RESULT/ FX	CRITICAL COND/ MY	RATIO/ MZ	LOADING/ LOCATION
(EUROPEAN SECTIONS)					
6 ST	PIP E	PASS	EC-6.2.3 (T)	0.118	1
		129.65 T	0.00	0.00	0.30

MATERIAL DATA

Grade of steel = S 460
 Modulus of elasticity = 210 kN/mm2
 Design Strength (py) = 460 N/mm2

SECTION PROPERTIES (units - cm)

Member Length = 30.00
 Gross Area = 28.27 Net Area = 28.27

	z-axis	y-axis
Moment of inertia	63.617	63.617
Plastic modulus	35.999	35.999
Elastic modulus	21.206	21.206
Shear Area	18.000	18.000
Radius of gyration	1.500	1.500
Effective Length	30.000	30.000

DESIGN DATA (units - kN,m) EUROCODE NO.3 /2005

Section Class : CLASS 1
 Squash Load : 1300.62
 Axial force/Squash load : 0.100
 GM0 : 1.15 GM1 : 1.15 GM2 : 1.25

	z-axis	y-axis
Slenderness ratio (KL/r)	20.0	20.0
Compression Capacity	1106.0	1106.0
Tension Capacity	1099.3	1099.3
Moment Capacity	14.4	14.4
Reduced Moment Capacity	14.0	14.0
Shear Capacity	415.7	415.7

BUCKLING CALCULATIONS (units - kN,m)

Lateral Torsional Buckling Moment MB = 16.6
 co-efficients C1_K : C1 =1.000 K =1.0, Effective Length= 0.300

TORSION CALCULATIONS (units - kN,m)

Total Torsional Load T = 0.0
 Effective Length for Torsion = 0.300
 END1: Torsion Fixed, Warping Fixed END2: Torsion Fixed, Warping Fixed

Max. section forces _capacities: [@ x = 0.000](units - kN,m)
 Torsion at section = 0.0
 Pure Torsion Component = 0.0
 Warping Torsion Component = 0.0
 Pure Torsion Capacity = 0.0
 Warping Torsion Capacity = 0.0

C:\Users\ss7n1827\Desktop\Offshore Technology\4th Semester\MSc Thesis\Calculations\Offshore Lift\Upper Pipe\lower p

Thursday, June 07, 2018, 12:45 PM

STAAD PLANE -- PAGE NO. 11

ALL UNITS ARE - KN METE (UNLESS OTHERWISE NOTED)

MEMBER	TABLE	RESULT/ FX	CRITICAL COND/ MY	RATIO/ MZ	LOADING/ LOCATION
--------	-------	---------------	----------------------	--------------	----------------------

CRITICAL LOADS FOR EACH CLAUSE CHECK (units- kN,m):

CLAUSE	RATIO	LOAD	FX	VY	VZ	MZ	MY
EC-6.2.3 (T)	0.118	1	-129.6	0.0	0.0	0.0	0.0

ADDITIONAL CLAUSE CHECKS FOR TORSION (units- kN,m):

CLAUSE	RATIO	LOAD	DIST	FX	VY	VZ	MZ	MY	MX
EC-6.2.7(5)	0.013	1	0.3	-129.6	0.0	0.0	0.0	0.0	0.0

C:\Users\ss7n1827\Desktop\Offshore Technology\4th Semester\MSc Thesis\Calculations\Offshore Lift\Upper Pipe\lower p

Thursday, June 07, 2018, 12:45 PM

STRAD PLANE -- PAGE NO. 12

ALL UNITS ARE - KN METE (UNLESS OTHERWISE NOTED)

MEMBER	TABLE	RESULT/ FX	CRITICAL COND/ MY	RATIO/ MZ	LOADING/ LOCATION
--------	-------	---------------	----------------------	--------------	----------------------

7	ST PIP E	(EUROPEAN SECTIONS)			
		PASS	EC-6.2.3 (T)	0.118	1
		129.65 T	0.00	0.00	0.30

MATERIAL DATA

Grade of steel = S 460
 Modulus of elasticity = 210 kN/mm²
 Design Strength (py) = 460 N/mm²

SECTION PROPERTIES (units - cm)

Member Length = 30.00
 Gross Area = 28.27 Net Area = 28.27

	z-axis	y-axis
Moment of inertia	63.617	63.617
Plastic modulus	35.999	35.999
Elastic modulus	21.206	21.206
Shear Area	18.000	18.000
Radius of gyration	1.500	1.500
Effective Length	30.000	30.000

DESIGN DATA (units - kN,m) EUROCODE NO.3 /2005

Section Class : CLASS 1
 Squash Load : 1300.62
 Axial force/Squash load : 0.100
 GM0 : 1.15 GM1 : 1.15 GM2 : 1.25

	z-axis	y-axis
Slenderness ratio (KL/r)	20.0	20.0
Compression Capacity	1106.0	1106.0
Tension Capacity	1099.3	1099.3
Moment Capacity	14.4	14.4
Reduced Moment Capacity	14.0	14.0
Shear Capacity	415.7	415.7

BUCKLING CALCULATIONS (units - kN,m)

Lateral Torsional Buckling Moment MB = 16.6
 co-efficients C1_K : C1 =1.000 K =1.0, Effective Length= 0.300

TORSION CALCULATIONS (units - kN,m)

Total Torsional Load T = 0.0
 Effective Length for Torsion = 0.300
 END1: Torsion Fixed, Warping Fixed END2: Torsion Fixed, Warping Fixed

Max. section forces _capacities: (@ x = 0.000)(units - kN,m)
 Torsion at section = 0.0
 Pure Torsion Component = 0.0
 Warping Torsion Component = 0.0
 Pure Torsion Capacity = 0.0
 Warping Torsion Capacity = 0.0

C:\Users\ss7n1827\Desktop\Offshore Technology\4th Semester\MSc Thesis\Calculations\Offshore Lift\Upper Pipe\lower p

Thursday, June 07, 2018, 12:45 PM

STAAD PLANE

-- PAGE NO. 13

ALL UNITS ARE - KN METE (UNLESS OTHERWISE NOTED)

MEMBER	TABLE	RESULT/ FX	CRITICAL COND/ MY	RATIO/ MZ	LOADING/ LOCATION
--------	-------	---------------	----------------------	--------------	----------------------

CRITICAL LOADS FOR EACH CLAUSE CHECK (units- kN,m):

CLAUSE	RATIO	LOAD	FX	VY	VZ	MZ	MY
EC-6.2.3 (T)	0.118	1	-129.6	0.0	0.0	0.0	0.0

ADDITIONAL CLAUSE CHECKS FOR TORSION (units- kN,m):

CLAUSE	RATIO	LOAD	DIST	FX	VY	VZ	MZ	MY	MX
EC-6.2.7(5)	0.013	1	0.3	-129.6	0.0	0.0	0.0	0.0	0.0

***** END OF TABULATED RESULT OF DESIGN *****

77. PERFORM ANALYSIS PRINT ALL

C:\Users\ss7n1827\Desktop\Offshore Technology\4th Semester\MSc Thesis\Calculations\Offshore Lift\Upper Pipe\lower p

Thursday, June 07, 2018, 12:45 PM

STAAD PLANE -- PAGE NO. 14

LOADING 1 LOADTYPE DEAD TITLE DESIGN LOAD CASE

SELFWEIGHT Y -3.620

ACTUAL WEIGHT OF THE STRUCTURE = 1.684 KN

MEMBER LOAD - UNII KN MEIE

MEMBER	UDL	L1	L2	CON	L	LIN1	LIN2
5				-21.1000	Y	0.94	
5				-21.1000	Y	0.47	
4				-21.1000	Y	0.94	
4				-21.1000	Y	0.00	
4				-21.1000	Y	0.47	
4				-21.1000	Y	1.41	
4				-21.1000	Y	1.88	
4				-21.1000	Y	2.35	
4				-21.1000	Y	2.82	
4				-21.1000	Y	3.29	
3				-21.1000	Y	0.94	
3				-21.1000	Y	0.47	

LOADING 2 LOADTYPE DEAD TITLE OPERATIONAL LOAD CASE

SELFWEIGHT Y -2.330

ACTUAL WEIGHT OF THE STRUCTURE = 1.684 KN

MEMBER LOAD - UNII KN MEIE

MEMBER	UDL	L1	L2	CON	L	LIN1	LIN2
5				-8.0000	Y	0.94	
5				-8.0000	Y	0.47	
4				-8.0000	Y	0.94	
4				-8.0000	Y	0.00	
4				-8.0000	Y	0.47	
4				-8.0000	Y	1.41	
4				-8.0000	Y	1.88	
4				-8.0000	Y	2.35	
4				-8.0000	Y	2.82	
4				-8.0000	Y	3.29	
3				-8.0000	Y	0.94	
3				-8.0000	Y	0.47	

ZERO STIFFNESS IN DIRECTION 6 AT JOINT 19 EQN.NO. 13
 LOADS APPLIED OR DISTRIBUTED HERE FROM ELEMENTS WILL BE IGNORED.
 THIS MAY BE DUE TO ALL MEMBERS AT THIS JOINT BEING RELEASED OR
 EFFECTIVELY RELEASED IN THIS DIRECTION.

C:\Users\ss7n1827\Desktop\Offshore Technology\4th Semester\MSc Thesis\Calculations\Offshore Lift\Upper Pipe\lower p

Thursday, June 07, 2018, 12:45 PM

STAAD PLANE -- PAGE NO. 15

ZERO STIFFNESS IN DIRECTION 6 AT JOINT 20 EQN.NO. 14

FOR LOADING - 1
 APPLIED JOINT EQUIVALENT LOADS

JOINT	FORCE-X	FORCE-Y	FORCE-Z	MOM-X	MOM-Y	MOM-Z
5	0.00000E+00	-2.17489E+01	0.00000E+00	0.00000E+00	0.00000E+00	-6.76383E+00
8	0.00000E+00	-1.07781E+02	0.00000E+00	0.00000E+00	0.00000E+00	-3.37345E+01
15	0.00000E+00	-1.07781E+02	0.00000E+00	0.00000E+00	0.00000E+00	3.37345E+01
18	0.00000E+00	-2.17489E+01	0.00000E+00	0.00000E+00	0.00000E+00	6.76383E+00
19	0.00000E+00	-1.17941E-01	0.00000E+00	0.00000E+00	0.00000E+00	0.00000E+00
20	0.00000E+00	-1.17941E-01	0.00000E+00	0.00000E+00	0.00000E+00	0.00000E+00

STATIC LOAD/REACTION/EQUILIBRIUM SUMMARY FOR CASE NO. 1
 LOADTYPE DEAD TITLE DESIGN LOAD CASE

CENTER OF FORCE BASED ON Y FORCES ONLY (METS).
 (FORCES IN NON-GLOBAL DIRECTIONS WILL INVALIDATE RESULTS)

X = 0.443961999E+01
 Y = 0.272910000E-03
 Z = 0.000000000E+00

***TOTAL APPLIED LOAD (KN METE) SUMMARY (LOADING 1)
 SUMMATION FORCE-X = 0.00
 SUMMATION FORCE-Y = -259.30
 SUMMATION FORCE-Z = 0.00

SUMMATION OF MOMENTS AROUND THE ORIGIN-
 MX= 0.00 MY= 0.00 MZ= -1151.17

***TOTAL REACTION LOAD (KN METE) SUMMARY (LOADING 1)
 SUMMATION FORCE-X = 0.00
 SUMMATION FORCE-Y = 259.30
 SUMMATION FORCE-Z = 0.00

SUMMATION OF MOMENTS AROUND THE ORIGIN-
 MX= 0.00 MY= 0.00 MZ= 1151.17

MAXIMUM DISPLACEMENTS (CM /RADIANS) (LOADING 1)
 MAXIMUMS AT NODE

X	0.00000E+00	0
Y	5.80966E-01	5
Z	0.00000E+00	0
RX	0.00000E+00	0
RY	0.00000E+00	0
RZ	1.06972E-02	15

C:\Users\ss7n1827\Desktop\Offshore Technology\4th Semester\MSc Thesis\Calculations\Offshore Lift\Upper Pipe\lower p

Thursday, June 07, 2018, 12:45 PM

STAD PLANE -- PAGE NO. 16

EXTERNAL AND INTERNAL JOINT LOAD SUMMARY (KN METE)-

JT	EXT FX/ INT FX	EXT FY/ INT FY	EXT FZ/ INT FZ	EXT MX/ INT MX	EXT MY/ INT MY	EXT MZ/ INT MZ	
							SUPPORT=1
19	0.00 0.00	-0.12 -129.53	0.00 0.00	0.00 0.00	0.00 0.00	0.00 0.00	111110
20	0.00 0.00	-0.12 -129.53	0.00 0.00	0.00 0.00	0.00 0.00	0.00 0.00	111110

FOR LOADING - 2

APPLIED JOINT EQUIVALENT LOADS

JOINT	FORCE-X	FORCE-Y	FORCE-Z	MOM-X	MOM-Y	MOM-Z
5	0.00000E+00	-8.41768E+00	0.00000E+00	0.00000E+00	0.00000E+00	-2.60482E+00
8	0.00000E+00	-4.14682E+01	0.00000E+00	0.00000E+00	0.00000E+00	-1.29696E+01
15	0.00000E+00	-4.14682E+01	0.00000E+00	0.00000E+00	0.00000E+00	1.29696E+01
18	0.00000E+00	-8.41768E+00	0.00000E+00	0.00000E+00	0.00000E+00	2.60482E+00
19	0.00000E+00	-7.59121E-02	0.00000E+00	0.00000E+00	0.00000E+00	0.00000E+00
20	0.00000E+00	-7.59121E-02	0.00000E+00	0.00000E+00	0.00000E+00	0.00000E+00

STATIC LOAD/REACTION/EQUILIBRIUM SUMMARY FOR CASE NO. 2
 LOADTYPE DEAD TITLE OPERATIONAL LOAD CASE

CENTER OF FORCE BASED ON Y FORCES ONLY (METE).
 (FORCES IN NON-GLOBAL DIRECTIONS WILL INVALIDATE RESULTS)

X = 0.443962006E+01
 Y = 0.455821118E-03
 Z = 0.000000000E+00

***TOTAL APPLIED LOAD (KN METE) SUMMARY (LOADING 2)
 SUMMATION FORCE-X = 0.00
 SUMMATION FORCE-Y = -99.92
 SUMMATION FORCE-Z = 0.00

SUMMATION OF MOMENTS AROUND THE ORIGIN-
 MX= 0.00 MY= 0.00 MZ= -443.62

***TOTAL REACTION LOAD(KN METE) SUMMARY (LOADING 2)
 SUMMATION FORCE-X = 0.00
 SUMMATION FORCE-Y = 99.92
 SUMMATION FORCE-Z = 0.00

SUMMATION OF MOMENTS AROUND THE ORIGIN-
 MX= 0.00 MY= 0.00 MZ= 443.62

C:\Users\ss7n1827\Desktop\Offshore Technology\4th Semester\MSc Thesis\Calculations\Offshore Lift\Upper Pipe\lower p

Thursday, June 07, 2018, 12:45 PM

STAAD PLANE

-- PAGE NO. 17

MAXIMUM DISPLACEMENTS (CM /RADIANS) (LOADING 2)
 MAXIMUMS AT NODE
 X = 0.00000E+00 0
 Y = 2.08670E-01 5
 Z = 0.00000E+00 0
 RX= 0.00000E+00 0
 RY= 0.00000E+00 0
 RZ= -4.03144E-03 8

EXTERNAL AND INTERNAL JOINT LOAD SUMMARY (KN METE)-

JT	EXT FX/ INT FX	EXT FY/ INT FY	EXT FZ/ INT FZ	EXT MX/ INT MX	EXT MY/ INT MY	EXT MZ/ INT MZ
						SUPPORT=1
19	0.00 0.00	-0.08 -49.89	0.00 0.00	0.00 0.00	0.00 0.00	0.00 0.00 111110
20	0.00 0.00	-0.08 -49.89	0.00 0.00	0.00 0.00	0.00 0.00	0.00 0.00 111110

***** END OF DATA FROM INTERNAL STORAGE *****

78. FINISH

***** END OF THE STAAD.Pro RUN *****

**** DATE= JUN 7,2018 TIME= 12:45: 5 ****

C:\Users\ss7n1827\Desktop\Offshore Technology\4th Semester\MSc Thesis\Calculations\Offshore Lift\Upper Pipe\lower p

Thursday, June 07, 2018, 12:45 PM

STAAD PLANE -- PAGE NO. 18

```
*****
*           For questions on STAAD.Pro, please contact           *
*           Bentley Systems or Partner offices                   *
*           *                                                     *
*           Telephone                                           Web / Email *
* USA      +1 (714) 974-2500                                     *
* UK       +44 (0) 808 101 9246                                 *
* SINGAPORE +65 6225-6158                                       *
* FRANCE   +33 (0) 1 55238400                                    *
* GERMANY  +49 0931 40468                                         *
* INDIA    +91 (033) 4006-2021                                    *
* JAPAN    +81 (03)5952-6500  http://www.ctc-g.co.jp *
* CHINA    +86 21 6288 4040                                       *
* THAILAND +66 (0)2645-1018/19 partha.p@reissoftwareth.com*
*           *                                                     *
* Worldwide http://selectservices.bentley.com/en-US/ *
*           *                                                     *
*****
```

C:\Users\ss7n1827\Desktop\Offshore Technology\4th Semester\MSc Thesis\Calculations\Offshore Lift\Upper Pipe\lower p

B.2 Cylindrical pipe (upper pipe)

```

                                                                    Thursday, June 07, 2018, 12:48 PM
                                                                    PAGE NO. 1
*****
*
*          STAAD.Pro V8i SELECTseries3          *
*          Version 20.07.08.20                  *
*          Proprietary Program of              *
*          Bentley Systems, Inc.               *
*          Date= JUN 7, 2018                   *
*          Time= 12:48: 3                      *
*
*          USER ID: Subsea 7                   *
*****

1. STAAD SPACE
INPUT FILE: upper pipe final OPERATIONAL.STD
2. START JOB INFORMATION
3. ENGINEER DATE 23-MAR-18
4. JOB NAME MASTER THESIS
5. JOB CLIENT UIS
6. JOB NO 3
7. ENGINEER NAME E.-CHATZIL
8. END JOB INFORMATION
9. INPUT WIDTH 79
10. UNIT METER KN
11. JOINT COORDINATES
12. 5 1.28462 0 0; 8 2.79462 0 0; 15 6.08462 0 0; 18 7.59462 0 0
13. MEMBER INCIDENCES
14. 3 18 15; 4 15 8; 5 8 5
15. DEFINE MATERIAL START
16. ISOTROPIC STEEL
17. E 2.1E+008
18. POISSON 0.3
19. DENSITY 76.8195
20. ALPHA 1.2E-005
21. DAMP 0.03
22. TYPE STEEL
23. STRENGTH FY 355000 FU 470000 RY 1.5 RT 1.2
24. END DEFINE MATERIAL
25. MEMBER PROPERTY EUROPEAN
26. 3 TO 5 TABLE ST 219.1X20CHS
27. CONSTANTS
28. MATERIAL STEEL ALL
29. SUPPORTS
30. 5 18 PINNED
31. LOAD 1 LOADTYPE DEAD TITLE LIFTING ONSHORE
32. SELFWEIGHT Y -3.62
33. MEMBER LOAD
34. 4 CON Y -130.3 0 0.10955
35. 4 CON Y -130.3 3.29 0.10955
36. LOAD 2 LOADTYPE DEAD TITLE OPERATIONAL
37. SELFWEIGHT Y -2.33
38. MEMBER LOAD
39. 4 CON Y -49.96 0 0.10955
40. 4 CON Y -49.96 3.29 0.10955

C:\Users\ss7n1827\Desktop\Offshore Technology\4th Semester\MSc Thesis\Calculations\Offshore Lift\Upper Pipe\upper p
  
```

Thursday, June 07, 2018, 12:48 PM

STAAD SPACE -- PAGE NO. 2

41. PERFORM ANALYSIS

PROBLEM STATISTICS

NUMBER OF JOINTS/MEMBER+ELEMENTS/SUPPORTS = 4/ 3/ 2

SOLVER USED IS THE OUT-OF-CORE BASIC SOLVER

ORIGINAL/FINAL BAND-WIDTH= 1/ 1/ 12 DOF
 TOTAL PRIMARY LOAD CASES = 2, TOTAL DEGREES OF FREEDOM = 18
 SIZE OF STIFFNESS MATRIX = 1 DOUBLE KILO-WORDS
 REQD/AVAIL. DISK SPACE = 12.0/ 22200.3 MB

*****WARNING - INSTABILITY AT JOINT 18 DIRECTION = MX**
 PROBABLE CAUSE SINGULAR-ADDING WEAK SPRING
 K-MATRIX DIAG= 5.9281965E+04 L-MATRIX DIAG= 7.2759576E-12 EQN NO 16
*****NOTE - VERY WEAK SPRING ADDED FOR STABILITY**

****NOTE**** STAAD DETECTS INSTABILITIES AS EXCESSIVE LOSS OF SIGNIFICANT DIGITS
 DURING DECOMPOSITION. WHEN A DECOMPOSED DIAGONAL IS LESS THAN THE
 BUILT-IN REDUCTION FACTOR TIMES THE ORIGINAL STIFFNESS MATRIX DIAGONAL,
 STAAD PRINTS A SINGULARITY NOTICE. THE BUILT-IN REDUCTION FACTOR
 IS 1.000E-09

THE ABOVE CONDITIONS COULD ALSO BE CAUSED BY VERY STIFF OR VERY WEAK
 ELEMENTS AS WELL AS TRUE SINGULARITIES.

- 42. PARAMETER 3
- 43. CODE EN 1993-1-1:2005
- 44. SGR 4 ALL
- 45. TORSION 2 ALL
- 46. GM0 1.15 ALL
- 47. GM1 1.15 ALL
- 48. TRACK 2 ALL
- 49. CHECK CODE ALL

STAAD.PRO CODE CHECKING - EN 1993-1-1:2005

 NATIONAL ANNEX - NOT USED

PROGRAM CODE REVISION V1.9 BS_EC3_2005/1

C:\Users\ss7n1827\Desktop\Offshore Technology\4th Semester\MSc Thesis\Calculations\Offshore Lift\Upper Pipe\upper p

Thursday, June 07, 2018, 12:48 PM

STAAD SPACE -- PAGE NO. 3

ALL UNITS ARE - KN METE (UNLESS OTHERWISE NOTED)

MEMBER	TABLE	RESULT/ FX	CRITICAL COND/ MY	RATIO/ MZ	LOADING/ LOCATION
3 ST	219.1X20CHS	(EUROPEAN SECTIONS)			
		PASS	EC-6.2.7(5)	0.886	1
		0.00	0.00	209.35	1.51

MATERIAL DATA

Grade of steel = S 460
Modulus of elasticity = 210 kN/mm2
Design Strength (py) = 460 N/mm2

SECTION PROPERTIES (units - cm)

Member Length = 151.00
Gross Area = 125.00 Net Area = 128.00

	z-axis	y-axis
Moment of inertia	: 6261.000	6261.000
Plastic modulus	: 795.000	795.000
Elastic modulus	: 571.520	571.520
Shear Area	: 79.577	79.577
Radius of gyration	: 7.077	7.077
Effective Length	: 151.000	151.000

DESIGN DATA (units - kN,m) EUROCODE NO.3 /2005

Section Class : CLASS 1
Squash Load : 5750.00
Axial force/Squash load : 0.000
GM0 : 1.15 GM1 : 1.15 GM2 : 1.25

	z-axis	y-axis
Slenderness ratio (KL/r)	: 21.3	21.3
Compression Capacity	: 4866.4	4866.4
Tension Capacity	: 4860.0	4860.0
Moment Capacity	: 318.0	318.0
Reduced Moment Capacity	: 318.0	318.0
Shear Capacity	: 1837.8	1837.8

BUCKLING CALCULATIONS (units - kN,m)

Lateral Torsional Buckling Moment MB = 365.7
co-efficients C1_K : C1 =1.000 K =1.0, Effective Length= 1.510

TORSION CALCULATIONS (units - kN,m)

Total Torsional Load T = 10.9
Effective Length for Torsion = 1.510
END1: Torsion Fixed, Warping Fixed END2: Torsion Fixed, Warping Fixed

Max. section forces _capacities: [@ x = 0.000] (units - kN,m)
Torsion at section = 28.5
Pure Torsion Component = 0.0
Warping Torsion Component = -28.5
Pure Torsion Capacity = 287.6
Warping Torsion Capacity = 0.0

C:\Users\ss7n1827\Desktop\Offshore Technology\4th Semester\MSc Thesis\Calculations\Offshore Lift\Upper Pipe\upper p

Thursday, June 07, 2018, 12:48 PM

STAD SPACE

-- PAGE NO. 4

ALL UNITS ARE - KN METE (UNLESS OTHERWISE NOTED)

MEMBER	TABLE	RESULT/ FX	CRITICAL COND/ MY	RATIO/ MZ	LOADING/ LOCATION
--------	-------	---------------	----------------------	--------------	----------------------

CRITICAL LOADS FOR EACH CLAUSE CHECK (units- kN,m):

CLAUSE	RATIO	LOAD	FX	VY	VZ	MZ	MY
EC-6.2.5	0.658	1	0.0	-136.0	0.0	209.4	0.0
EC-6.2.6-(Y)	0.077	1	0.0	141.3	0.0	0.0	0.0
EC-6.3.2 LTB	0.572	1	0.0	-136.0	0.0	209.4	0.0

ADDITIONAL CLAUSE CHECKS FOR TORSION (units- kN,m):

CLAUSE	RATIO	LOAD	DIST	FX	VY	VZ	MZ	MY	MX
EC-6.2.7(1)	0.099	1	0.0	0.0	141.3	0.0	0.0	0.0	28.5
EC-6.2.7(9)	0.083	1	0.0	0.0	141.3	0.0	0.0	0.0	28.5
EC-6.2.7(5)	0.886	1	1.5	0.0	-136.0	0.0	209.4	0.0	28.5

C:\Users\ss7n1827\Desktop\Offshore Technology\4th Semester\MSc Thesis\Calculations\Offshore Lift\Upper Pipe\upper p

Thursday, June 07, 2018, 12:48 PM

STAD SPACE -- PAGE NO. 5

ALL UNITS ARE - KN METE (UNLESS OTHERWISE NOTED)

MEMBER	TABLE	RESULT/ FX	CRITICAL COND/ MY	RATIO/ MZ	LOADING/ LOCATION
4 ST	219.1X20CHS	(EUROPEAN SECTIONS)			
		PASS	EC-6.2.7(5)	0.896	1
		0.00	0.00	213.92	1.92

MATERIAL DATA

Grade of steel = S 460
 Modulus of elasticity = 210 kN/mm2
 Design Strength (py) = 460 N/mm2

SECTION PROPERTIES (units - cm)

Member Length = 329.00
 Gross Area = 125.00 Net Area = 125.00

	z-axis	y-axis
Moment of inertia	: 6261.000	6261.000
Plastic modulus	: 795.000	795.000
Elastic modulus	: 571.520	571.520
Shear Area	: 79.577	79.577
Radius of gyration	: 7.077	7.077
Effective Length	: 329.000	329.000

DESIGN DATA (units - kN,m) EUROCODE NO.3 /2005

Section Class : CLASS 1
 Squash Load : 5750.00
 Axial force/Squash load : 0.000
 GM0 : 1.15 GM1 : 1.15 GM2 : 1.25

	z-axis	y-axis
Slenderness ratio (KL/r)	: 46.5	46.5
Compression Capacity	: 4255.8	4255.8
Tension Capacity	: 4860.0	4860.0
Moment Capacity	: 318.0	318.0
Reduced Moment Capacity	: 318.0	318.0
Shear Capacity	: 1837.8	1837.8

BUCKLING CALCULATIONS (units - kN,m)

Lateral Torsional Buckling Moment MB = 365.7
 co-efficients C1_K : C1 =1.000 K =1.0, Effective Length= 3.290

TORSION CALCULATIONS (units - kN,m)

Total Torsional Load T = 10.9
 Effective Length for Torsion = 3.290
 END1: Torsion Fixed, Warping Fixed END2: Torsion Fixed, Warping Fixed

Max. section forces _capacities: [@ x = 3.290](units - kN,m)
 Torsion at section = 28.5
 Pure Torsion Component = 0.0
 Warping Torsion Component = -28.5
 Pure Torsion Capacity = 287.6
 Warping Torsion Capacity = 0.0

C:\Users\ss7n1827\Desktop\Offshore Technology\4th Semester\MSc Thesis\Calculations\Offshore Lift\Upper Pipe\upper p

Thursday, June 07, 2018, 12:48 PM

STAAD SPACE -- PAGE NO. 6

ALL UNITS ARE - KN METE (UNLESS OTHERWISE NOTED)

MEMBER	TABLE	RESULT/ FX	CRITICAL COND/ MY	RATIO/ MZ	LOADING/ LOCATION
--------	-------	---------------	----------------------	--------------	----------------------

CRITICAL LOADS FOR EACH CLAUSE CHECK (units- kN,m):

CLAUSE	RATIO	LOAD	FX	VY	VZ	MZ	MY
EC-6.2.5	0.673	1	0.0	0.0	0.0	214.1	0.0
EC-6.2.6-(Y)	0.074	1	0.0	136.0	0.0	209.4	0.0
EC-6.3.2 LTB	0.585	1	0.0	0.0	0.0	214.1	0.0

ADDITIONAL CLAUSE CHECKS FOR TORSION (units- kN,m):

CLAUSE	RATIO	LOAD	DIST	FX	VY	VZ	MZ	MY	MX
EC-6.2.7(1)	0.099	1	3.3	0.0	136.0	0.0	209.4	0.0	28.5
EC-6.2.7(9)	0.080	1	3.3	0.0	136.0	0.0	209.4	0.0	28.5
EC-6.2.7(5)	0.896	1	1.9	0.0	-1.0	0.0	213.9	0.0	28.5

C:\Users\ss7n1827\Desktop\Offshore Technology\4th Semester\MSc Thesis\Calculations\Offshore Lift\Upper Pipe\upper p

Thursday, June 07, 2018, 12:48 PM

STAAD SPACE -- PAGE NO. 7

ALL UNITS ARE - KN METE (UNLESS OTHERWISE NOTED)

MEMBER	TABLE	RESULT/ FX	CRITICAL COND/ MY	RATIO/ MZ	LOADING/ LOCATION
5 ST	219.1X20CHS	(EUROPEAN SECTIONS)			
		PRSS	EC-6.2.7(5)	0.847	1
		0.00	0.00	209.35	0.00

MATERIAL DATA

Grade of steel = S 460
 Modulus of elasticity = 210 kN/mm2
 Design Strength (py) = 460 N/mm2

SECTION PROPERTIES (units - cm)

Member Length = 151.00
 Gross Area = 125.00 Net Area = 125.00

	z-axis	y-axis
Moment of inertia	: 6261.000	6261.000
Plastic modulus	: 795.000	795.000
Elastic modulus	: 571.520	571.520
Shear Area	: 79.577	79.577
Radius of gyration	: 7.077	7.077
Effective Length	: 151.000	151.000

DESIGN DATA (units - kN,m) EUROCODE NO.3 /2005

Section Class : CLASS 1
 Squash Load : 5750.00
 Axial force/Squash load : 0.000
 GM0 : 1.15 GM1 : 1.15 GM2 : 1.25

	z-axis	y-axis
Slenderness ratio (KL/r)	: 21.3	21.3
Compression Capacity	: 4866.4	4866.4
Tension Capacity	: 4860.0	4860.0
Moment Capacity	: 318.0	318.0
Reduced Moment Capacity	: 318.0	318.0
Shear Capacity	: 1837.8	1837.8

BUCKLING CALCULATIONS (units - kN,m)

Lateral Torsional Buckling Moment MB = 365.7
 co-efficients C1_K : C1 =1.000 K =1.0, Effective Length= 1.510

TORSION CALCULATIONS (units - kN,m)

Total Torsional Load T = 0.0
 Effective Length for Torsion = 1.510
 END1: Torsion Fixed, Warping Fixed END2: Torsion Fixed, Warping Fixed

Max. section forces _capacities: [0 x = 3.290] (units - kN,m)
 Torsion at section = 28.5
 Pure Torsion Component = 0.0
 Warping Torsion Component = -28.5
 Pure Torsion Capacity = 287.6
 Warping Torsion Capacity = 0.0

C:\Users\ss7n1827\Desktop\Offshore Technology\4th Semester\MSc Thesis\Calculations\Offshore Lift\Upper Pipe\upper p

Thursday, June 07, 2018, 12:48 PM

STAAD SPACE

-- PAGE NO. 8

ALL UNITS ARE - KN METE (UNLESS OTHERWISE NOTED)

MEMBER	TABLE	RESULT/ FX	CRITICAL COND/ MY	RATIO/ MZ	LOADING/ LOCATION
--------	-------	---------------	----------------------	--------------	----------------------

CRITICAL LOADS FOR EACH CLAUSE CHECK (units- kN,m):

CLAUSE	RATIO	LOAD	FX	VY	VZ	MZ	MY
EC-6.2.5	0.658	1	0.0	-136.0	0.0	209.4	0.0
EC-6.2.6-(Y)	0.077	1	0.0	141.3	0.0	0.0	0.0
EC-6.3.2 LTB	0.572	1	0.0	-136.0	0.0	209.4	0.0

ADDITIONAL CLAUSE CHECKS FOR TORSION (units- kN,m):

CLAUSE	RATIO	LOAD	DIST	FX	VY	VZ	MZ	MY	MX
EC-6.2.7(9)	0.077	1	1.5	0.0	141.3	0.0	0.0	0.0	0.0
EC-6.2.7(5)	0.847	1	0.0	0.0	-136.0	0.0	209.4	0.0	0.0

***** END OF TABULATED RESULT OF DESIGN *****

50. PERFORM ANALYSIS PRINT ALL

C:\Users\ss7n1827\Desktop\Offshore Technology\4th Semester\MSc Thesis\Calculations\Offshore Lift\Upper Pipe\upper p

Thursday, June 07, 2018, 12:48 PM

STAD SPACE -- PAGE NO. 9

LOADING 1 LOADTYPE DEAD TITLE LIFTING ONSHORE

SELFWEIGHT Y -3.620

ACTUAL WEIGHT OF THE STRUCTURE = 6.059 KN

MEMBER LOAD - UNIT KN METE

MEMBER	UDL	L1	L2	CON	L	LIN1	LIN2
4				-130.3000 Y	0.00		
4				-130.3000 Y	3.29		

LOADING 2 LOADTYPE DEAD TITLE OPERATIONAL

SELFWEIGHT Y -2.330

ACTUAL WEIGHT OF THE STRUCTURE = 6.059 KN

MEMBER LOAD - UNIT KN METE

MEMBER	UDL	L1	L2	CON	L	LIN1	LIN2
4				-49.9600 Y	0.00		
4				-49.9600 Y	3.29		

***WARNING - INSTABILITY AT JOINT 18 DIRECTION = MX
 PROBABLE CAUSE SINGULAR-ADDING WEAK SPRING
 K-MATRIX DIAG= 5.9281965E+04 L-MATRIX DIAG= 7.2759576E-12 EQN NO 16
 ***NOTE - VERY WEAK SPRING ADDED FOR STABILITY

NOTE STAAD DETECTS INSTABILITIES AS EXCESSIVE LOSS OF SIGNIFICANT DIGITS
 DURING DECOMPOSITION. WHEN A DECOMPOSED DIAGONAL IS LESS THAN THE
 BUILT-IN REDUCTION FACTOR TIMES THE ORIGINAL STIFFNESS MATRIX DIAGONAL,
 STAAD PRINTS A SINGULARITY NOTICE. THE BUILT-IN REDUCTION FACTOR
 IS 1.000E-09

THE ABOVE CONDITIONS COULD ALSO BE CAUSED BY VERY STIFF OR VERY WEAK
 ELEMENTS AS WELL AS TRUE SINGULARITIES.

FOR LOADING - 1

APPLIED JOINT EQUIVALENT LOADS

JOINT	FORCE-X	FORCE-Y	FORCE-Z	MOM-X	MOM-Y	MOM-Z
5	0.00000E+00-2.62444E+00	0.00000E+00	0.00000E+00	0.00000E+00	0.00000E+00	-6.60485E-01
8	0.00000E+00-1.38643E+02	0.00000E+00	-1.42744E+01	0.00000E+00	-2.47532E+00	
15	0.00000E+00-1.38643E+02	0.00000E+00	-1.42744E+01	0.00000E+00	2.47533E+00	
18	0.00000E+00-2.62444E+00	0.00000E+00	0.00000E+00	0.00000E+00	0.00000E+00	6.60485E-01

C:\Users\ss7n1827\Desktop\Offshore Technology\4th Semester\MSc Thesis\Calculations\Offshore Lift\Upper Pipe\upper p

Thursday, June 07, 2018, 12:48 PM

STAAD SPACE

-- PAGE NO. 10

STATIC LOAD/REACTION/EQUILIBRIUM SUMMARY FOR CASE NO. 1
 LOADTYPE DEAD TITLE LIFTING ONSHORE

CENTER OF FORCE BASED ON Y FORCES ONLY (METS).
 (FORCES IN NON-GLOBAL DIRECTIONS WILL INVALIDATE RESULTS)

X = 0.443962000E+01
 Y = 0.000000000E+00
 Z = -0.101045261E+00

***TOTAL APPLIED LOAD (KN METE) SUMMARY (LOADING 1)
 SUMMATION FORCE-X = 0.00
 SUMMATION FORCE-Y = -282.53
 SUMMATION FORCE-Z = 0.00

SUMMATION OF MOMENTS AROUND THE ORIGIN-
 MX= -28.55 MY= 0.00 MZ= -1254.34

***TOTAL REACTION LOAD(KN METE) SUMMARY (LOADING 1)
 SUMMATION FORCE-X = 0.00
 SUMMATION FORCE-Y = 282.53
 SUMMATION FORCE-Z = 0.00

SUMMATION OF MOMENTS AROUND THE ORIGIN-
 MX= 0.00 MY= 0.00 MZ= 1254.34

MAXIMUM DISPLACEMENTS (CM /RADIANS) (LOADING 1)

	MAXIMUMS	AT NODE
X =	0.00000E+00	0
Y =	-5.26702E+00	15
Z =	0.00000E+00	0
RX=	-4.26230E+04	8
RY=	0.00000E+00	0
RZ=	3.86821E-02	18

EXTERNAL AND INTERNAL JOINT LOAD SUMMARY (KN METE)-

JT	EXT FX/	EXT FY/	EXT FZ/	EXT MX/	EXT MY/	EXT MZ/	
	INT FX	INT FY	INT FZ	INT MX	INT MY	INT MZ	
							SUPPORT=1
5	0.00	-2.62	0.00	0.00	0.00	-0.66	
	0.00	-138.64	0.00	0.00	0.00	0.66	111000
18	0.00	-2.62	0.00	0.00	0.00	0.66	
	0.00	-138.64	0.00	-28.55	0.00	-0.66	111000

FOR LOADING - 2

APPLIED JOINT EQUIVALENT LOADS

JOINT	FORCE-X	FORCE-Y	FORCE-Z	MOM-X	MOM-Y	MOM-Z
5	0.00000E+00	-1.68921E+00	0.00000E+00	0.00000E+00	0.00000E+00	-4.25119E-01
8	0.00000E+00	-5.53297E+01	0.00000E+00	-5.47312E+00	0.00000E+00	-1.59314E+00

C:\Users\ss7n1827\Desktop\Offshore Technology\4th Semester\MSc Thesis\Calculations\Offshore Lift\Upper Pipe\upper p

Thursday, June 07, 2018, 12:48 PM

STAAD SPACE -- PAGE NO. 11

APPLIED JOINT EQUIVALENT LOADS

JOINT	FORCE-X	FORCE-Y	FORCE-Z	MOM-X	MOM-Y	MOM-Z
15	0.00000E+00	-5.53297E+01	0.00000E+00	-5.47312E+00	0.00000E+00	1.59315E+00
18	0.00000E+00	-1.68921E+00	0.00000E+00	0.00000E+00	0.00000E+00	4.25119E-01

STATIC LOAD/REACTION/EQUILIBRIUM SUMMARY FOR CASE NO. 2
LOADTYPE DEAD TITLE OPERATIONAL

CENTER OF FORCE BASED ON Y FORCES ONLY (METS) .
(FORCES IN NON-GLOBAL DIRECTIONS WILL INVALIDATE RESULTS)

X = 0.443962001E+01
Y = 0.000000000E+00
Z = -0.959877871E-01

***TOTAL APPLIED LOAD (KN METE) SUMMARY (LOADING 2)

SUMMATION FORCE-X = 0.00
SUMMATION FORCE-Y = -114.04
SUMMATION FORCE-Z = 0.00

SUMMATION OF MOMENTS AROUND THE ORIGIN-

MX= -10.95 MY= 0.00 MZ= -506.28

***TOTAL REACTION LOAD(KN METE) SUMMARY (LOADING 2)

SUMMATION FORCE-X = 0.00
SUMMATION FORCE-Y = 114.04
SUMMATION FORCE-Z = 0.00

SUMMATION OF MOMENTS AROUND THE ORIGIN-

MX= 0.00 MY= 0.00 MZ= 506.28

MAXIMUM DISPLACEMENTS (CM /RADIANS) (LOADING 2)

	MAXIMUMS	AT NODE
X	0.00000E+00	0
Y	-2.11786E+00	8
Z	0.00000E+00	0
RX	-1.63426E+04	5
RY	0.00000E+00	0
RZ	1.55518E-02	18

EXTERNAL AND INTERNAL JOINT LOAD SUMMARY (KN METE)-

JT	EXT FX/	EXT FY/	EXT FZ/	EXT MX/	EXT MY/	EXT MZ/	
	INT FX	INT FY	INT FZ	INT MX	INT MY	INT MZ	
							SUPPORT=1
5	0.00	-1.69	0.00	0.00	0.00	-0.43	
	0.00	-55.33	0.00	0.00	0.00	0.43	111000
18	0.00	-1.69	0.00	0.00	0.00	0.43	
	0.00	-55.33	0.00	-10.95	0.00	-0.43	111000

C:\Users\ss7n1827\Desktop\Offshore Technology\4th Semester\MSc Thesis\Calculations\Offshore Lift\Upper Pipe\upper p

Thursday, June 07, 2018, 12:48 PM

STAAD SPACE

-- PAGE NO. 12

***** END OF DATA FROM INTERNAL STORAGE *****

51. FINISH

***** END OF THE STAAD.Pro RUN *****

**** DATE= JUN 7,2018 TIME= 12:48: 4 ****

* For questions on STAAD.Pro, please contact *
* Bentley Systems or Partner offices *
* *
* Telephone Web / Email *
* USA +1 (714) 974-2500 *
* UK +44 (0) 808 101 9246 *
* SINGAPORE +65 6225-6158 *
* FRANCE +33 (0) 1 55238400 *
* GERMANY +49 0931 40468 *
* INDIA +91 (033) 4006-2021 *
* JAPAN +81 (03)5952-6500 <http://www.ctc-g.co.jp> *
* CHINA +86 21 6288 4040 *
* THAILAND +66 (0)2645-1018/19 partha.p@reisoftwareth.com*
* *
* Worldwide <http://selectservices.bentley.com/en-US/> *
* *

C:\Users\ss7n1827\Desktop\Offshore Technology\4th Semester\MSc Thesis\Calculations\Offshore Lift\Upper Pipe\upper p

APPENDIX C:

Inventor spur gear design

Spur Gears Component Generator

Design Calculation

Common

Design Guide: Module and Number of Teeth

Pressure Angle: 20 deg

Helix Angle: 0deg

Desired Gear Ratio: 4.5

Module: 4.000 mm

Center Distance: 195

Unit Corrections Guide: In Gear Ratio

Total Unit Correction: 0.2548 ul

Preview...

Gear 1

Component: Cylindrical Face

Number of Teeth: 18 ul

Facewidth: 50 mm

Unit Correction: 0.0473 ul

Gear 2

Component: Cylindrical Face

Number of Teeth: 79 ul

Facewidth: 50 mm

Unit Correction: 0.2075 ul

Results:

ϵ : 1.6303 ul

Gear 1

d_a : 80.340 mm

d : 72.000 mm

d_f : 62.378 mm

x_z : 0.5871 ul

x_p : 0.0327 ul

x_d : -0.1482 ul

s_a : 0.6688 ul

b_r : 0.6944 ul

Gear 2

d_a : 325.622 mm

d : 316.000 mm

d_f : 307.660 mm

ϵ : 1.7747 ul

Calculate OK Cancel <<

Input Type: Gear Ratio Number of Teeth

Size Type: Module Diametral Pitch

Reaching Center Distance: Teeth Correction Helix Angle

Unit Tooth Sizes:

Addendum: a^* Gear 1: 1.0000 ul, Gear 2: 1.0000 ul

Clearance: c^* Gear 1: 0.2500 ul, Gear 2: 0.2500 ul

Root Fillet: r_f^* Gear 1: 0.2500 ul, Gear 2: 0.2500 ul

Spur Gears Component Generator

Design Calculation

Method of Strength Calculation: ANSI/AGMA 2001-D04:2005

Loads:

Power: Gear 1: 11.356 kW, Gear 2: 10.788 kW

Speed: Gear 1: 40 rpm, Gear 2: 9.11 rpm

Torque: Gear 1: 2711 N m, Gear 2: 11303.364 N m

Efficiency: η : 0.95 ul

Material Values:

Gear 1: 14NiCr18

Gear 2: 14NiCr18

Allowable Bending Stress: s_{at} Gear 1: 483.0 MPa, Gear 2: 483.0 MPa

Allowable Contact Stress: s_{ac} Gear 1: 1550.0 MPa, Gear 2: 1550.0 MPa

Modulus of Elasticity: E Gear 1: 206000 MPa, Gear 2: 206000 MPa

Poisson's Ratio: μ Gear 1: 0.300 ul, Gear 2: 0.300 ul

Required Life: L_h : 10000 hr

Factors Accuracy

Results:

F_t : 74919.373 N

F_r : 28447.609 N

F_a : 0.000 N

F_n : 80138.498 N

v : 0.151 mps

n_{E1} : 18343.160 rpm

Gear 1

k_f : 0.531 ul

k_n : 0.545 ul

Gear 2

k_f : 0.577 ul

k_n : 0.566 ul

Calculate OK Cancel >>

Spur Gears Component Generator (Version: 2015 (Build 190159000, 159))

25/5/2018

Design Guide - Module and Number of Teeth

Unit Corrections Guide - In Gear Ratio

Type of Load Calculation - Power calculation for the specified torque and speed

Type of Strength Calculation - Check Calculation

Method of Strength Calculation - ANSI/AGMA 2001-D04:2005

Common Parameters

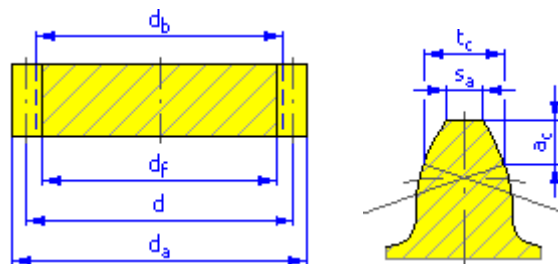
Gear Ratio	i	4.3889 ul
Desired Gear Ratio	i_{in}	4.5000 ul
Module	m	4.000 mm
Helix Angle	β	0.0000 deg
Pressure Angle	α	20.0000 deg
Center Distance	a_w	195.000 mm
Product Center Distance	a	194.000 mm
Total Unit Correction	Σx	0.2548 ul

Circular Pitch	p	12.566 mm
Base Circular Pitch	ptb	11.809 mm
Operating Pressure Angle	α_w	20.7923 deg
Contact Ratio	ϵ	1.6303 ul
Limit Deviation of Axis Parallelity	f_x	0.0140 mm
Limit Deviation of Axis Parallelity	f_y	0.0070 mm

☐ Gears

		Gear 1	Gear 2
Type of model		Component	Component
Number of Teeth	z	18 ul	79 ul
Unit Correction	x	0.0473 ul	0.2075 ul
Pitch Diameter	d	72.000 mm	316.000 mm
Outside Diameter	d_a	80.340 mm	325.622 mm
Root Diameter	d_f	62.378 mm	307.660 mm
Base Circle Diameter	d_b	67.658 mm	296.943 mm
Work Pitch Diameter	d_w	72.371 mm	317.629 mm
Facewidth	b	50.000 mm	50.000 mm
Facewidth Ratio	b_r	0.6944 ul	0.1582 ul
Addendum	a^*	1.0000 ul	1.0000 ul
Clearance	c^*	0.2500 ul	0.2500 ul
Root Fillet	r_f^*	0.2500 ul	0.2500 ul
Tooth Thickness	s	6.421 mm	6.887 mm
Tangential Tooth Thickness	s_t	6.421 mm	6.887 mm
Chordal Thickness	t_c	5.670 mm	6.082 mm
Chordal Addendum	a_c	3.138 mm	3.704 mm
Chordal Dimension	W	30.659 mm	117.174 mm
Chordal Dimension Teeth	z_w	3.000 ul	10.000 ul
Dimension Over (Between) Wires	M	85.327 mm	329.429 mm
Wire Diameter	d_M	8.007 mm	7.500 mm
Limit Deviation of Helix Angle	F_β	0.0140 mm	0.0150 mm
Limit Circumferential Run-out	F_r	0.0220 mm	0.0380 mm
Limit Deviation of Axial Pitch	f_{pt}	0.0090 mm	0.0110 mm
Limit Deviation of Basic Pitch	f_{pb}	0.0085 mm	0.0100 mm
Virtual Number of Teeth	z_v	18.000 ul	79.000 ul

Virtual Pitch Diameter	d_n	72.000 mm	316.000 mm
Virtual Outside Diameter	d_{an}	80.340 mm	325.622 mm
Virtual Base Circle Diameter	d_{bn}	67.658 mm	296.943 mm
Unit Correction without Tapering	x_z	0.5871 ul	-1.2742 ul
Unit Correction without Undercut	x_p	0.0327 ul	-3.5351 ul
Unit Correction Allowed Undercut	x_d	-0.1482 ul	-3.7160 ul
Addendum Truncation	k	0.0048 ul	0.0048 ul
Unit Outside Tooth Thickness	s_a	0.6688 ul	0.7779 ul
Tip Pressure Angle	α_a	32.6328 deg	24.2272 deg



⊞ Loads

		Gear 1	Gear 2
Power	P	11.356 kW	10.788 kW
Speed	n	40.00 rpm	9.11 rpm
Torque	T	2711.000 N m	11303.364 N m
Efficiency	η	0.950 ul	
Radial Force	F_r	28447.609 N	
Tangential Force	F_t	74919.373 N	
Axial Force	F_a	0.000 N	
Normal Force	F_n	80138.498 N	
Circumferential Speed	v	0.151 mps	
Resonance Speed	n_{E1}	18343.160 rpm	

⊞ Material

		Gear 1	Gear 2
		14NiCr18	14NiCr18
Ultimate Tensile Strength	S_u	MPa	MPa
Yield Strength	S_y	MPa	MPa
Modulus of Elasticity	E	MPa	MPa
Poisson's Ratio	μ	0.300 ul	0.300 ul
Allowable Bending Stress	s_{at}	483.0 MPa	483.0 MPa
Allowable Contact Stress	s_{ac}	1550.0 MPa	1550.0 MPa

Hardness in Tooth Core	JHV	210 ul	210 ul
Type of Treatment	type	4 ul	4 ul

Strength Calculation

Factors of Additional Load

Overload Factor	Ko	1.000 ul	
Dynamic Factor	Kv	1.014 ul	
Size Factor	Ks	1.000 ul	1.000 ul
Reliability Factor	KR	1.000 ul	
Temperature Factor	kt	1.000 ul	
Load Distribution Factor	Km	1.114 ul	1.114 ul
Lead Correction Factor	Cmc	1.000 ul	1.000 ul
Mesh Alignment Correction Factor	Ce	1.000 ul	
Pinion Proportion Modifier	Cpm	1.000 ul	
Mesh Alignment Factor	Cma	Commercial Enclosed Gear Units (0.0578)	

Factors for Contact

Surface Condition Factor	Cf	1.000 ul	1.000 ul
Stress Cycle Factor	ZN	0.952 ul	1.034 ul
Hardness Ratio Factor	CH	1.000 ul	1.000 ul
Elastic Factor	Cp	2285.933 ul	
Geometry Factor	I	0.109 ul	

Factors for Bending

Reverse Loading Factor	Ya	1.000 ul	1.000 ul
Rim Thickness Factor	KB	1.000 ul	1.000 ul
Stress Cycle Factor	YN	0.972 ul	1.020 ul
Geometry Factor	J	0.492 ul	0.487 ul

Results

Factor of Safety from Pitting	kf	0.531 ul	0.577 ul
Factor of Safety from Tooth Breakage	kn	0.545 ul	0.566 ul
Check Calculation	Negative		

APPENDIX D:

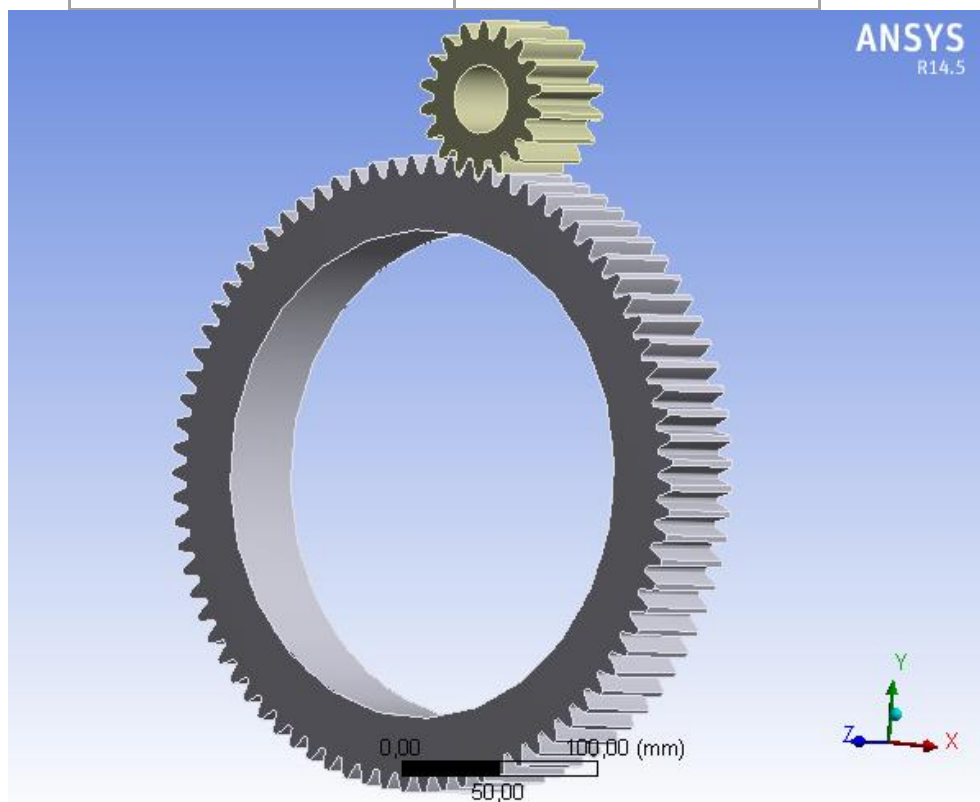
Ansysis report

3. juni 2018
16:14



Project

First Saved	Wednesday, May 23, 2018
Last Saved	Sunday, June 03, 2018
Product Version	14.5.7 Release
Save Project Before Solution	No
Save Project After Solution	No



Contents

- [Units](#)
- [Model \(A4\)](#)
 - [Geometry](#)
 - [Parts](#)
 - [Coordinate Systems](#)
 - [Connections](#)
 - [Contacts](#)
 - [Frictionless - thesispinion To thesisgear](#)
 - [Mesh](#)
 - [Face Sizing](#)
 - [Static Structural \(A5\)](#)
 - [Analysis Settings](#)
 - [Loads](#)
 - [Solution \(A6\)](#)
 - [Solution Information](#)
 - [Results](#)
 - [Contact Tool](#)
 - [Results](#)
- [Material Data](#)
 - [Structural Steel](#)

Units

TABLE 1

Unit System	Metric (mm, kg, N, s, mV, mA) Degrees rad/s Celsius
Angle	Degrees
Rotational Velocity	rad/s
Temperature	Celsius

Model (A4)

Geometry

TABLE 2

Model (A4) > Geometry

Object Name	Geometry
State	Fully Defined
Definition	
Source	C:\Users\ss7n1827\Desktop\Thesis\thesis_renos1.stp
Type	Step
Length Unit	Meters
Element Control	Program Controlled

Display Style	Body Color
Bounding Box	
Length X	325,98 mm
Length Y	425,96 mm
Length Z	50, mm
Properties	
Volume	1,6495e+006 mm ³
Mass	12,949 kg
Scale Factor Value	1,
Statistics	
Bodies	2
Active Bodies	2
Nodes	289226
Elements	64827
Mesh Metric	None
Basic Geometry Options	
Solid Bodies	Yes
Surface Bodies	Yes
Line Bodies	No
Parameters	Yes
Parameter Key	DS
Attributes	No
Named Selections	No
Material Properties	No
Advanced Geometry Options	
Use Associativity	Yes
Coordinate Systems	No
Reader Mode Saves Updated File	No

Use Instances	Yes
Smart CAD Update	No
Attach File Via Temp File	Yes
Temporary Directory	C:\Users\ss7n1827\AppData\Local\Temp
Analysis Type	3-D
Mixed Import Resolution	None
Decompose Disjoint Geometry	Yes
Enclosure and Symmetry Processing	Yes

TABLE 3
Model (A4) > Geometry > Parts

Object Name	thesisgear	thesispinion
State	Meshed	
Graphics Properties		
Visible	Yes	
Transparency	1	
Definition		
Suppressed	No	
Stiffness Behavior	Flexible	
Coordinate System	Default Coordinate System	
Reference Temperature	By Environment	
Material		
Assignment	Structural Steel	
Nonlinear Effects	Yes	
Thermal Strain Effects	Yes	
Bounding Box		
Length X	325,98 mm	80,777 mm
Length Y	325,93 mm	80,171 mm
Length Z	50, mm	

Properties		
Volume	1,4957e+006 mm ³	1,5384e+005 mm ³
Mass	11,741 kg	1,2076 kg
Centroid X	-4,9852e-002 mm	21,194 mm
Centroid Y	7,2334e-003 mm	193,87 mm
Centroid Z	25, mm	
Moment of Inertia Ip1	1,2367e+005 kg·mm ²	748,73 kg·mm ²
Moment of Inertia Ip2	1,236e+005 kg·mm ²	748,73 kg·mm ²
Moment of Inertia Ip3	2,4231e+005 kg·mm ²	995,21 kg·mm ²
Statistics		
Nodes	66119	223107
Elements	13336	51491
Mesh Metric	None	

Coordinate Systems

TABLE 4

Model (A4) > Coordinate Systems > Coordinate System

Object Name	Global Coordinate System
State	Fully Defined
Definition	
Type	Cartesian
Coordinate System ID	0,
Origin	
Origin X	0, mm
Origin Y	0, mm
Origin Z	0, mm
Directional Vectors	
X Axis Data	[1, 0, 0,]
Y Axis Data	[0, 1, 0,]
Z Axis Data	[0, 0, 1,]

Connections

TABLE 5
Model (A4) > Connections

Object Name	Connections
State	Fully Defined
Auto Detection	
Generate Automatic Connection On Refresh	Yes
Transparency	
Enabled	Yes

TABLE 6
Model (A4) > Connections > Contacts

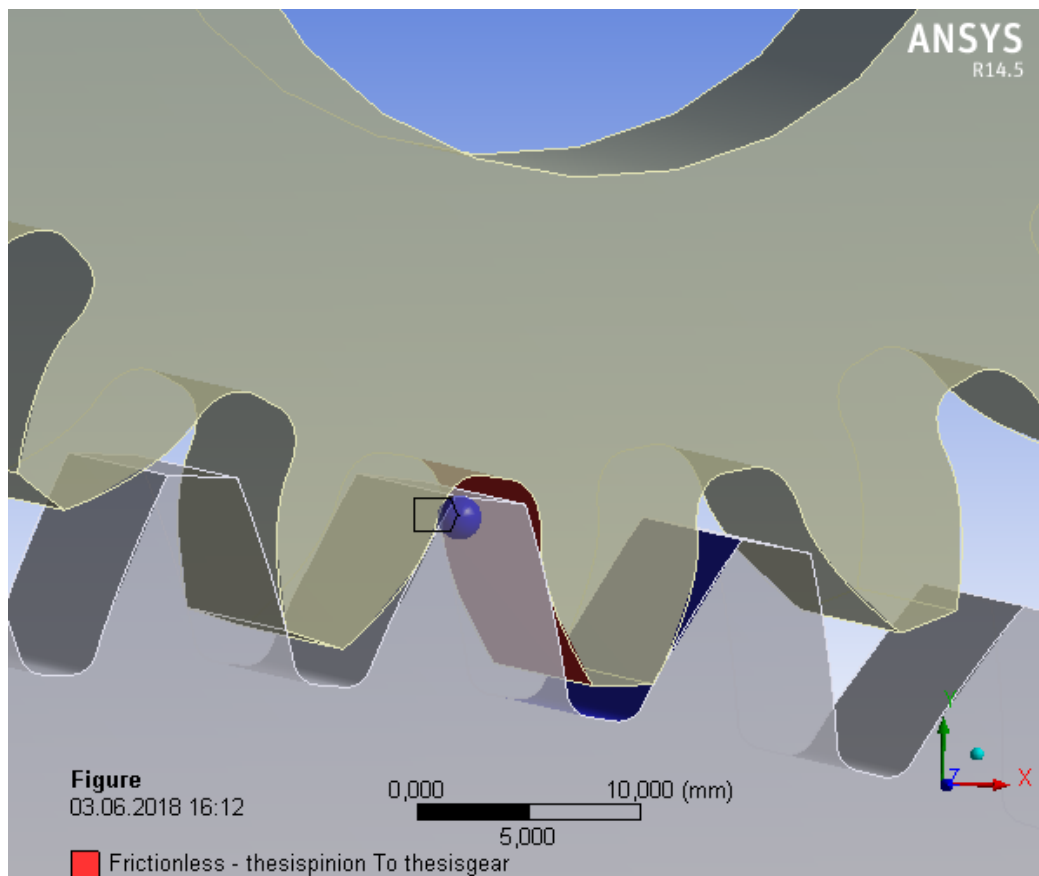
Object Name	Contacts
State	Fully Defined
Definition	
Connection Type	Contact
Scope	
Scoping Method	Geometry Selection
Geometry	All Bodies
Auto Detection	
Tolerance Type	Slider
Tolerance Slider	0,
Tolerance Value	1,4144 mm
Use Range	No
Face/Face	Yes
Face/Edge	No
Edge/Edge	No
Priority	Include All
Group By	Bodies
Search Across	Bodies

TABLE 7
Model (A4) > Connections > Contacts > Contact Regions

Object Name	Frictionless - thesispinion To thesisear
--------------------	--

State	Fully Defined
Scope	
Scoping Method	Geometry Selection
Contact	1 Face
Target	1 Face
Contact Bodies	thesispinion
Target Bodies	thesisgear
Definition	
Type	Frictionless
Scope Mode	Manual
Behavior	Program Controlled
Trim Contact	Program Controlled
Suppressed	No
Advanced	
Formulation	Augmented Lagrange
Detection Method	Program Controlled
Penetration Tolerance	Program Controlled
Interface Treatment	Adjust to Touch
Normal Stiffness	Manual
Normal Stiffness Factor	1,
Update Stiffness	Program Controlled
Stabilization Damping Factor	0,
Pinball Region	Radius
Pinball Radius	1, mm
Time Step Controls	None

FIGURE 1
 Model (A4) > Connections > Contacts > Frictionless - thesispinion To thesisgear > Figure



Mesh

TABLE 8

Model (A4) > Mesh

Object Name	Mesh
State	Solved
Defaults	
Physics Preference	Mechanical
Relevance	0
Sizing	
Use Advanced Size Function	Off
Relevance Center	Coarse
Element Size	Default
Initial Size Seed	Active Assembly
Smoothing	Medium
Transition	Fast

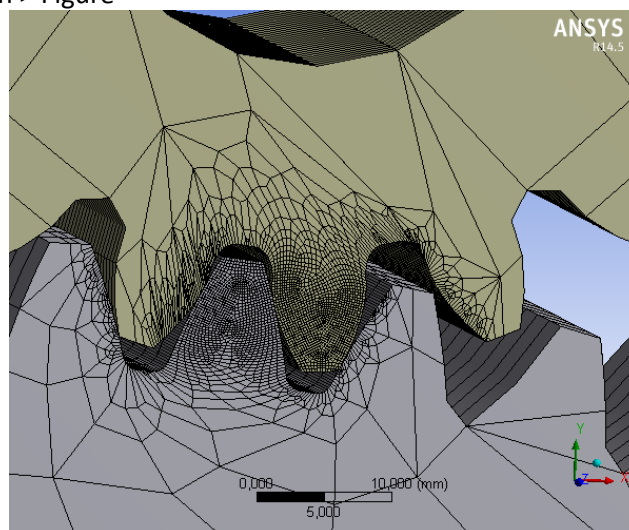
Span Angle Center	Coarse
Minimum Edge Length	2,67530 mm
Inflation	
Use Automatic Inflation	None
Inflation Option	Smooth Transition
Transition Ratio	0,272
Maximum Layers	5
Growth Rate	1,2
Inflation Algorithm	Pre
View Advanced Options	Yes
Collision Avoidance	Stair Stepping
Gap Factor	0,5
Maximum Height over Base	1
Growth Rate Type	Geometric
Maximum Angle	140,0 °
Fillet Ratio	1
Use Post Smoothing	Yes
Smoothing Iterations	5
Patch Conforming Options	
Triangle Surface Mesher	Program Controlled
Advanced	
Shape Checking	Standard Mechanical
Element Midside Nodes	Kept
Straight Sided Elements	No
Number of Retries	0
Extra Retries For Assembly	Yes
Rigid Body Behavior	Dimensionally Reduced
Mesh Morphing	Disabled
Defeaturing	

Pinch Tolerance	Please Define
Generate Pinch on Refresh	No
Automatic Mesh Based Defeaturing	On
Defeaturing Tolerance	Default
Statistics	
Nodes	289226
Elements	64827
Mesh Metric	None

TABLE 9
 Model (A4) > Mesh > Mesh Controls

Object Name	Face Sizing
State	Fully Defined
Scope	
Scoping Method	Geometry Selection
Geometry	6 Faces
Definition	
Suppressed	No
Type	Element Size
Element Size	0,2 mm
Behavior	Soft

FIGURE 2
 Model (A4) > Mesh > Figure



Static Structural (A5)

TABLE 10
Model (A4) > Analysis

Object Name	Static Structural (A5)
State	Solved
Definition	
Physics Type	Structural
Analysis Type	Static Structural
Solver Target	Mechanical APDL
Options	
Environment Temperature	22, °C
Generate Input Only	No

TABLE 11
Model (A4) > Static Structural (A5) > Analysis Settings

Object Name	Analysis Settings
State	Fully Defined
Step Controls	
Number Of Steps	1,
Current Step Number	1,
Step End Time	1, s
Auto Time Stepping	Program Controlled
Solver Controls	
Solver Type	Program Controlled
Weak Springs	Program Controlled
Large Deflection	Off
Inertia Relief	Off
Restart Controls	
Generate Restart Points	Program Controlled
Retain Files After Full Solve	No
Nonlinear Controls	

Force Convergence	Program Controlled
Moment Convergence	Program Controlled
Displacement Convergence	Program Controlled
Rotation Convergence	Program Controlled
Line Search	Program Controlled
Stabilization	Off
Output Controls	
Stress	Yes
Strain	Yes
Nodal Forces	No
Contact Miscellaneous	No
General Miscellaneous	No
Store Results At	All Time Points
Max Number of Result Sets	Program Controlled
Analysis Data Management	
Solver Files Directory	\\noforufs02\home\$\SS7N1827\dp0\SYS\MECH\
Future Analysis	None
Scratch Solver Files Directory	
Save MAPDL db	No
Delete Unneeded Files	Yes
Nonlinear Solution	Yes
Solver Units	Active System
Solver Unit System	nmm

FIGURE 3
 Model (A4) > Static Structural (A5) > Figure

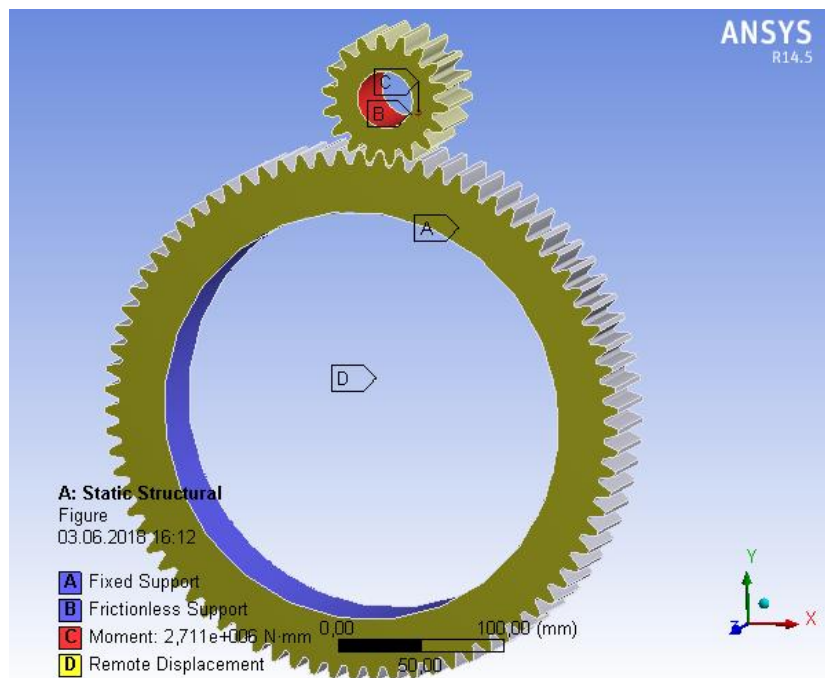


TABLE 12
Model (A4) > Static Structural (A5) > Loads

Object Name	Fixed Support	Frictionless Support	Moment	Remote Displacement
State	Fully Defined			
Scope				
Scoping Method	Geometry Selection			
Geometry	1 Face			4 Faces
Coordinate System				Global Coordinate System
X Coordinate				1,9054 mm
Y Coordinate				17,85 mm
Z Coordinate				25, mm
Location				Defined
Definition				
Type	Fixed Support	Frictionless Support	Moment	Remote Displacement
Suppressed	No			

Define By			Vector	
Magnitude			2,711e+006 N-mm (ramped)	
Direction			Defined	
Behavior			Deformable	
X Component				0, mm (ramped)
Y Component				0, mm (ramped)
Z Component				0, mm (ramped)
Rotation X				Free
Rotation Y				Free
Rotation Z				Free
Advanced				
Pinball Region			All	

FIGURE 4
Model (A4) > Static Structural (A5) > Moment

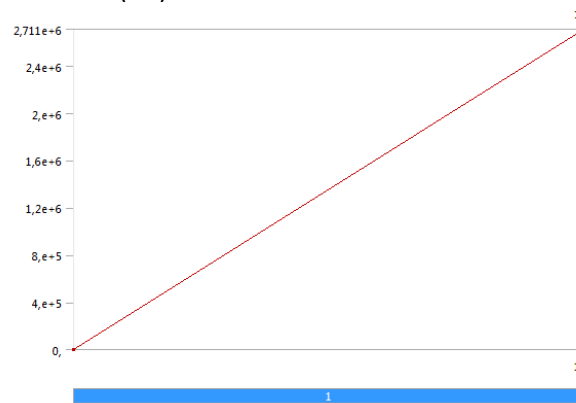
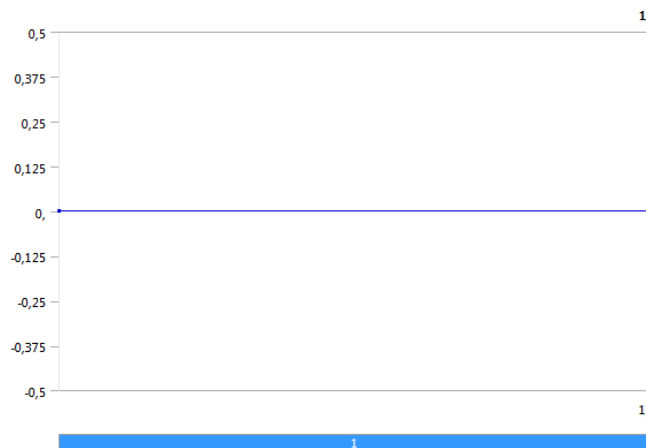


FIGURE 5
Model (A4) > Static Structural (A5) > Remote Displacement



Solution (A6)

TABLE 13

Model (A4) > Static Structural (A5) > Solution

Object Name	Solution (A6)
State	Solved
Adaptive Mesh Refinement	
Max Refinement Loops	1,
Refinement Depth	2,
Information	
Status	Done

TABLE 14

Model (A4) > Static Structural (A5) > Solution (A6) > Solution Information

Object Name	Solution Information
State	Solved
Solution Information	
Solution Output	Solver Output
Newton-Raphson Residuals	0
Update Interval	2,5 s
Display Points	All
FE Connection Visibility	
Activate Visibility	Yes
Display	All FE Connectors
Draw Connections Attached To	All Nodes

Line Color	Connection Type
Visible on Results	No
Line Thickness	Single
Display Type	Lines

TABLE 15
Model (A4) > Static Structural (A5) > Solution (A6) > Results

Object Name	Equivalent Stress	Total Deformation
State	Solved	
Scope		
Scoping Method	Geometry Selection	
Geometry	All Bodies	
Definition		
Type	Equivalent (von-Mises) Stress	Total Deformation
By	Time	
Display Time	Last	
Calculate Time History	Yes	
Identifier		
Suppressed	No	
Integration Point Results		
Display Option	Averaged	
Results		
Minimum	5,7436e-003 MPa	0, mm
Maximum	1074,6 MPa	0,37979 mm
Minimum Occurs On	thesisgear	
Maximum Occurs On	thesispinion	
Information		
Time	1, s	
Load Step	1	
Substep	1	
Iteration Number	4	

FIGURE 6
Model (A4) > Static Structural (A5) > Solution (A6) > Equivalent Stress > Figure 3

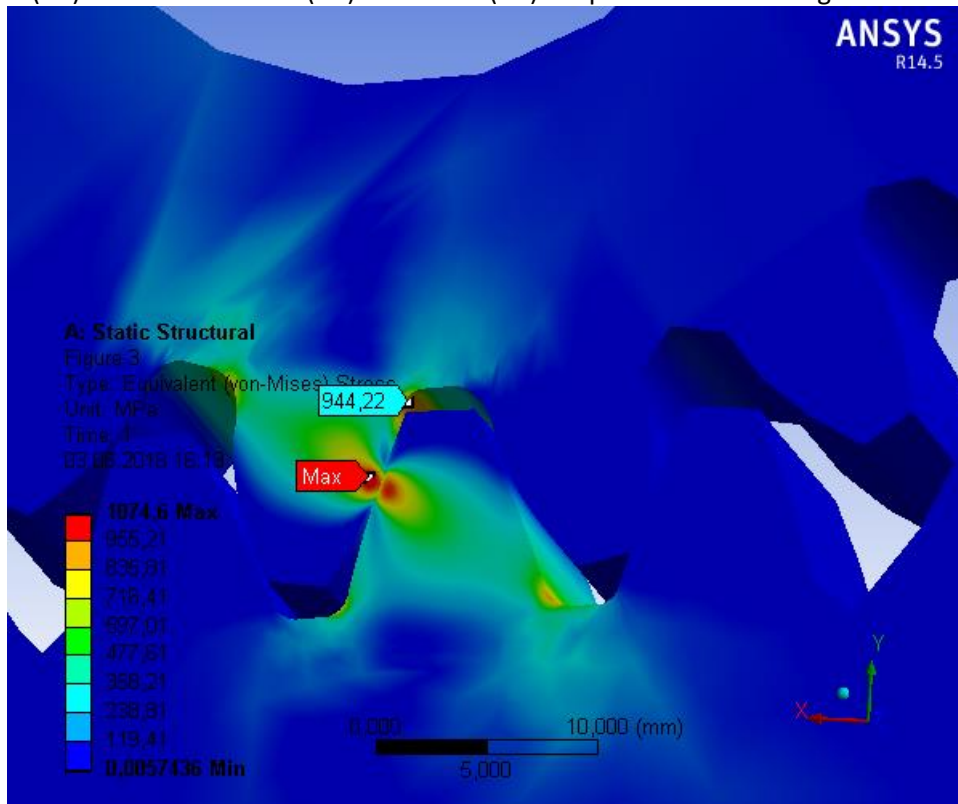


TABLE 16
Model (A4) > Static Structural (A5) > Solution (A6) > Contact Tools

Object Name	Contact Tool
State	Solved
Scope	
Scoping Method	Geometry Selection
Geometry	2 Faces

Model (A4) > Static Structural (A5) > Solution (A6) > Contact Tool

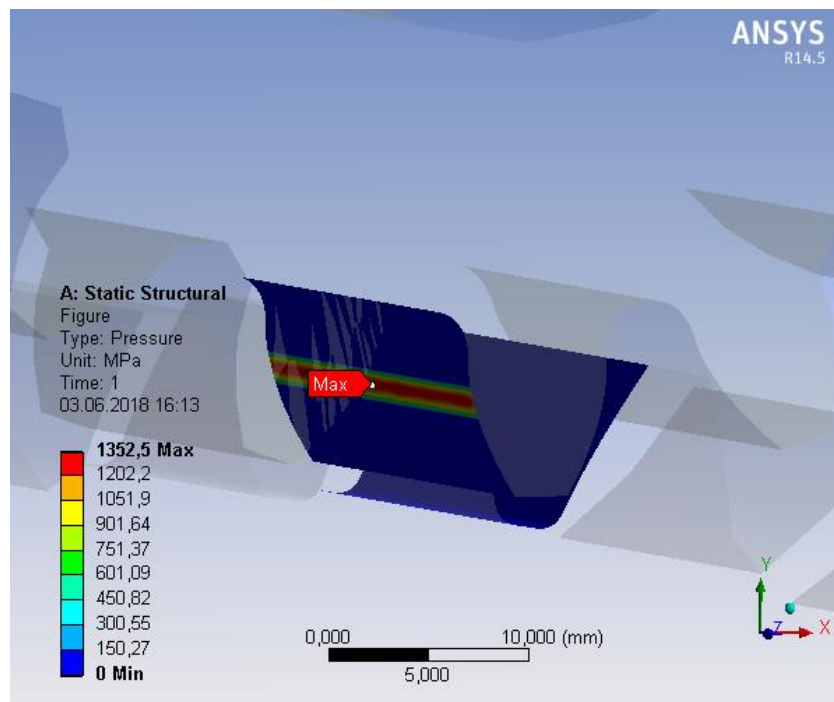
Name	Contact Side
Frictionless - thesispinion To thesisgear	Both

TABLE 17
Model (A4) > Static Structural (A5) > Solution (A6) > Contact Tool > Results

Object Name	Status	Pressure
State	Solved	
Definition		
Type	Status	Pressure

By	Time	
Display Time	Last	
Calculate Time History	Yes	
Identifier		
Suppressed	No	
Integration Point Results		
Display Option	Averaged	
Information		
Time	1, s	
Load Step	1	
Substep	1	
Iteration Number	4	
Results		
Minimum		0, MPa
Maximum		1352,5 MPa
Minimum Occurs On		thesisgear
Maximum Occurs On		thesispinion

FIGURE 7
 Model (A4) > Static Structural (A5) > Solution (A6) > Contact Tool > Pressure > Figure



Material Data

Structural Steel

TABLE 18

Structural Steel > Constants

Density	7,85e-006 kg mm ⁻³
Coefficient of Thermal Expansion	1,2e-005 C ⁻¹
Specific Heat	4,34e+005 mJ kg ⁻¹ C ⁻¹
Thermal Conductivity	6,05e-002 W mm ⁻¹ C ⁻¹
Resistivity	1,7e-004 ohm mm

TABLE 19

Structural Steel > Compressive Ultimate Strength

Compressive Ultimate Strength MPa
850,

TABLE 20

Structural Steel > Compressive Yield Strength

Compressive Yield Strength MPa
550,

TABLE 21

Structural Steel > Tensile Yield Strength

Tensile Yield Strength MPa
885,

TABLE 22
Structural Steel > Tensile Ultimate Strength

Tensile Ultimate Strength MPa
1130,

TABLE 23
Structural Steel > Isotropic Secant Coefficient of Thermal Expansion

Reference Temperature C
22,

TABLE 24
Structural Steel > Alternating Stress Mean Stress

Alternating Stress MPa	Cycles	Mean Stress MPa
3999,	10,	0,
2827,	20,	0,
1896,	50,	0,
1413,	100,	0,
1069,	200,	0,
441,	2000,	0,
262,	10000	0,
214,	20000	0,
138,	1,e+005	0,
114,	2,e+005	0,
86,2	1,e+006	0,

TABLE 25
Structural Steel > Strain-Life Parameters

Strength Coefficient MPa	Strength Exponent	Ductility Coefficient	Ductility Exponent	Cyclic Strength Coefficient MPa	Cyclic Strain Hardening Exponent
920,	-0,106	0,213	-0,47	1000,	0,2

TABLE 26
Structural Steel > Isotropic Elasticity

Temperature C	Young's Modulus MPa	Poisson's Ratio	Bulk Modulus MPa	Shear Modulus MPa
	206000	0,30	67647	79300

TABLE 27
Structural Steel > Isotropic Relative Permeability

Relative Permeability
10000

Inserted from
[<file:///C:/Users/ss7n1827/AppData/Roaming/Ansys/v145/Mechanical_Report/Mechanical_Report.htm>](file:///C:/Users/ss7n1827/AppData/Roaming/Ansys/v145/Mechanical_Report/Mechanical_Report.htm)

APPENDIX E:

Structural checks

Project: Master Thesis 2018	Multi-handling mechanism	Page: 1 of 11
Client: UiS		Originator: Eirinaios Chatzillari
		Checker:

Structural checks for the final handling mechanism

References

- /1/ EN1993-1-8 Eurocode 3: Design of Steel Structures, part 1-1: General Rules and Rules for Buildings
- /2/ EN1993-1-8 Eurocode 3: Design of Steel Structures, part 1-8: Design of Joints, 2005
- /3/ DNV-OS-C101, Design of Offshore Steel Structures, General, 2004
- /4/ Norsok N-004, Structural Design
- /5/ www.astrup.no/Materialer-Produkter/Materialer/Plast-Teknisk/PA-POM-PET
- /6/ EN ISO 13628-8:2006: Part 8: Remotely Operated Vehicle (ROV) interfaces on subsea production systems
- /7/ Arthur P. Boresi and Richard J. Schmidt, Advanced Mechanics of Materials, 6th ed., Wiley, New York, 2003, pp.589-623.

General:

This calculation sheet covers the structural checks of the following components:

- a) Panel plate and POM cross section resistance against contact compressive forces
- b) Structural integrity of ROV bucket bolts
- c) Weld check of the stem

Units: $\frac{kN}{mm^2} := 1000\text{-newton}$ $\frac{g}{mm} := 9.81m \cdot s^{-2}$ $Te := 1\text{tonne}$ $\frac{MPa}{mm^2} := 1 \cdot N \cdot mm^{-2}$ $kNm := kN \cdot m$

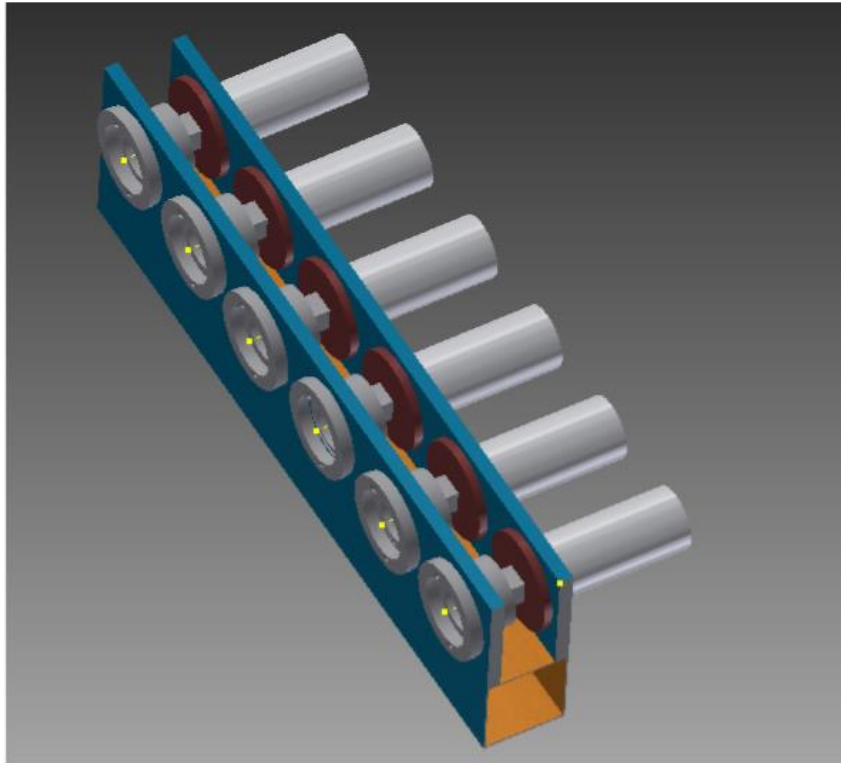
GENERIC INPUT PARAMETERS

	Yield strength	Tensile strength
Material S355, $t \leq 40\text{mm}$ (Ref /1/):	$f_y := 355\text{MPa}$	$f_u := 510\text{MPa}$
Welding material 355:	$f_{yw_355} := 355\text{MPa}$	$f_{uw_355} := 490\text{MPa}$
Poisson's ratio in elastic stage:	$\nu := 0.30$	
Density steel:	$\rho_{st} := 7850 \frac{kg}{m^3}$	
Elasticity modulus	$E := 210000 \frac{N}{mm^2}$	
Shear modulus	$G = \frac{E}{2 \cdot (1 + \nu)} = 80769.23 \frac{N}{mm^2}$	
Cross-section resistance factor:	$\gamma_{M0} := 1.15$	(ref. to /1/)
Resistance factor of members to instability:	$\gamma_{M1} := 1.15$	(ref. to /1/)
Resistance factor of cross-section in tension to fracture:	$\gamma_{M2} := 1.25$	(ref. to /1/)
Weld correlation factor steel:	$\beta_w := 0.9$	(ref. to /2/)
Load factor:	$\gamma_f := 1.30$	(ref. to /3/)

Project: **Master Thesis 2018**
 Client: UiS

Multi-handling mechanism

Page: 2 of 11
 Originator: Eirinaios Chatzillari
 Checker:



The concrete handling mechanism consists of: one panel plate (2.55m x 0.40 m) with 6 bores, 6 circular end-flanges, 6 stems welded on the end-flanges, one plate with 6 bores for attachment of 6 ROV buckets and 6 RPV buckets. The supporting frame beam is not within the scope of the present analysis.

The ROV buckets, the stems and the circular plates are excepted from the structural checks as the first two are standardized according to /6/, and the latter just holds the upper pipe from falling and no axial forces exist.

1)Panel plate and POM cross section resistance

Inside the bores of the panel acting as support ground for the upper pipe, a plastic material (PO6) with very low friction is inserted. Which is subjected to the vertical loads due to mattress selfweight take from Staad.Pro,

Structural checks.xmcd

13.06.2018

Project: Master Thesis 2018	Multi-handling mechanism	Page: 3 of 11
Client: UiS		Originator: Eirinaios Chatzillari
		Checker:

Loads acting on POM face:

Axial: $N_{Ed} := 0\text{kN}$

Shear-Y: $V_{Ed,y} := 130.3\text{kN}$

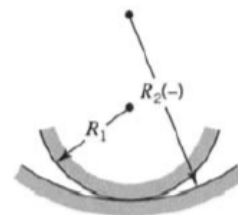
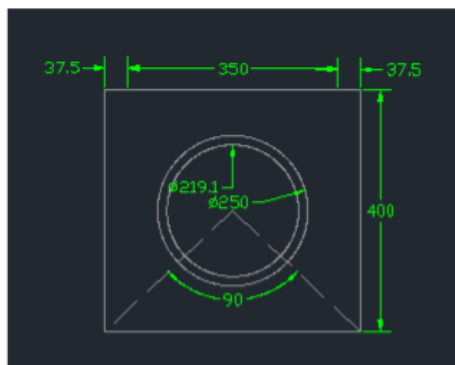
Shear-Z: $V_{Ed,z} := 0\text{kN}$

Mom-Y: $M_{Ed,y} := 0\text{kNm}$

Mom-Z: $M_{Ed,z} := 0\text{kNm}$

Geometry of the panel plate:

The total length of the panel plate is 2.55 m and the height is 0.40 m. It contains six bores, where the upper pipes are located, acting as pin foundation for them. Only one piece of the plate is examined, as is assumed that they are far enough to affect each other. The considered area is the following (dimensions in mm).



Calculation of contact stresses with reference to //:

	<u>Upper pipe</u>	<u>POM cylindrical surface</u>
Modulus of elasticity:	$E_1 := E$	$E_2 := \frac{2300\text{MPa} + 2800\text{MPa}}{2} = 2.55 \times 10^3 \cdot \text{MPa}(\text{Reference } /5/)$
Poisson ratio:	$\nu_1 := \nu$	$\nu_2 := 0.35$
Radius	$R_1 := 219.1\text{mm}$	$R_2 := R_1$

Project: Master Thesis 2018	Multi-handling mechanism	Page: 4 of 11
Client: UiS		Originator: Eirinaios Chatzillari
		Checker:

Assume a thickness for the section of the plastic material.

Thickness of POM: $t_{PO6} := 30\text{mm}$

Yield strength: $f_{y,PO6} := 67\text{MPa}$ (Reference /5/)

Factors for determining the equivalent stress according to /7/:

Load per unit length: $w_c := \frac{V_{Ed,y}}{t_{PO6}} = 4.34 \times 10^3 \frac{\text{kN}}{\text{m}}$

$$\Delta := \left(\frac{1 - \nu_1^2}{E_1} + \frac{1 - \nu_2^2}{E_2} \right) \cdot R_1 = 7.63 \times 10^{-11} \frac{\text{m}^2 \cdot \text{s}^2}{\text{kg}}$$

$$b := \sqrt{\frac{(2 \cdot V_{Ed,y}) \cdot \Delta}{t_{PO6} \cdot \pi}} = 0.01\text{m}$$

Maximum octahedral shear stress (equivalent stress): $\tau_{eq,max} := 0.27 \cdot \frac{b}{\Delta} = 51.38\text{MPa}$

Utilization ratio due to contact stresses:

$$UR_{cont,POM} := \frac{\tau_{eq,max}}{\frac{f_{y,PO6}}{\gamma_{M0}}} = 0.88$$

---> OK

Resistance in compression Ref. /1:Clause 6.2.4/

Diameter of upper pipe: $OD_{pipe} := 219.1\text{mm}$

Circumference of upper pipe $S_{pipe} := 2 \cdot \pi \cdot \frac{OD_{pipe}}{2} = 688.32\text{mm}$

Assume an arch of load distribution of 90 degrees.

$$S_{arch} := \frac{S_{pipe}}{4} = 172.08\text{mm}$$

$$A_{arch} := S_{arch} \cdot t_{PO6} = 5.16 \times 10^3 \cdot \text{mm}^2$$

The design value of the compression force N_{Ed} at each cross-section shall satisfy:

$$\frac{N_{Ed}}{N_{c,Rd}} \leq 1$$

$$N_{c,Rd,PO6} := \frac{0.50 A_{arch} f_{y,PO6}}{\gamma_{M0}} = 150.38\text{kN} \quad (\text{Conservative})$$

Project: Master Thesis 2018	Multi-handling mechanism	Page: 5 of 11
Client: UiS		Originator: Eirinaios Chatzillari
		Checker:

$$N_{Ed,PO6} := V_{Ed,y} = 130.3 \text{ kN}$$

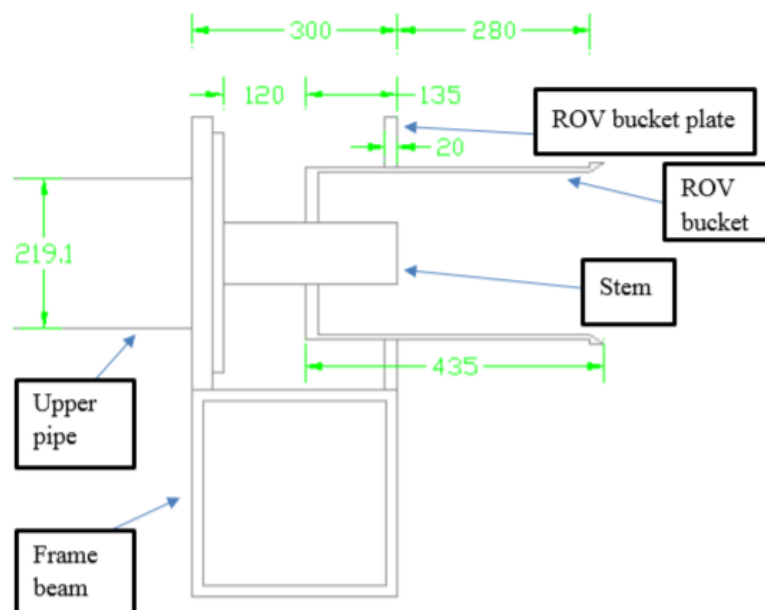
Utilization ratio due to compression:

$$UR_{com} := \frac{N_{Ed,PO6}}{N_{c,Rd,PO6}} = 0.87 \quad \rightarrow \text{OK}$$

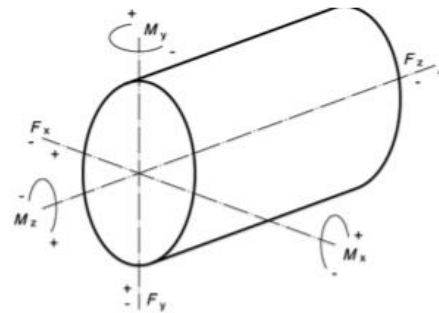
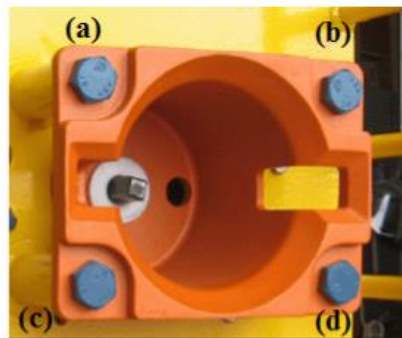
The steel panel plate has higher strength and therefore is waived from the check.

2(Bolting structural integrity)

The side view of the mechanism is depicted in the following figure. Each bucket is mounted with 4 bolts to the plate.



Project: **Master Thesis 2018** **Multi-handling mechanism** Page: 6 of 11
 Client: UiS Originator: Eirinaios Chatzillari
 Checker:



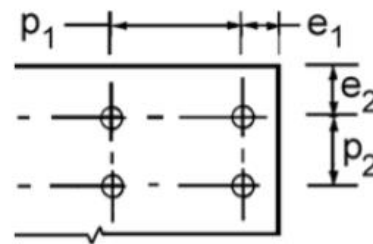
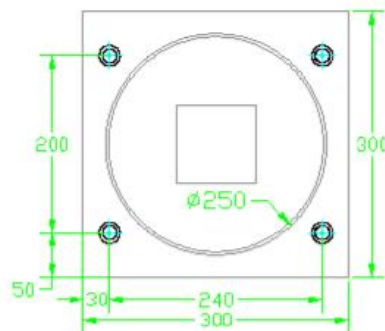
M_x	$\pm 1\,570\text{ N}\cdot\text{m}$ (1 158 lbf)	F_x	$\pm 3\,800\text{ N}$ (854 lbf)
M_y	$\pm 6\,080\text{ N}\cdot\text{m}$ (4 484 lbf)	F_y	$\pm 980\text{ N}$ (220 lbf)
M_z	—	F_z	$\pm 5\,060\text{ N}$ (1 137 lbf)

Thickness of the ROV bucket plate for bolting:

$$t_{\text{ROV.rec}} := 15\text{mm}$$

Diameter of ROV bucket:

$$\text{OD}_{\text{ROV.b}} := 250\text{mm}$$



Distances:

$$\begin{aligned} e_1 &:= 30\text{mm} & B_{\text{bucket.pl}} &:= 300\text{mm} \\ e_2 &:= 50\text{mm} & H_{\text{bucket.pl}} &:= 300\text{mm} \\ p_1 &:= 240\text{mm} \\ p_2 &:= 200\text{mm} \end{aligned}$$

Loads acting on the interface /6/:

$$\begin{aligned} \text{Axial:} & & N_{\text{Ed.int}} &:= 5.06\text{kN} \\ \text{Shear-Y:} & & V_{\text{Ed.y.int}} &:= 0.98\text{kN} \\ \text{Shear-X:} & & V_{\text{Ed.x.int}} &:= 3.8\text{kN} \end{aligned}$$

Project: Master Thesis 2018	Multi-handling mechanism	Page: 7 of 11
Client: UiS		Originator: Eirinaios Chatzillari
		Checker:

Mom-Y: $M_{Ed,y,int} := 6.08 \text{ kNm}$

Mom-X: $M_{Ed,x,int} := 1.57 \text{ kNm}$

Shear stress caused by torsion moment To: $T_{Ed} := 10.87 \text{ kNm}$

Torsion accounting the load factor: $M_{Ed,z,int} := \gamma_F T_{Ed} = 14.13 \text{ kNm}$

It is considered that the loads act simultaneously on the interface. The My moment creates a tensile force on the bolts (a) and (c), while the Mx moment creates a tensile force on the (a) and (b) bolts. Therefore, bolt (a) is the critical component, as subjected to 2 tensile forces. In addition, the tangential shear force and the tensile axial force will be accounted in the calculations.

Choose a M20 8.8 class bolt size:

Bolt class	4.6	4.8	5.6	5.8	6.8	8.8	10.9
$f_b \text{ (N/mm}^2\text{)}$	240	320	300	400	480	640	900
$f_{ub} \text{ (N/mm}^2\text{)}$	400	400	500	500	600	800	1000

The category of the connection is: Category C

c) Category C: Slip-resistant at ultimate limit state

In this category preloaded bolts in accordance with 3.1.2(1) should be used. Slip should not occur at the ultimate limit state. The design ultimate shear load should not exceed the design slip resistance, obtained from 3.9, nor the design bearing resistance, obtained from 3.6 and 3.7. In addition for a connection in tension, the design plastic resistance of the net cross-section at bolt holes $N_{net,Rd}$, (see 6.2 of EN 1993-1-1), should be checked, at the ultimate limit state.

Diameter of bolt: $od_{bolt} := 20 \text{ mm}$

Hole diameter for one bolt: $od_{bolt,o} := od_{bolt} + 2 \text{ mm} = 22 \text{ mm}$

Resistant area of one bolt: $A_{res} := 245 \text{ mm}^2$

Number of bolts each side: $n_{bolt} := 4$

Total resistance area for 4 bolts: $A_{res,t} := 4 \cdot A_{res} = 980 \cdot \text{mm}^2$

Capacity of bolt: $f_{u,bolt} := 800 \text{ MPa}$

Check if distances satisfy the requirements of /2/:

$e_1 = 30 \text{ mm}$ $e_1 \geq 1.2 \cdot od_{bolt,o} = 1$ \rightarrow OK (1 stands for true and 0 for false)

Project: Master Thesis 2018	Multi-handling mechanism	Page: 8 of 11
Client: UiS		Originator: Eirinaios Chatzillari
		Checker:

$$\begin{aligned}
 e_2 &= 50 \text{ mm} & e_2 &\geq 1.2 \cdot od_{\text{bolt.o}} = 1 \quad \rightarrow \text{OK} \\
 p_1 &= 240 \text{ mm} & p_1 &\leq \min(28 \cdot t_{\text{ROV.rec}}, 400 \text{ mm}) = 1 \quad \rightarrow \text{OK} \\
 p_2 &= 200 \text{ mm} & p_2 &\leq \min(14 \cdot t_{\text{ROV.rec}}, 200 \text{ mm}) = 1 \quad \rightarrow \text{OK}
 \end{aligned}$$

Partial safety factors for joints /2/:

$$\gamma_{M3} := 1.25$$

$$\gamma_{M7} := 1.10$$

Other parameters:

$$a_b := \min\left(\frac{f_u \cdot \text{bolt}}{f_u}, \frac{e_1}{3 \cdot od_{\text{bolt.o}}}, 1\right) = 0.45$$

Bearing resistance factors:

$$k_1 := \min\left(2.8 \cdot \frac{e_2}{od_{\text{bolt.o}}} - 1.7, 2.5\right) = 2.5$$

Tension resistance factor:

$$k_2 := 0.9$$

Slip resistance factors:

$$\mu := 0.3$$

$$k_3 := 1$$

$$n := 1$$

Resistance of bolt (a):

$$\text{Shear resistance: } F_{v.Rd} := 0.6 \cdot \frac{A_{res} \cdot f_u \cdot \text{bolt}}{\gamma_{M2}} = 94.08 \cdot \text{kN}$$

$$\text{Tension resistance: } F_{t.Rd} := k_2 \cdot \frac{A_{res} \cdot f_u \cdot \text{bolt}}{\gamma_{M2}} = 141.12 \cdot \text{kN}$$

Loads acting on the bolts:

$$\text{Tangential action from ROV intervention loads: } F_{v.Ed1} := \sqrt{V_{Ed.y.int}^2 + V_{Ed.x.int}^2} = 3.92 \cdot \text{kN}$$

$$\text{Shear force due to Mz moment: } F_{v.Ed2} := \frac{M_{Ed.z.int}}{\frac{OD_{ROV.b}}{2}} = 113.05 \cdot \text{kN}$$

Project: Master Thesis 2018	Multi-handling mechanism	Page: 9 of 11
Client: UIS		Originator: Eirinaios Chatzillari
		Checker:

Tensile force due to My:

$$F_{ty} := \frac{M_{Ed,y,int}}{OD_{ROV,b} - 2 \cdot \frac{od_{bolt}}{2}} = 26.43 \text{ kN}$$

Tensile force due to Mx:

$$F_{tx} := \frac{M_{Ed,x,int}}{OD_{ROV,b} - 2 \cdot \frac{od_{bolt}}{2}} = 6.83 \text{ kN}$$

Tensile force due to axial force:

$$F_{tz} := N_{Ed,int} = 5.06 \text{ kN}$$

Total tensile force on bolt (a):

$$F_{t,Ed,a} := \frac{F_{ty} + F_{tx}}{2} + \frac{F_{tz}}{4} = 17.9 \text{ kN}$$

Total shear force on bolt (a):

$$F_{v,Ed,a} := \frac{F_{v,Ed1} + F_{v,Ed2}}{4} = 29.24 \text{ kN}$$

Utilization ratio due to tension:

$$UR_{t,a} := \frac{F_{t,Ed,a}}{F_{t,Rd}} = 0.13$$

Utilization ratio due to shear:

$$UR_{t,s} := \frac{F_{v,Ed,a}}{F_{v,Rd}} = 0.31$$

Combined shear and tension:

$$\frac{F_{t,Ed,a}}{1.4F_{t,Rd}} + \frac{F_{v,Ed,a}}{F_{v,Rd}} = 0.4 < 1 \quad \rightarrow \text{OK}$$

Resistance of the connection:

$$0.8 \cdot F_{t,Ed,a} = 14.32 \text{ kN}$$

Bolt preload:

$$F_{p,Cd} := 0.7 \cdot f_{u,bolt} \cdot A_{res} = 137.2 \text{ kN}$$

Slip resistance:

$$F_{s,Rd} := \frac{k_s \cdot n \cdot \mu}{\gamma_{M3}} \cdot (F_{p,Cd} - 0.8 \cdot F_{t,Ed,a}) = 29.49 \text{ kN}$$

Bearing resistance:

$$F_{b,Rd} := \frac{(k_1 \cdot a_b \cdot f_{u,bolt} \cdot 10 \text{ mm} \cdot od_{bolt})}{\gamma_{M2}} = 145.45 \text{ kN}$$

Project: Master Thesis 2018	Multi-handling mechanism	Page: 10 of 11
Client: UIS		Originator: Eirinaios Chatzillari
		Checker:

Utilization ratio due to slip: $UR_{t,slip} := \frac{F_{v,Ed,a}}{F_{s,Rd}} = 0.99 < 1 \rightarrow OK$

Utilization ratio of bearing: $UR_{t,bearing} := \frac{F_{v,Ed1} + F_{v,Ed2}}{F_{b,Rd}} = 0.8 < 1 \rightarrow OK$

Control check of the bolting plate of the ROV bucket according to /1/:

$$A_{bucket,pl} := B_{bucket,pl} \cdot H_{bucket,pl} - \pi \cdot \left(\frac{OD_{ROV,b}}{2} \right)^2 = 4.09 \times 10^4 \text{ mm}^2$$

$$A_{net} := A_{bucket,pl} - n_{bolt} \cdot od_{bolt,o} \cdot t_{ROV,rec} = 3.96 \times 10^4 \text{ mm}^2$$

$$N_{net,Rd} := \frac{0.9 \cdot f_u \cdot A_{net}}{\gamma_{M2}} = 1.45 \times 10^4 \text{ kN}$$

Utilization ratio of bolting plate: $UR := \frac{F_{v,Ed1} + F_{v,Ed2}}{N_{net,Rd}} = 0.008 < 1 \rightarrow OK$

3) Weld check of the stem

Shear stress caused by torsion moment T_o : $T_o := 10.87 \text{ kNm}$

Torsion accounting the load factor: $T_{Ed,o} := \gamma_f \cdot T_o = 14.13 \text{ kNm}$

Square stem with height and width equal to 88.90 mm.

$$H_{st} := 88.90 \text{ mm}$$

$$B_{st} := H_{st}$$

Assume a weld throat thickness: $a := 5 \text{ mm}$

Weld contour:  $A = a \cdot 2 \cdot (H + B)$

Full weld length: $A_{st} := a \cdot 2 \cdot (H_{st} + B_{st}) = 1.78 \times 10^3 \cdot \text{mm}^2$

Project: Master Thesis 2018	Multi-handling mechanism	Page: 11 of 11
Client: UiS		Originator: Eirinaios Chatzillari
		Checker:

Polar moment of inertia: $J_{st} := a \cdot \frac{(H_{st} + B_{st})^3}{6} = 4.68 \times 10^6 \cdot \text{mm}^4$

X - component of stress

$$\tau_{xT} := \frac{T_{Ed.o} \cdot \frac{(H_{st})}{2}}{J_{st}} = 134.1 \cdot \text{MPa}$$

Y - component of stress

$$\tau_{yT} := \frac{T_{Ed.o} \cdot \frac{B_{st}}{2}}{J_{st}} = 134.1 \cdot \text{MPa}$$

Total shear stress: $\tau_{shear} := \sqrt{\tau_{xT}^2 + \tau_{yT}^2} = 189.65 \cdot \text{MPa}$

Utilization of weld due to shear: $UR_{w, shear} := \frac{\tau_{shear}}{\frac{f_{uW, 355} \cdot \beta_w}{\gamma_{M2}}} = 0.54 \quad \rightarrow \text{OK}$

Stress Analysis Report



Analyzed File:	ROV_plate.ipt
Autodesk Inventor Version:	2015 (Build 190159000, 159)
Creation Date:	5/6/2018, 15:15
Simulation Author:	EirinaiosChatz
Summary:	Docking stress analysis

Project Info (iProperties)

- ▣ Summary
- ▣ Project
- ▣ Status
- ▣ Physical

Simulation:1

General objective and settings:

Design Objective	Single Point
Simulation Type	Static Analysis
Last Modification Date	5/6/2018, 15:11
Detect and Eliminate Rigid Body Modes	No

Mesh settings:

Avg. Element Size (fraction of model diameter)	0.1
Min. Element Size (fraction of avg. size)	0.2
Grading Factor	1.5
Max. Turn Angle	60 deg
Create Curved Mesh Elements	Yes

Material(s)

Operating conditions

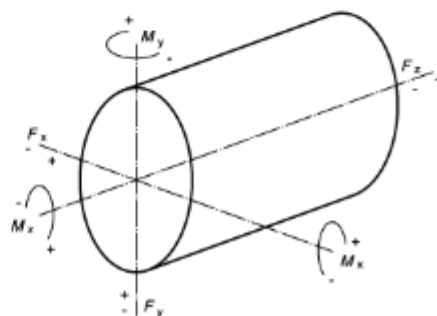
Moment:1

Load Type	Moment
Magnitude	6080.000 N mm
Vector X	0.000 N mm
Vector Y	0.000 N mm
Vector Z	6080.000 N mm

Selected Face(s)

Moment:2

Load Type	Moment
Magnitude	1570.000 N mm
Vector X	0.000 N mm
Vector Y	1570.000 N mm



M_x	$\pm 1\,570\text{ N}\cdot\text{m}$ (1 158 lbf)	F_x	$\pm 3\,800\text{ N}$ (854 lbf)
M_y	$\pm 6\,080\text{ N}\cdot\text{m}$ (4 484 lbf)	F_y	$\pm 980\text{ N}$ (220 lbf)
M_z	—	F_z	$\pm 5\,060\text{ N}$ (1 137 lbf)

Figure 8 — Docking receptacle loading

5/6/2018

Stress Analysis Report

Vector Z 0.000 N mm

Selected Face(s)

Force:1

Load Type	Force
Magnitude	5060 N
Vector X	5060 N
Vector Y	0.000 N
Vector Z	0.000 N

Selected Face(s)

Force:2

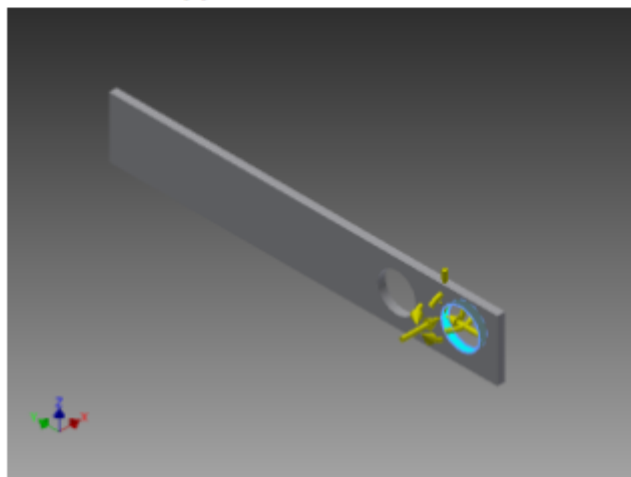
Load Type	Force
Magnitude	3800.000 N
Vector X	0.000 N
Vector Y	3800.000 N
Vector Z	0.000 N

Selected Face(s)

Force:3

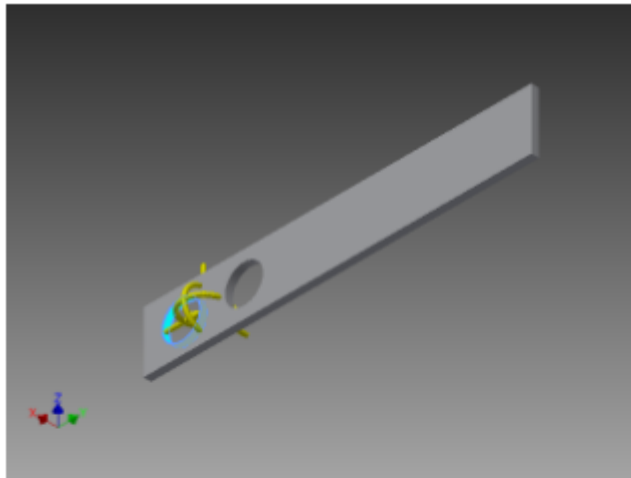
Load Type	Force
Magnitude	980.000 N
Vector X	0.000 N
Vector Y	0.000 N
Vector Z	-980.000 N

Selected Face(s)



5/6/2018

Stress Analysis Report



[-] Fixed Constraint:1

Constraint Type Fixed Constraint

[-] Selected Face(s)

[-] Results

[-] Reaction Force and Moment on Constraints

Constraint Name	Reaction Force		Reaction Moment	
	Magnitude	Component (X,Y,Z)	Magnitude	Component (X,Y,Z)
Fixed Constraint:1	3924.34 N	-5060 N	216.055 N m	-215.748 N m
		-3800 N		-2.62693 N m
		980 N		-11.2207 N m

[-] Result Summary

Name	Minimum	Maximum
Volume	46091300 mm ³	
Mass	368.73 kg	
Von Mises Stress	0.00017726 MPa	0.512313 MPa
1st Principal Stress	-0.023343 MPa	0.486224 MPa
3rd Principal Stress	-0.474811 MPa	0.125694 MPa
Displacement	0 mm	0.000984397 mm
Safety Factor	15 ul	15 ul
Stress XX	-0.0732697 MPa	0.183837 MPa
Stress XY	-0.0196821 MPa	0.0285784 MPa
Stress XZ	-0.0407585 MPa	0.0447272 MPa
Stress YY	-0.458757 MPa	0.220002 MPa
Stress YZ	-0.113212 MPa	0.255939 MPa
Stress ZZ	-0.347717 MPa	0.478032 MPa
X Displacement	-0.0000197689 mm	0.000320233 mm
Y Displacement	0 mm	0.000926966 mm
Z Displacement	-0.000158756 mm	0.000221288 mm
Equivalent Strain	0.000000000796271 ul	0.00000233415 ul
1st Principal Strain	0.000000000599489 ul	0.00000208558 ul
3rd Principal Strain	-0.00000256538 ul	-0.000000000739254 ul
Strain XX	-0.000000608312 ul	0.000000723444 ul
Strain XY	-0.000000132574 ul	0.000000192497 ul
Strain XZ	-0.000000274539 ul	0.000000301271 ul
Strain YY	-0.0000023755 ul	0.00000104484 ul

5/6/2018

Stress Analysis Report

Strain YZ	-0.000000762566 ul	0.00000172394 ul
Strain ZZ	-0.00000179957 ul	0.00000205721 ul

Figures

Von Mises Stress

